The Canadian Journal of Chemical Engineering

formerly

CANADIAN JOURNAL OF TECHNOLOGY

CONTENTS

Heat Transfer to High-Quality Steam-Water Mixtures Flowing in a Horizontal Rectangular Duct	*E. J. Davis* *M. M. David*	**99**
Fluid Friction and Heat Transfer in Cyclindrical Pipes: Relationship Between Lumped and Distributed Parameters	*Julian C. Smith*	**106**
Fundamental Aspects of Solids-Gas Flow: Part VI: Multiparticle Behavior in Turbulent Fluids	*L. B. Torobin* *W. H. Gauvin*	**113**
Optimal Bypass Rates for Sequences of Stirred Tank Reactors	*Rutherford Aris*	**121**
The Effect of Intraparticle Temperature Distribution on the Catalytic Effectiveness Factor of a Porous Catalyst	*T. Akehata* *S. Namkoong* *H. Kubota* *M. Shindo*	**127**
A Design Parameter for Multicomponent Tray Design Estimates	*Alfred J. Surowiec*	**130**
Factorial Design in the Study of Acid Leaching of Pegmatitic Uranium Ores	*D. G. Fisher* *R. G. McIntosh* *R. L. Eager* *A. B. Van Cleave*	**139**
Industrial Section		
Reactions in a Fluidized Coke Bed, with Self-Resistive Heating	*H. S. Johnson*	**145**

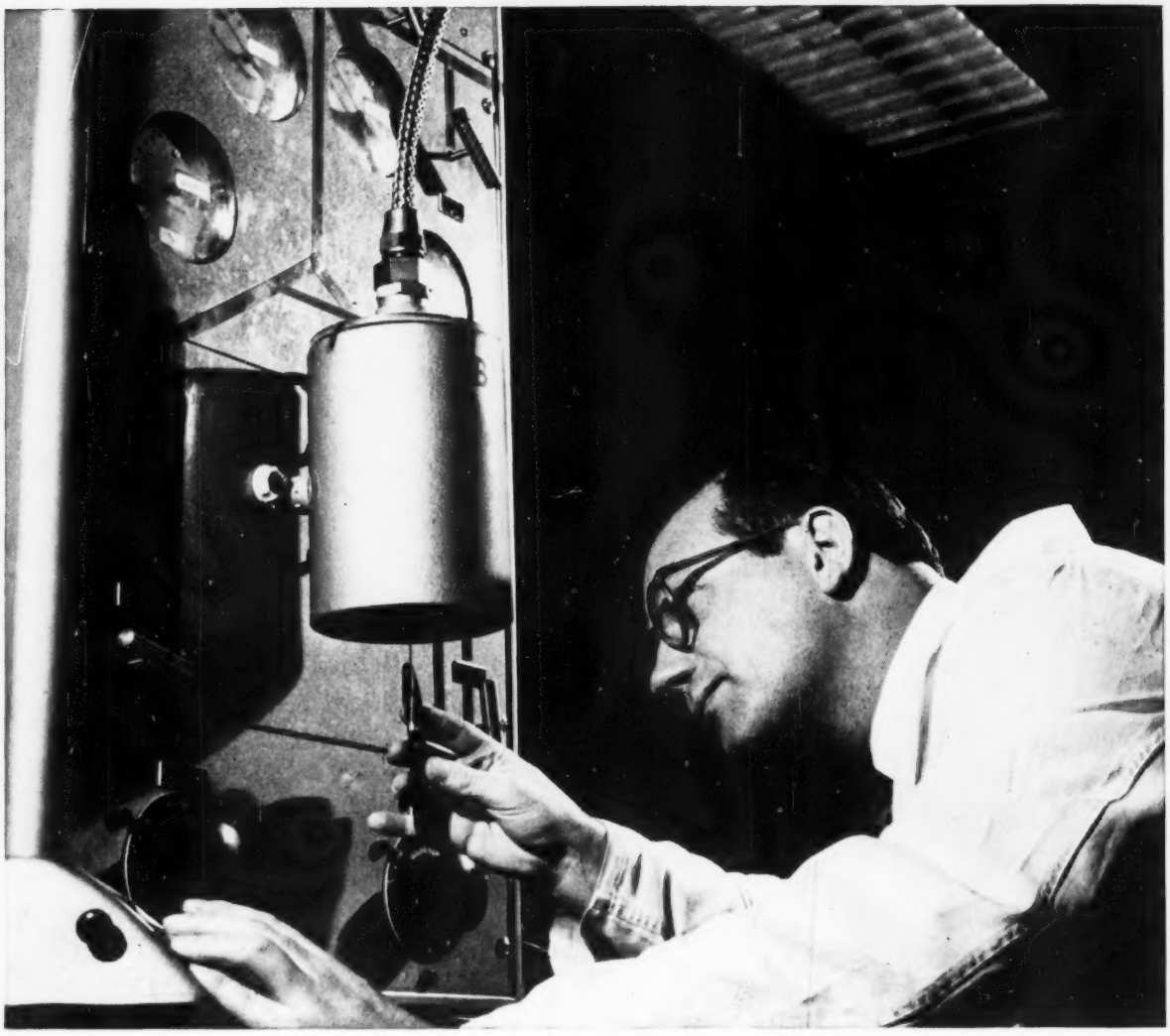

Photograph taken at C-I-L Central Research Laboratory, McMasterville, Que.

Plastics Detective

This photograph shows the High Shear Viscometer, designed and built at our Central Research Laboratory, used to investigate factors involved in complex flow behaviour of molten thermo-plastics during commercial processing.

Information on this newly developed pressure-driven capillary Viscometer has been made available to industry by C-I-L, and many industrial laboratories in the United States, England, India and Australia have built identical machines.

Such C-I-L research contributes to higher standards of performance in the plastics industry, to new and better plastics products and—through better technical service—to greater success in the application of these new materials to modern living.

C-I-L **CANADIAN INDUSTRIES LIMITED**

Serving Canadians Through Chemistry

Agricultural Chemicals • Ammunition • Coated Fabrics — Industrial Chemicals • Commercial Explosives • Paints • Plastics • Textile Fibres

The Canadian Journal of Chemical Engineering

formerly

Canadian Journal of Technology

Published by The Chemical Institute of Canada

VOLUME 39 JUNE, 1961 NUMBER 3

Authorized as second class mail, Post Office Department, Ottawa. Printed in Canada

Manuscripts for publication should be submitted to the Editor: Dr. A. Cholette, Faculty of Science, Laval University, Boulevard de l'Entente, Quebec, Que. (Instructions to authors are on the next page).

Editorial, Production and Circulation Offices: 48 Rideau Street, Ottawa 2, Ont.

Advertising Office: C. N. McCuaig, manager of advertising sales, *The Canadian Journal of Chemical Engineering*, Room 601, 217 Bay Street, Toronto, Ont. Telephone—EMpire 3-3871.

Plates and Advertising Copy: Send to *The Canadian Journal of Chemical Engineering*, 48 Rideau Street, Ottawa 2, Ont.

Subscription Rates: In Canada—$6.00 per year and $1.25 per single copy; U.S. and U.K.—$7.00, Foreign—$7.50.

Change of Address: Advise Circulation Department in advance of change of address, providing old as well as new address. Enclose address label if possible.

The Canadian Journal of Chemical Engineering is published by The Chemical Institute of Canada every two months.

The Canadian Journal of Chemical Engineering

INSTRUCTIONS TO AUTHORS

Manuscript Requirements for Articles

1. The manuscript should be in English or French.
2. The original and two copies of the manuscript should be supplied. These are to be on 8½ x 11 inch sheets, typewritten, and double spaced. Each page should be numbered.
3. Symbols should conform to American Standards Association. An abridged set of acceptable symbols is found in the third edition of Perry's Chemical Engineers' Handbook. Greek letters and subscripts and superscripts should be carefully made.
4. Abstracts of not more than 200 words in English indicating the scope of the work and the principal findings should accompany all technical papers.
5. References should be listed in the order in which they occur in the paper, after the text, using the form shown here: "Othmer, D. F., Jacobs, Jr., J. J., and Levy, J. F., Ind. Eng. Chem. **34**, 286 (1942). Abbreviations of journal names should conform to the "List of Periodicals Abstracted by Chemical Abstracts". Abbreviations of the common journals are to be found in Perry's Handbook also. All references should be carefully checked with the original article.
6. Tables should be numbered in Arabic numerals. They should have brief descriptive titles and should be appended to the paper. Column headings should be brief. Tables should contain a minimum of descriptive material.
7. All figures should be numbered from 1 up, in Arabic numerals. Drawings should be carefully made with India ink on white drawing paper or tracing linen. All lines should be of sufficient thickness to reproduce well, especially if the figure is to be reduced. Letters and numerals should be carefully and neatly made, with a stencil. Generally speaking, originals should not be more than twice the size of the desired reproduction; final engravings being 3¼ in. or 7 in. wide depending on whether one column or two is used. For further details ask the Editor for the Guide for Drawings.
8. Photographs should be made on glossy paper with strong contrasts. Photographs or groups of photographs should not be larger than three times the size of the desired reproduction.
9. All tables and figures should be referred to in the text.

Submission of Manuscripts

1. The three copies of the manuscript, including figures and tables, should be sent directly to:

   DR. A. CHOLETTE, editor,
   The Canadian Journal of Chemical Engineering,
   Faculty of Science, Laval University,
   Boulevard de l'Entente,
   Quebec, Que.
2. The authors addresses and titles should be submitted with the manuscript.
3. The author may suggest names of reviewers for his article, but the selection of the reviewers will be the responsibility of the editor. Each paper or article is to be reviewed by two chemical engineers familiar with the topic. Reviewers will remain anonymous.
4. All correspondence regarding reviews should be directed to the editor.

Reprints

1. At least 50 free "tear sheets" of each paper will be supplied.
2. Additional reprints may be purchased at cost. An estimated cost of reprints, with an attached order form, will be sent to the author with the galley proofs.
3. Orders for reprints must be made before the paper has appeared in the Journal.

Communications, Letters and Notes to the Editor

Short papers, as described below, will be considered for publication in this Journal. Their total length should be such that they will not occupy more than one page of the Journal.

Communications

A communication is a prompt preliminary report of observations made which are judged to be sufficiently important to warrant expedited publication. It usually calls for a more expanded paper in which the original matter is republished with more details.

Letters

A letter consists of comments or remarks submitted by readers or authors in connection with previously published material. It may deal with various forms of discussion arising out of a publication or it may simply report and correct inadvertent errors.

Notes

A note is a short paper which describes a piece of work not sufficiently important or complete to make it worth a full article. It may refer to a study or piece of research which, while it is not finished and may not be finished, offers interesting aspects or facts. As in the case of an article a note is a final publication.

* * *

Heat Transfer to High-Quality Steam-Water Mixtures Flowing in a Horizontal Rectangular Duct[1]

E. J. DAVIS[2] *and M. M. DAVID*[3]

Heat transfer and pressure drop were investigated for steam-water mixtures flowing in an electrically heated horizontal duct of rectangular cross-section. The investigation was primarily concerned with the region of high vapor fractions and mass flow rates, where two-phase convention-controlled heat transfer predominated.

The experimental data were found to be in good agreement with those of other studies in which circular tubes were used. The data in the convection-controlled region were correlated by equations developed from two flow models, a separated-annular model and a homogeneous model.

Two phase pressure drop data were correlated satisfactorily by the Lockhart-Martinelli correlation.

In the vaporization of a liquid stream flowing through a closed channel, three regimes of heat transfer can occur—nucleate boiling, forced convection-controlled heat transfer, and a regime of liquid deficiency or burnout, which occurs beyond the point of maximum heat transfer coefficient. The first regime is characterized by bubble growth and nucleation at the heat transfer surface, and the heat transfer coefficient is a function of the heat flux. In the convection-controlled regime the heat transfer coefficient is independent of the heat flux, as in single-phase convection heat transfer. The third regime is characterized by a liquid deficient condition at the wall and occurs when the vapor mass fraction becomes so large that the liquid film on the wall is removed.

Nucleate boiling has been the object of many pool boiling and flow boiling studies in recent years, and numerous theoretical and experimental investigations in this field have been reported. Two-phase convection-controlled heat transfer has been studied much less extensively; and only a very small amount of work has been reported in the liquid-deficient range other than flow boiling burnout measurements. Much of the early work in two-phase flow heat transfer was concerned with situations where both convection and nucleate boiling contributed to the heat transfer process[1,2,3,4,5,6], and the work was generally uncoordinated with other investigations and limited to specialized studies and to the measurement of average overall or integral coefficients which shed little light on the mechanisms involved. More recent two-phase convection studies have measured and correlated point coefficients and avoided other complications of earlier studies. Dengler[7,8], Silvestri and coworkers[9], Fikry[10], Kvamme[11], Rohsenow and Clark[12,13], and Mumm[14,15] have studied the steam-water system; Johnson and Abou-Sabe[16], Groothuis and Hendal[17], and Fried[18] have investigated the air-water system; and McNelly[19,20] and Guerrieri and Talty[21] have studied various organic two-phase systems. However, the published correlations and data are still limited in breadth of applicability and are often inconsistent.

The present investigation, although extending into the nucleate boiling and liquid-deficient ranges of operation, was particularly concerned with two-phase convection-controlled heat transfer with the steam-water system. The study used high quality (usually above 30% steam) mixtures, flowing in a horizontal duct with rectangular cross section, which was heated on one vertical face only.

Apparatus

The overall apparatus is shown schematically in Figure 1. Metered water and steam streams were mixed by spraying water into the steam to produce a mixture of the desired quality and at the desired pressure. This mixture was passed through the heat transfer test section, and then led to condensing tees where the mixture was condensed and cooled.

The enthalpy of all entering and leaving liquid streams was measured by calibrated chromel-alumel thermocouples installed in the flowing streams, and the steam enthalpy was measured by a throttling calorimeter. Flow rates were measured by calibrated orifices. These measurements plus that of the heat input to the test section permitted mass and heat balances to be made around the system for each run, and the enthalpy balance was usually found to be accurate to within 5%.

The heat transfer test section, shown in Figure 2, was designed to measure heat transfer coefficients in essentially a differential length, which has a rectangular cross section 0.769-in. high by 0.260-in. wide. The test section consisted of an 8.25-in. long converging inlet portion, a 7.25-in. calming portion, a 6.0-in. heating portion heated electrically on one vertical face, a 2.50-in. unheated portion, a 3.00-in. window section, another 3.50-in. section, and a 4.00-in. expansion section. The window section, which had the same internal dimensions as the rectangular heated section, was installed to permit visual or photographic observation of the flow patterns. Pressure taps were located on the wall opposite the heater area and were connected to seal pots or manifolds which led, through ⅛-in. needle valves, to calibrated pressure guages and a manometer system. The pressure measurements permitted determination of both the temperature of the two-phase mixture in the heated section and the pressure drop along the test section.

The rectangular duct was constructed from 26-gauge type 302 stainless steel whose thickness was accurately measured

[1]*Manuscript received October 12, 1960; accepted March 15, 1961.*
[2]*Chemical Engineering Department, Gonzaga University, Spokane, Wash., U.S.A.*
[3]*Department of Chemical Engineering, University of Washington, Seattle, Wash., U.S.A.*
Contribution from the Department of Chemical Engineering, University of Washington, Seattle, Wash., U.S.A. Based on a paper presented at the Chemical Engineering Conference, Quebec City, November 7-9, 1960.

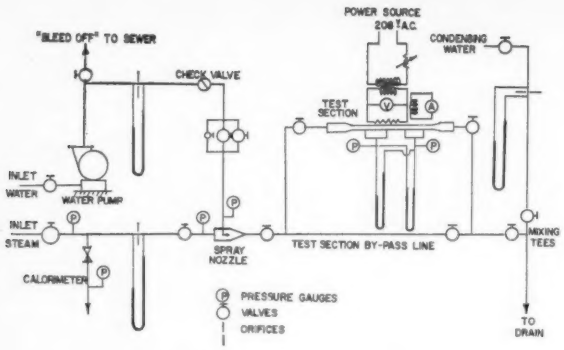

Figure 1—Schematic diagram of the apparatus.

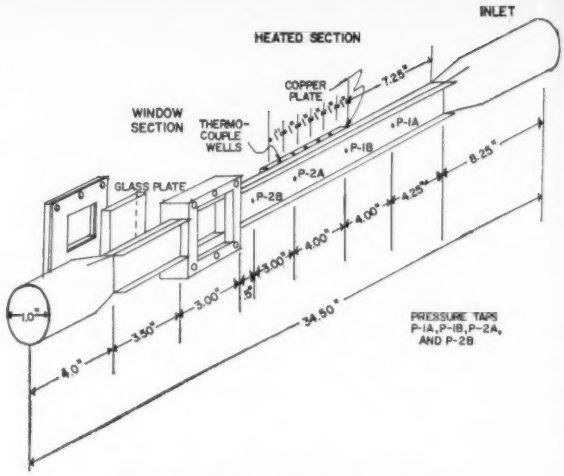

Figure 2—Heat transfer test section.

before the duct was fabricated. A thin-walled duct was used to minimize longitudinal heat transfer from the heated area, and heavy steel back-up plates were clamped on, but insulated from, the vertical sides to eliminate the possibility of bowing at the higher pressures used. To permit obtaining the inside wall temperature of the thin-walled duct, provide an accurately known heat transfer area, and ensure a uniform distribution of the heat flux, a 0.100-in. layer of pure copper was electroplated on one vertical face of the 6.00-in. heated section. Five calibrated chromel-alumel thermocouples were mounted in 0.032-in. diameter holes drilled vertically along the center of the copper plate, at the positions indicated in Figure 2, and the inside wall temperature was determined by correcting for the temperature drop across half the thickness of the copper and across the duct wall. The high thermal conductivity of the copper and the small size of the thermocouple holes make the accuracy of this method essentially dependent upon the accuracy of the thermal conductivity data for the stainless steel, for approximately 90% of the calculated temperature drop from the thermocouples to the inside of the wall occurs in the stainless steel. Thermal conductivity data from a number of sources were compared, and the data published by Smith[22] were used in the present work. The thermocouples were calibrated before and after installation and are estimated to be accurate to within ±1.0°F.

The heat flux was supplied electrically by means of a stainless steel heater strip with the same area as the copper plate, with heavy copper leads fastened to the two ends. The copper leads were connected to an 18 K.V.A. transformer which supplied the power at low voltages and high currents (less than 10 volts and up to 400 amperes). The heater strip was clamped to the outer surface of the copper and separated from it by a layer of isomica 0.0009-in. thick. The heat input was determined by the power supplied to the heater strip, corrected for losses along the leads and to the surroundings. The test section was insulated with glass wool and the remainder of the installation with standard pipe insulation.

The heat losses from the test section could not be determined by an overall enthalpy balance because the heat input was only a small fraction of the total enthalpy of the flowing stream. The heater was therefore calibrated, both by heating a stream of water and measuring the temperature rise and by measuring the power input with stagnant air inside the test section, with the test section at the operating temperature.

The extent of temperature elevation (above the temperature of the two-phase mixture) of the duct walls adjacent to the copper-plated heating section was investigated both by rough calculations and experimentally by thermocouples mounted on the outer surface of the duct, as close to the copper strip as possible without actually touching it. Both methods indicated that longitudinal conduction of heat (horizontal conduction, in the case of the top and bottom of the duct) through the duct walls, away from the heated section, was negligible. From the calibration studies, it is estimated that the heat flux was known to ±3%.

*Experimental Data**

Experimental data were taken over a range of total mass flow rates from 50,000 to 600,000 lbs./hr.-ft.^{2}, qualities from 30% to 90% steam, pressures from 25 to 150 p.s.i.a. ,and heat fluxes from 60,000 to 260,000 B.t.u./hr.-ft.^{2}. The upper flow rate limit for the 25 and 50 p.s.i.a. runs was determined by the occurrence of critical flow. The heat transfer coefficients calculated from the data are estimated to have an accuracy of 5%-10%, except for runs at very high flow rates where the film temperature drop ($T_w - T_s$) was low. For these latter data an accuracy of 15%-20% is estimated, excluding possibly two runs where the film temperature differences were as low as 3.6°F. Generally the differences were greater than about 6.0°F.

To determine if the data were in the convection regime, log-log plots of heat flux versus the film temperature difference ($T_w - T_s$) were prepared as in Figures 3 and 4. The slope of these lines is 1.0 at the higher flow rates, indicating that the heat transfer coefficient is independent of the heat flux. At lower flow rates the slope was found to increase with a decrease in either quality or flow rate, as in Figure 5. It is probable that this increase of coefficient with an increase in heat flux is due to a nucleate boiling contribution, for a convection mechanism does explain this phenomenon. At the higher flow rates nucleate boiling is probably suppressed because the wall temperature is too low to foster nucleation and bubble growth, and it was found that Dengler's correlation (8) for the minimum temperature difference required to initiate nucleate boiling, would predict this result.

$$\Delta T_i = 10(G_L V_L/3600 R_L)^{0.3}$$

At each pressure investigated, the data for the convection-controlled runs, smoothed by the above plots, were plotted on log-log plots of the heat transfer coefficient versus the superficial vapor mass velocity, as illustrated in Figure 6. The data were then found to fit equations of the form:

$$h_{TP} = B(G_g')^{0.87} \quad \ldots\ldots\ldots\ldots\ldots\ldots\ldots\ldots (1)$$

where the exponent, 0.87 was the average slope for the four pressures studied, and the values of the pressure dependent constant, B, are listed in Table 1.

*A complete tabulation of data and results, as well as further details of the apparatus, procedure, and other phases of the study are given by Davis [22].

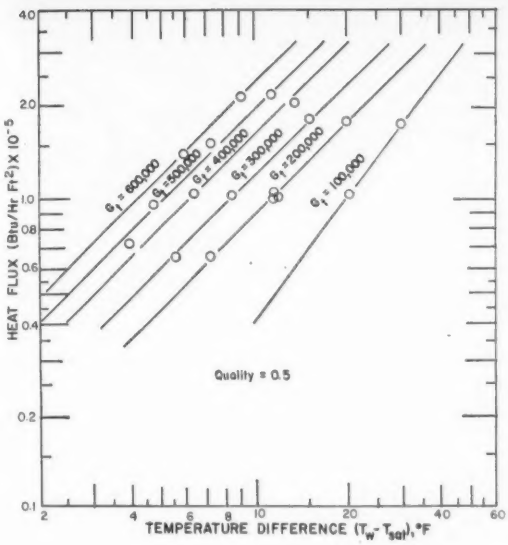

Figure 3—Experimental data at 100 p.s.i.a.

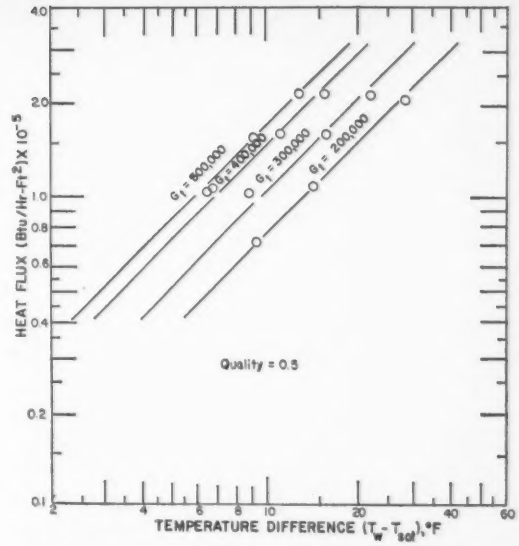

Figure 4—Experimental data at 150 p.s.i.a.

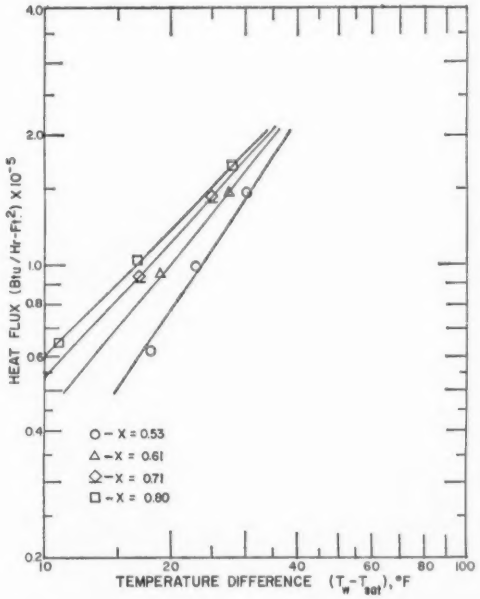

Figure 5—Experimental data for $P = 25$ p.s.i.a. and $G_t = 75{,}000$ lb./hr. ft.^{2}.

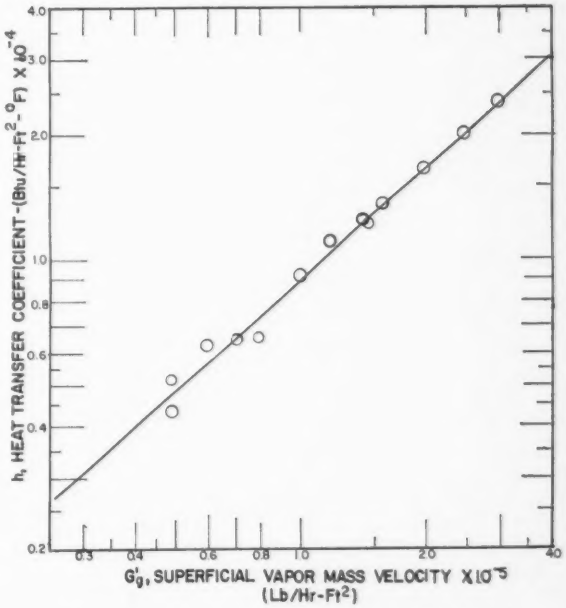

Figure 6—Experimental results at 100 p.s.i.a.

TABLE 1

VALUE OF THE PRESSURE DEPENDENT CONSTANT, B, IN EQUATION (1) FROM THE EXPERIMENTAL DATA

B	Pressure, p.s.i.a.
0.449	25
0.429	50
0.400	100
0.346	150

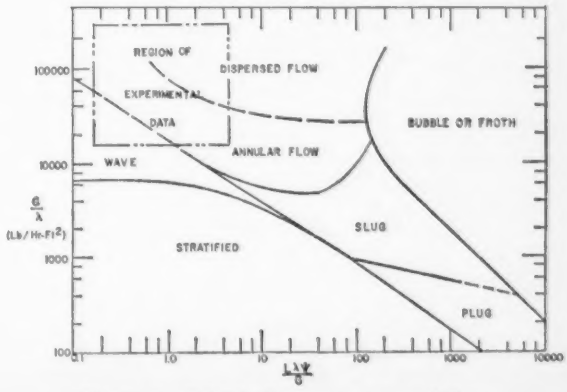

Figure 7—Baker's flow pattern correlation.

A maximum heat transfer coefficient was found to occur for each pressure and flow rate in the region of 80%-90% steam, but the phenomenon was not studied in sufficient detail to permit prediction of the maximum coefficient, because of the danger of burnout of the test section. Visual observation of the flow patterns indicated that for runs below the maximum heat transfer coefficient a thin liquid layer existed on the wall, and either annular flow or dispersed-annular flow occurred. The flow patterns were in general agreement with Baker's flow patterns correlation[24], as shown in Figure 7.

Correlation of Results

Based upon the observed flow patterns and the correlation of the experimental data by the superficial vapor mass velocity, two models are postulated to predict the two-phase heat transfer coefficients for a vapor-liquid system.

Separated-Annular Flow Model: Two alternate approaches were developed based upon a separated-annular flow model — a slip ratio equation and a void fraction equation. For both approaches it is assumed that:

(1) Nucleate boiling does not occur, because of suppression by two-phase forced convection heat transfer.

(2) The resistance to heat transfer occurs within the thin layer of liquid at the wall.

(3) The Reynolds number of the liquid and the physical properties of the liquid determine the convection heat transfer rate from the wall to the liquid film.

(4) An equation of the following form can be used to predict the heat transfer coefficients for heat transfer from the wall to the liquid film:

$$\frac{hD_e}{k_L} = a\left(\frac{D_eG_L}{\mu_L}\right)^b\left(\frac{C_p\mu}{k}\right)^c_L \qquad \text{.....(2)}$$

The liquid mass velocity in Equation (2) can be related to the vapor mass velocity by the equation of continuity for each phase and by the slip ratio definition:

$$\rho_g u_g = G_g, \text{ and } \rho_L u_L = G_L$$
$$\alpha = u_g/u_L = \text{slip ratio}$$

Solving for G_L:

$$G_L = \frac{G_g\rho_L}{\alpha\rho_g}$$

Substituting in Equation (2) for G_L:

$$\frac{hD_e}{k_L} = a\left(\frac{D_eG_g\rho_L}{\mu_L\alpha\rho_g}\right)^b\left(\frac{C_p\mu}{k}\right)^c_L \qquad \text{.....(2a)}$$

Because in the high vapor mass fraction range the vapor phase occupies practically all of the cross sectional area of the duct, the actual vapor mass velocity can be approximated by the superficial vapor mass velocity, and Equation (2a) can be written:

$$\frac{hD_e}{k_L} = a\left(\frac{D_eG_g'\rho_L}{\mu_L\alpha\rho_g}\right)^{0.87}\left(\frac{C_p\mu}{k}\right)^{0.4} \qquad \text{.....(3a)}$$

Because slip ratio data are not available for the range of pressures, qualities, and flow rates studied in the present investigation, it is not possible to assess the value of Equation (3a) per se for correlating the experimental data. Slip ratio data can be obtained from void fraction data to obtain the void fraction equation, as discussed below, but an alternate approach based upon Equation (3a) was developed to provide an empirical correlation of the experimental data.

By including the values of the physical properties for each pressure studied in Equation (3a) and equating Equations (3a) and (1), the numerical values of $a/\alpha^{0.87}$ can be calculated for each pressure, as tabulated in Table 2. In the computations the equivalent diameter, D_e, was taken as defined for single-phase flow:

$$D_e = \frac{4(\text{cross sectional area for flow})}{\text{wetted perimeter}}$$

However, there is no theoretical justification for this usage.

TABLE 2

THE VARIATION OF $a/\alpha^{0.87}$ WITH PRESSURE

$a/\alpha^{0.87}x10^3$	Pressure, p.s.i.a.
1.051	25
1.530	50
2.385	100
2.745	150

The term, $a/\alpha^{0.87}$, was found to be correlated by a log-log plot of the term versus the absolute pressure and also versus the liquid-vapor density ratio, ρ_L/ρ_g. The latter log-log plot results in an excellent fit of the variables by a straight line having a slope of -0.59, and this correlation can be included in Equation (3a) to give:

$$\frac{hD_e}{k_L} = 0.060\left(\frac{\rho_L}{\rho_g}\right)^{-0.59}\left(\frac{D_eG_g'\rho_L}{\mu_L\rho_g}\right)^{0.87}\left(\frac{C_p\mu}{k}\right)^{0.4}_L \qquad \text{.....(4)}$$

By relating the superficial vapor mass velocity to the total mass velocity, the equation can be written in final form:

$$\frac{hD_e}{k_L} = 0.060\left(\frac{\rho_L}{\rho_g}\right)^{0.28}\left(\frac{D_exG_t}{\mu_L}\right)^{0.87}\left(\frac{C_p\mu}{k}\right)^{0.4}_L \qquad \text{.....(4a)}$$

Equation (4a) was used to correlate the data in the convection-controlled heat transfer region of the present investigation to within $\pm 15\%$, as shown in Figure 8.

Although the range of values for the physical properties of the liquid film was too small in the present study to permit independent determination of the effects of these properties on the heat transfer coefficient, inclusion of these properties in Equation (4a) produced a slightly better correlation of results

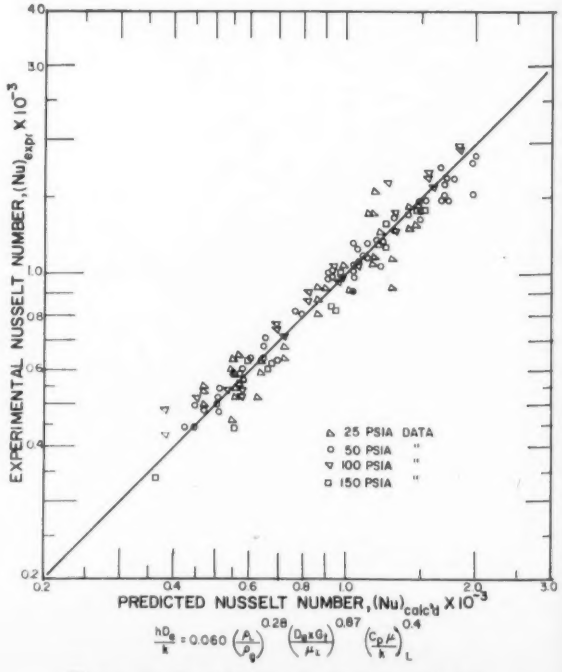

Figure 8—Correlation of experimental data.

TABLE 3

Author	Pressure p.s.i.a.	Quality %	Heat Flux B.t.u./hr.-ft.^{2}	Mass Velocity lb./hr.-ft.^{2}	Equiv. Dia. ft.
Present	25-150	30-80	60,000-260,000	75,000-600,000	0.0324
Kvamme-Yamazaki	18-86	10-94	25,600- 50,200	85,000-189,000	0.0313
Dengler	10-29	15-83	27,600-198,000	41,000-284,500	0.0833

than was obtained from a generalized correlation of either a form similar to Equation (1), or to Equation (4a) used without the Prandtl number.

The two-phase convection heat transfer data of Kvamme and Yamazaki[11] and Dengler[7,8] for circular tubes were also correlated adequately by Equation (4a), as shown in Figure 9. (Because of the large scatter in the individual point heat transfer coefficients measured along Kvamme's test section, the average heat transfer coefficient for each of his runs was used.) Table 3 lists the range of variables involved in the data correlated by Equation (4a).

The ability of the correlating equation to predict the various data adequately indicates that the data are in agreement, that the equivalent diameter used is satisfactory, and that the model might be correct. However, because slip ratio data are not available, the model cannot be thoroughly tested, and the correlation must be considered as a purely empirical approach.

The separated-annular flow model can also be developed using void fraction data to calculate the slip ratio. The liquid void fraction is defined as:

$$R_L = A_L/A_t = A_L/(A_L + A_g)$$

By use of equations of continuity for each phase, and the definitions of the void fraction and slip ratio, the slip ratio can be obtained in terms of the void fraction:

$$a = u_g/u_L = \frac{x}{(1-x)}\frac{\rho_L}{\rho_g}\frac{R_L}{(1-R_L)}$$

Substituting in Equation (2) for a, the following correlating equation is obtained:

$$\frac{hD_e}{k_L} = a\left[\frac{D_e(1-x)G_t}{\mu_L R_L}\right]^{0.87}\frac{C_p\mu}{k}^{0.4} \quad \ldots\ldots\ldots\ldots(5)$$

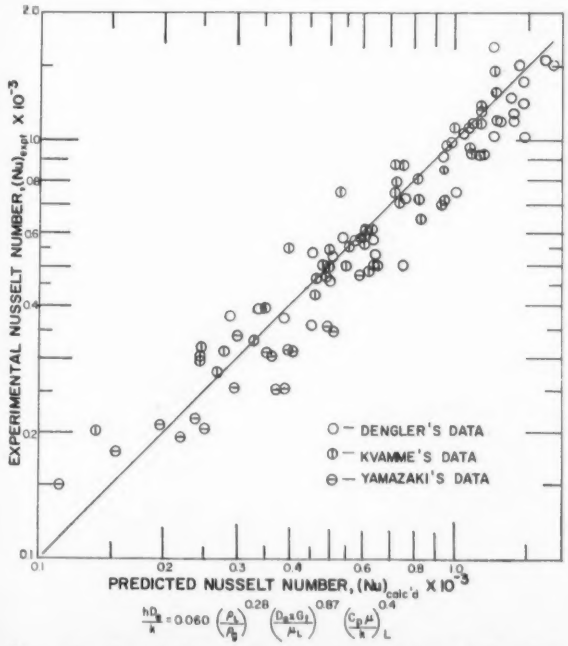

Figure 9—Correlation of the experimental data of Dengler, Kvamme, and Yamazaki.

In Equation (5), the void fraction equation, the exponents and the equivalent diameter are taken as in Equation (3a). The constant, a, was determined to be 0.017 be fitting the equation to the data of the present study, using the liquid void fraction data of Smith and Hoe[28], who correlated their data by the Lockhart-Martinelli method[20]. Figure 10 is a comparison between the experimental data at a pressure of 50 p.s.i.a. and Equation (5). The correlation is unsatisfactory at both high and low qualities, but it cannot be determined whether the heat transfer equation, Equation (5), is unsuitable or whether the void fraction correlation of Smith and Hoe is unsatisfactory in the high flow rate region.

Equation (5) is similar to the correlating equation proposed by Kvamme[11]:

$$h_{TP}/h_L = 1.5\,[(1-x)/R_L]^{0.8}$$

where:

$$h_L = 0.023\,\frac{k}{D}\left(\frac{DG_t}{\mu_L}\right)^{0.8}\left(\frac{C_p\mu}{k}\right)^{0.4}$$

However, Equation (5) predicts two-phase heat transfer coefficients that are about 20% higher than Kvamme's correlation.

Homogeneous Model: The second correlating approach, the homogeneous model, was used because the flow pattern was dispersed or dispersed-annular for many of the heat transfer runs. With this model it is assumed that the heat transfer occurs to a very thin film of liquid on the wall, and the flow characteristics of the film are a function of the Reynolds number of the homogenous core. The equation used is:

$$\frac{hD_e}{k_L} = a\left(\frac{D_e\rho_{TP}u_{TP}}{\mu_{TP}}\right)^{0.87}\left(\frac{C_p\mu}{k}\right)^{0.4}_L$$

By considering a unit volume of duct, assuming no slip occurs, and that thermodynamic equilibrium exists between the two

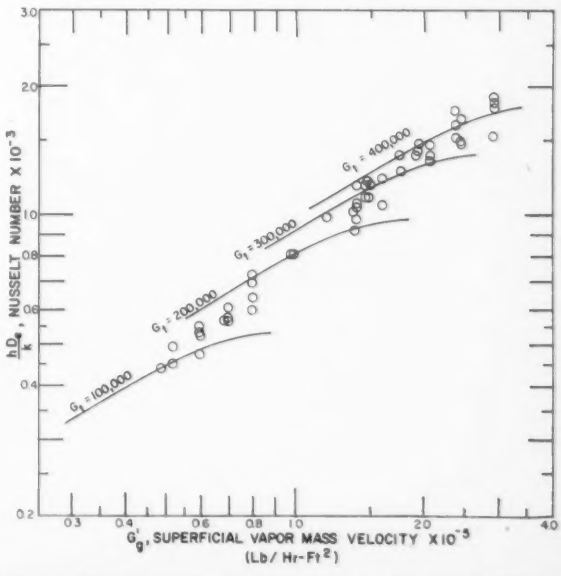

Figure 10—Comparison of the void fraction model (Equation 5) with the experimental data at 50 p.s.i.a.

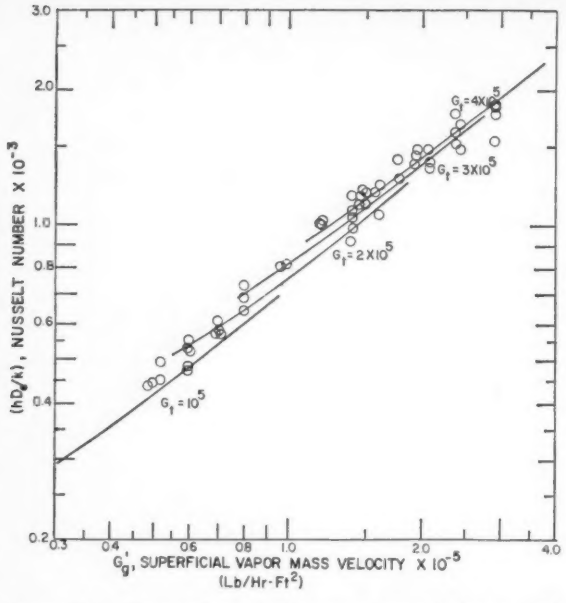

Figure 11—Correlation of the experimental data at 50 p.s.i.a. by the homogeneous model.

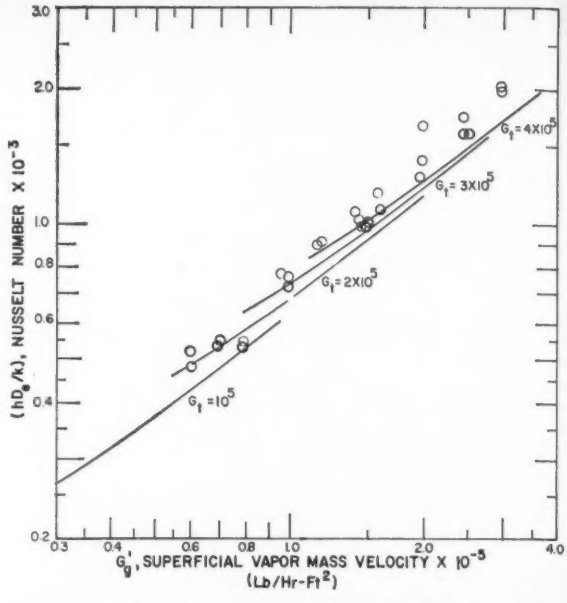

Figure 12—Correlation of the experimental data at 100 p.s.i.a. by the homogeneous model.

phases, the following relations can be derived for the homogeneous average linear velocity and the density of the homogeneous mixture:

$$u_{TP} = [x/\rho_g + (1-x)/\rho_L]G_t \quad \ldots\ldots(7)$$

$$1/\rho_{TP} = x/\rho_g + (1-x)/\rho_L \quad \ldots\ldots(8)$$

It is assumed that the viscosity of the two-phase dispersed core can be defined in a manner analogous to the density. McAdams and Woods[16] have used a similar definition in their two-phase pressure drop correlation:

$$1/\mu_{TP} = x/\mu_g + (1-x)/\mu_L \quad \ldots\ldots(9)$$

The correlating equation developed from this model is:

$$\frac{hD_e}{k_L} = 0.033\left(\frac{D_eG_t}{\mu_{TP}}\right)^{0.87}\left(\frac{C_p\mu}{k}\right)_L^{0.4} \quad (10)$$

Figures 11 and 12 show Equation (10) compared to the experimental data of the present investigation; the data are correlated to within ±15%. Each curve on the figures represents a range of qualities from 30% to 90% at some constant total mass velocity.

Equation (10) is strikingly similar to a correlation recently published by Groothuis and Hendal[17] for heat transfer to air-water mixtures flowing in a circular duct:

$$Nu = 0.029\ Re_2^{0.87}\ Pr^{1/3}(\mu_b/\mu_w)^{0.14} \quad \ldots\ldots(11)$$

where:

$$Re_2 = \frac{D\rho_g u_g'}{\mu_g} + \frac{D\rho_L u_L'}{\mu_L}$$

Equation (11) can be rewritten as follows:

$$\frac{hD_e}{k_L} = 0.029\left(\frac{DG_g'}{\mu_g} + \frac{DG_L'}{\mu_L}\right)^{0.87}\left(\frac{C_p\mu}{k}\right)^{1/3}\left(\frac{\mu_b}{\mu_w}\right)^{0.14} \quad \ldots\ldots(12)$$

but:

$$G_g' = xG_t, \text{ and } G_L' = (1-x)G_t$$

Therefore:

$$\frac{hD_e}{k_L} = 0.029\left(\frac{DG_t}{\mu_{TP}}\right)^{0.87}\left(\frac{C_p\mu}{k}\right)^{1/3}\left(\frac{\mu_b}{\mu_w}\right)^{0.14} \quad \ldots\ldots(13)$$

Equations (10) and (13) predict heat transfer coefficients within 10% of each other for the steam-water data taken in the present investigation. The agreement between the two equations is excellent, and indicates remarkable agreement between steam-water and air-water data for the wide range of flow rates, vapor mass fractions, and pressures studied. However, the highly empirical form of the equation does not attest to the theoretical correctness of the homogeneous model.

Pressure Drop Correlation

The pressure drop data taken with the rectangular duct of the present investigation were adequately correlated by the Lockhart-Martinelli correlation for isothermal two-phase flow[26], as shown in Figure 13. In preparing the experimental data for Figure 13, the single-phase friction factors needed were taken from a plot prepared from single-phase pressure drop measurements on water and superheated steam in the test section of this study; and the pressure drop due to acceleration was neglected. However, the acceleration pressure drop was estimated to be significant at higher heat fluxes and lower flow rates, where the quality increase in the test section was greatest. For most of the runs, because of the short heated length (6.0-in.) and short pressure drop length (4.0 to 11.0-in.), the acceleration pressure drop was usually less than 15% of the total pressure drop (frictional plus acceleration). The acceleration pressure drop was estimated by a momentum balance around the pressure drop section as suggested by Martinelli and Nelson[27], using both a separated-annular flow model and a homogeneous flow model.

Conclusions

The heat transfer coefficients for two-phase vapor-liquid flow at high vapor qualities can be predicted from equations similar to the Dittus-Boelter or Sieder-Tate equations for single-phase flow. Two models, a separated-annular flow model and a homogeneous model, have been used to develop such equations for two-phase flow. A slip ratio approach provided a correlation for much of the available steam-water data in the region of high vapor mass velocities:

$$\frac{hD_e}{k_L} = 0.060\left(\frac{\rho_L}{\rho_g}\right)^{0.28}\left(\frac{D_exG_t}{\mu_L}\right)^{0.87}\left(\frac{C_p\mu}{k}\right)_L^{0.4} \quad \ldots\ldots(4a)$$

Equation (4a) has been used to correlate the data of the present investigation to within ±15% and the data of Kvamme,

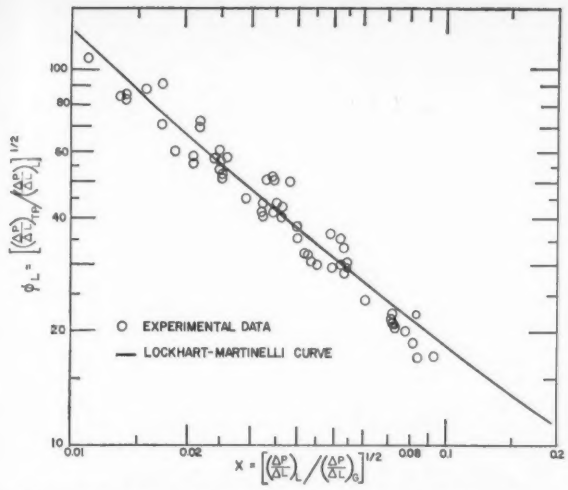

Figure 13—Experimental two-phase pressure drop data.

Yamazaki, and Dengler to ±20%. An alternate equation based on a void fraction approach (Equation 15) proved relatively unsatisfactory. A homogeneous model correlated the data to approximately ±15%, and the equation developed and given below was found to be in excellent agreement with the Groothuis-Hendal correlation for air-water flow:

$$\frac{hD_e}{k_L} = 0.033 \left(\frac{D_e G_t}{\mu_{TP}}\right)^{0.87} \left(\frac{C_p \mu}{k}\right)_L^{0.4} \quad \ldots\ldots\ldots\ldots (10)$$

The non-isothermal two-phase pressure drop data were found to be correlated adequately by the Lockhart-Martinelli correlation for isothermal flow.

Acknowledgement

The authors wish to express their appreciation to the Boeing Airplane Co. and to the Leeds and Northrup Co. for their financial aid during the course of this investigation.

Nomenclature

a = Dimensionless constant
A = Cross sectional area of tube or duct, ft.²
b = Dimensionless exponent
B = Pressure dependent constant in the equation, $h_{TP} = B(G_g')^{0.87}$
c = Dimensionless exponent
C_p = Heat capacity at constant pressure, B.t.u./lb.-°F.
D = Tube diameter, ft.
D_e = Equivalent diameter of a tube of duct, ft.
G = Mass velocity, lb./hr.-ft.²
G' = Superficial mass velocity, lb./hr.-ft.²
h = Heat transfer coefficient, B.t.u./hr.-ft.²-°F.
h_L = Heat transfer coefficient based on the total flow rate as liquid, B.t.u./hr.-ft.²-°F.
h_{TP} = Two-phase heat transfer coefficient, B.t.u./hr.-ft.²-°F.
k = Thermal Conductivity, B.t.u./hr.-ft.²-°F./ft.
L = Superficial mass velocity of liquid phase, lb./hr.-ft.² (In Baker correlation, Figure 7)
$R_L = A_L/A_t$ = Liquid void fraction, dimensionless
$R_g = A_g/A_t$ = Vapor void fraction, dimensionless
Re_2 = Reynolds number defined by Groothuis and Hendal, dimensionless
T = Temperature, °F.
ΔT_i = The minimum temperature difference required to initiate nucleate boiling, °F.
u = Average linear velocity of a phase, ft./sec.
u_{TP} = Average linear velocity of a homogeneous mixture, ft./sec.
V_L = Specific volume of the liquid phase, ft.³/lb.
w = Mass flow rate, lb./sec. or lb./hr.
x = Vapor mass fraction, dimensionless
$X_L = \left[\frac{(\Delta P/\Delta L)_{TP}}{(\Delta P/\Delta L)_L}\right]^{1/2}$ Martinelli's pressure drop parameter, dimensionless

Greek Letters

α = The slip ratio, dimensionless, equals u_g/u_L
λ = Baker's flow pattern parameter, dimensionless
μ = Viscosity, lb./hr.-ft.
μ_{TP} = Viscosity of a two-phase homogeneous mixture, lb./hr.-ft.
ρ = Density, lb./ft.³
ρ_{TP} = Density of a two-phase homogeneous mixture, lb./ft.³
$\phi_L = \left[\frac{(\Delta P/\Delta L)_{TP}}{(\Delta P/\Delta L)_L}\right]^{1/2}$ Martinelli's pressure drop parameter, dimensionless
ψ = Dimensionless flow pattern parameter used in Baker correlation

Subscripts

b = Refers to a physical property at the bulk temperature
g = Refers to the vapor phase
L = Refers to the liquid phase
s = Refers to saturation temperature
t = Refers to a total value
TP = Refers to two-phase flow or to a homogeneous two-phase property
w = Refers to a physical property at the wall temperature or to the wall temperature

References

(1) Baker, N., Touloukian, Y. S., Hawkins, G. H., Refrig. Eng., **61,** 986 (1953).
(2) Kirschbaum, E., Chem. Ing. Tech., **27,** 248-257 (1955).
(3) Kirschbaum, E., Ingenieur, **67,** 39-48 (1955).
(4) McAdams, W. H., Woods, W. K., and Heroman, L. C., Jr., Trans. Am. Soc. Mech. Engrs., **64,** 193 (1942).
(5) McAdams, W. H., Woods, W. K., and Bryan, R. L., Trans. Am. Soc. Mech. Engrs., **63,** 545-552 (1941).
(6) Witzig, W. F., Penney, G. W., and Cyphers, J. A., Refrig. Engr., **56,** 153 (1948).
(7) Dengler, C. E., Ph.D. Thesis, M.I.T. (1952).
(8) Dengler, C. E., and Addoms, J. N., Chem. Engr. Progr. Symposium Series, **52** (1956).
(9) Silvestri, M., Finzi, S., Roseo, L., Schiavon, M., and Zavattarelli, R., AEC Report, A/Conf. 15/P/1367 (June, 1958).
(10) Fikry, M. M., Ph.D. Thesis, Imp. Coll. Sci. Tech., London University (1953).
(11) Kvamme, A., M.S. Thesis, Univ. Minn., Minneapolis, Minnesota (1959).
(12) Rohsenow, W. M., and Clark, J. A., Trans. Am. Soc. Mech. Engrs., **73,** 609-616 (1951).
(13) Rohsenow, W. M., and Clark, J. A., AEC Reports, NP-3385 (Apr., 1951), NP-3443 (July, 1951), and NO-3461 (1951).
(14) Mumm, J. F., AEC Report, BNL-2446 (1955).
(15) Mumm, J. F., AEC Report, ANL-5276 (1954).
(16) Johnson, H. A., and Abou-Sabe, A. H., Trans. Am. Soc. Mech. Engrs., **74,** 977-983 (1952).
(17) Groothuis, H., and Hendal, W. P., Chem. Engr. Sci., **XI,** 212 (1959).
(18) Fried, L., Chem. Engr. Progr. Symposium Series, **50,** 47-51 (1954).
(19) McNelly, M. J., Ph.D. Thesis, Imp. Coll. Sci. Tech., London Univ. (1953).
(20) McNelly, M. J., J. Imp. Coll. Chem. Soc., **7,** 18 (1953).
(21) Guerrieri, S. A., and Talty, R. D., Chem. Engr. Progr. Symposium Series, **52** (1956).
(22) Smith, A. K., AEC Report, WIAP-M-38 (1954).
(23) Davis, E. J., Ph.D. Thesis, Univ. Wash., Seattle, Washington (1960).
(24) Baker, O., Oil Gas J., **53,** 185 (1954).
(25) Smith, G. M., and Hoe, Y. L., C.E. 174, Report No. DL 118/6, Dom. Lab., Dept. Sci. Ind. Res., New Zealand (1956).
(26) Lockhart, R. W., and Martinelli, R. C., Chem. Engr. Progr., **45,** 39 (1945).
(27) Martinelli, R. C., and Nelson, D. B., Trans. Am. Soc. Mech. Engrs., **70,** 695 (1948).

★ ★ ★

Fluid Friction and Heat Transfer in Cylindrical Pipes: Relationship between Lumped and Distributed Parameters[1]

JULIAN C. SMITH[2]

Physical phenomena may be described from the "microscopic" point of view, in terms of distributed parameters, or from the "macroscopic" viewpoint, using lumped parameters. Engineering correlations almost always involve lumped parameters. A lumped parameter is equal or proportional to some average value of the corresponding distributed parameter. Like any average quantity it gives no information regarding the form of the distribution. The use of lumped parameters therefore requires some assumptions, expressed or implied, regarding the form of the distribution within the system.

The characteristic lumped parameters used in problems of heat transfer and fluid friction are overall or average fluxes of heat energy or momentum, arbitrarily defined as described in this paper. Common dimensionless groups, such as f, N_{Re}, N_{St} and others are ratios of these energy or momentum fluxes. Such dimensionless groups, since they are ratios of lumped parameters, are themselves lumped parameters. In their definition, therefore, several assumptions regarding the distributions of velocity and temperature are implicit. When these assumptions are not valid, correction factors such as diffusivity ratios or length-to-length ratios are needed to allow for deviations from the distributions used for reference.

Using this approach the form of empirical equations becomes easy to predict. Dimensional analysis is not needed. In addition, this approach suggests that some accepted correlations may contain weaknesses not predicted by other methods.

Phenomena occurring in a physical system may be analyzed in terms of the behavior of the entire system, or in terms of events taking place at individual locations within the systems. From the internal or "microscopic" viewpoint transfer phenomena are described by differential equations relating the distributed parameters of the system. From the external or "macroscopic" point of view phenomena are described by lumped parameters which are characteristic of the whole system. Lumped parameters are usually restricted in their application to a particular system or to a small group of highly similar systems. However, they are of direct practical use, whereas distributed parameters ordinarily are not. Engineers are therefore much more often concerned with lumped parameters than with distributed parameters.

Full understanding of external behavior, however, demands a knowledge of internal events and of the relationship of one to the other. The transition from microscopic to macroscopic, from distributed parameters to lumped parameters, may be made in several ways. In a few cases the differential equations may be integrated analytically. Usually, however, this is not possible and the transition must be made by dimensional analysis of the pertinent differential equations[1] or by application of the principles of similitude[2,3]. Unfortunately these methods do not make it easy to visualize the underlying physical relationships, nor do they emphasize the assumptions involved. This paper suggests a way of interpreting some commonly used lumped parameters in terms of the corresponding distributed parameters, to bring out these relationships and assumptions.

Fluid Friction

The relationships between lumped and distributed parameters in a flowing fluid will be developed for a specific and rather simple case — that of steady fully developed flow of an incompressible fluid in a horizontal cylindrical pipe of constant cross section. In this system the relationships are reasonably clear. Many of the commonly used lumped parameters appear to have been originally defined with reference to this system, though they have since been applied — with more or less success — to other more complex situations. The concepts presented here may also be applied, with some modifications, to other physical systems.

Distributed Parameters. Consider the cross section of a horizontal cylindrical pipe of diameter D in which an incompressible fluid of density ρ is flowing in steady, fully developed flow. Assume for the present that viscosity μ is constant. Flow may be laminar or turbulent, but the bulk motion of the fluid is unidirectional and parallel to the pipe axis.

The distributed parameters are the fluid velocity u, pressure p, and shear stress τ, which is related to the transfer flux* of momentum j_M by the equation

$$j_M = -\tau g_c \qquad (1)$$

Since μ and ρ are assumed constant they need not be considered as distributed parameters. Furthermore, p is nearly constant across the pipe cross section. Only the velocity and the transfer flux of momentum vary significantly from point to point.

[1]*Manuscript received September 24, 1960; accepted March 6, 1961.*
[2]*School of Chemical and Metallurgical Engineering, College of Engineering, Cornell University, Ithaca, New York, U.S.A.*
Based on a paper presented at the 4th National Heat Transfer Conference, A.I.Ch.E.-A.S.M.E., Buffalo, New York, August, 1960.

*A "transfer flux" is the flux resulting from a potential gradient. A "convective flux" is the flux resulting from motion of the fluid.

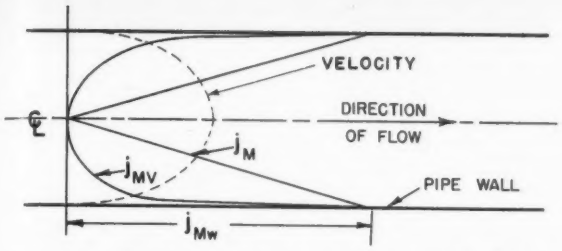

Figure 1 — Profiles of velocity and momentum flux in turbulent flow.

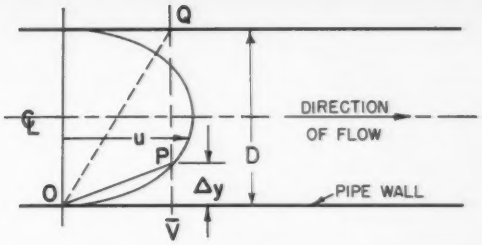

Figure 2—Definition of "average" velocity gradient.

The nature of this variation is indicated by the velocity and flux profiles in Figure 1. The velocity is zero at the pipe wall and a maximum at centerline. Flux j_M is zero at the centerline and rises to a maximum of j_{Mw} at the pipe wall. If p is constant across the cross section the variation of j_M is linear with radial distance from the pipe axis.

In general the total momentum flux is made up of two parts: the flux caused by viscous action, j_{MV}, and the flux caused by turbulent action, j_{MT}. When flow is laminar j_{MT} is zero and $j_{MV} = j_M$. With turbulent flow the flux by viscous action is normally a very small part of the total flux except near the pipe wall. Nevertheless it is not zero except at the pipe axis. It typically varies with radial distance as indicated in Figure 1. The viscous flux j_{MV} is therefore a distributed parameter, given by the equation

$$j_{MV} = -\mu \frac{du}{dy} \qquad (2)$$

Quantity j_{Mw}, a particular local value of a distributed parameter, is of especial interest to the engineer, because from it he can find the frictional pressure drop by the relation

$$\frac{dp}{dx} = -\frac{4\tau_w}{D} = \frac{4j_{Mw}}{Dg_c} \qquad (3)$$

where τ_w is the shear stress at the pipe wall. When the velocity profile may be calculated mathematically, as in the fully developed isothermal laminar flow of a Newtonian fluid in a cylindrical pipe, τ_w may be calculated directly from the relation

$$\tau_w g_c = \mu \left(\frac{du}{dy}\right)_w \qquad (4)$$

where $(du/dy)_w$ is the velocity gradient at the wall. This leads to the Hagen-Poiseuille equation for frictional pressure drop in laminar flow. When the shape of the velocity profile is unknown, however, $(du/dy)_w$ cannot be found directly, and empirical correlations using lumped parameters must be employed.

Lumped Parameters in Fluid Flow. An important group of lumped parameters is comprised of the overall convective fluxes; that is, the convective flux caused by the motion of all the fluid passing through a pipe cross section. First is the average velocity $\bar{V}$, which is the overall convective flux of volume (total volume flowing through a unit cross sectional area per unit time). Other overall convective fluxes are the products of $\bar{V}$ with "concentration". The overall convective flux of mass is $\bar{V}\rho$ or G, since ρ is the "concentration" of mass. The average "concentration" of momentum in an incompressible fluid equals $\rho\bar{V}$, and the overall convective flux of momentum, J_M, is given by*

$$J_M = \rho\bar{V}\bar{V} = \rho\bar{V}^2 \qquad (5)$$

*Rigorously $J_M = \rho\overline{u^2}$ or $\rho\bar{V}^2/\beta$, where β is a "convective flux correction factor." For fully developed laminar flow in a cylindrical pipe $\beta = 0.75$; for turbulent flow it is almost unity.

An important but loosely defined lumped parameter is the average value of j_{MV} in the pipe. As shown later, this average is not used without modification and thus for present purposes it may be defined in any convenient way so long as the same definition is always used. One such way is illustrated by Figure 2, which shows a typical velocity profile in the fluid. Point P is the point on the profile where the local velocity u equals $\bar{V}$. The slope of the line OP may be taken as a measure of the average velocity gradient in the fluid, and an "average" value of j_{MV} defined by

$$\bar{j}_{MV} \equiv -\mu \frac{\bar{V}}{\Delta y} \qquad (6)$$

where Δy is the radial distance from Point P to the pipe wall.

This "average", however, is valueless as a lumped parameter, for Δy is unknown unless the shape of the velocity profile is known. A useful lumped parameter, however, is formed by defining a "modified average" transfer flux, $\bar{j}'_{MV}$, by the equation

$$\bar{j}'_{MV} \equiv \bar{j}_{MV}\frac{\Delta y}{D} \equiv -\mu \frac{\bar{V}}{D} \qquad (7)$$

where D is the pipe diameter. Flux $\bar{j}'_{MV}$ may be regarded as the viscous flux of momentum corresponding to a "modified average" velocity gradient, which is the slope of line OQ in Figure 2.

Flux Ratios. Friction Factor. A secondary or derived lumped parameter is the ratio of the scalar magnitude of the transfer flux at the wall to that of the total convective flux of momentum. These flux vectors are shown in Figure 3. This ratio, by definition, is proportional to a friction factor. Specifically, the Fanning friction factor is defined by the equation

$$\frac{f}{2} \equiv -\frac{j_{Mw}}{J_M} \qquad (8)$$

Substitution from Equations (3) and (5) into Equation (8) gives the more familiar definition

$$f \equiv -\frac{dp}{dx}\cdot\frac{Dg_c}{2\rho\bar{V}^2} \qquad (9)$$

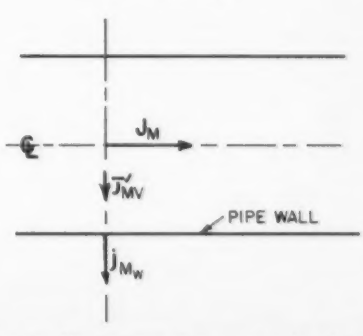

Figure 3—Momentum flux vectors in pipe flow.

Ratio of Convective Flux to "Modified Average" Transfer Flux. Pipe Reynolds Number. Another secondary lumped parameter is the pipe Reynolds number, which is proportional to the ratio of the total convective flux to the "modified average" transfer flux. It is defined by

$$N_{Re} \equiv -\frac{J_M}{\bar{j}'_{MV}} \quad \ldots\ldots\ldots\ldots\ldots\ldots\ldots\ldots (10)$$

Substitution from Equations (5) and (7) into Equation (10) gives

$$N_{Re} = \frac{\rho \bar{V}^2}{\mu \bar{V}/D} = \frac{D\bar{V}\rho}{\mu} \quad \ldots\ldots\ldots\ldots\ldots\ldots\ldots\ldots (11)$$

Note that $\bar{j}'_{MV}$ contains an average flux $\bar{j}_{MV}$ which, however defined, may be considered proportional to the true average momentum flux in the fluid, and also a term $\Delta y/D$ which depends on the shape of the velocity profile. Thus the significance of the Reynolds number depends on the shape of the velocity profile, even when all other characteristics of the system are held constant. As stated by McAdams[4]: "In two geometrically and *kinematically* similar systems, equal Reynolds numbers assure dynamic similarity." This assumption of kinematic similarity in the use of the Reynolds number is often overlooked.

Relationship between Friction Factor and Reynolds Number. The friction factor is proportional to the lumped parameter J_M and the local value of the distributed parameter, the transfer flux at the wall, j_{Mw}. The Reynolds number is also proportional to J_M and to another lumped parameter, $\bar{j}'_{MV}$, which is a "modified average" value of the viscous transfer flux of momentum. If it is assumed that the transfer flux at the wall depends on the "average" viscous transfer flux, then there must be a functional relationship between f and N_{Re}.

This relationship is simple in fully developed laminar flow, in which the transfer flux everywhere in the fluid is by viscous action and the velocity profile is parabolic. The conditions of kinematic similarity are met, and there can be no variation in the ratio $\Delta y/D$. Under these conditions the Reynolds number and friction factor are both proportional (though in different ways) to the same physical quantities. The one-to-one relationship between them is given by the simple equation

$$f = \frac{16}{N_{Re}} \quad \ldots\ldots\ldots\ldots\ldots\ldots\ldots\ldots (12)$$

When flow is turbulent the relationship is more tenuous, for f and N_{Re} are no longer measures of the same physical quantities. Unless the average viscous flux always bears the same relation to the total transfer flux, the Reynolds number cannot be uniquely related to the friction factor. This requirement is satisfied if kinematic similarity is assumed. Anything which changes the shape of the velocity profile, however, changes the friction factor even though the Reynolds number is held constant.

The roughness of the pipe wall has this effect and the conventional friction-factor plot contains lines for different pipe roughnesses. For a pipe of given roughness a unique relationship between f and N_{Re} is assumed; that is, it is assumed that at a given Reynolds number the shape of the velocity profile is always the same. This may or may not be a valid assumption. It is equivalent to assuming that the Prandtl mixing length is independent of molecular viscosity, or, alternatively, that the eddy diffusivity of momentum, at a given point in the fluid and at a given Reynolds number, bears a constant relationship to the molecular viscosity. If, for example, the fluid viscosity is increased but N_{Re} is held constant, by changing D or $\bar{V}$, then ϵ_M at corresponding points in the fluid must increase in exact proportion to the increase in ν. Otherwise the shape of the velocity profile would change and f would not bear the same relationship to N_{Re}.

Exactly proportional increase of the turbulent and molecular diffusivities at all points seems improbable, and some change in the shape of the velocity profile with molecular viscosity might be expected. The possibility of such a change is suggested in the analysis of turbulent-flow velocity profiles by Hanratty and Flint[5].

Published data do not indicate any variation of f with ν at a given N_{Re}. The range of viscosities studied, however, has been rather narrow. From a practical standpoint the variation, if it exists, is probably insignificant. Furthermore, it is difficult to study, for to create turbulence in a highly viscous liquid causes so much energy loss by viscous dissipation that the assumptions of isothermal flow and constant viscosity are no longer valid. On the other hand, as pointed out by White and Churchill[6], the fact that experimental measurements (especially of transfer rates) appear to agree with an integral equation is no assurance that the differential model which leads to the integral equation is valid. It seems probable that in the intermediate range of turbulence f and N_{Re} are not uniquely related for a pipe of given wall roughness, but existing data are not sufficient to indicate whether or not this is true.

Though unimportant in most practical engineering calculations, the question is conceptually important. Many empirical correlations, in heat transfer as well as fluid dynamics, may be regarded as using the fully developed velocity profile of a constant-viscosity fluid as a reference or standard. A given Reynolds number under these conditions is assumed to imply a velocity profile of a given shape. Actually there are two "standard" profiles: one for laminar and one for turbulent flow. Any variations in the shape of the turbulent-flow profile with molecular viscosity are ignored.

At high turbulence the viscous transfer flux is a negligible part of the total, and variations in its average value have no effect on the transfer flux at the pipe wall. Changes in $\bar{j}'_{MV}$ do not affect j_{Mw}. As shown by Equations (8) and (10), f and N_{Re} in this region are therefore measures of unrelated physical quantities and are independent of each other.

Effect of Temperature Variation. When the temperature of a Newtonian fluid varies across the pipe, the changes in viscosity alter the form of the velocity profile. This effect is illustrated in Figure 4. The velocity gradient at the pipe wall becomes steeper, and the momentum transfer flux at the wall becomes

$$j_{Mw} = -\mu_w \left(\frac{du}{dy}\right)_w \quad \ldots\ldots\ldots\ldots\ldots\ldots\ldots\ldots (13)$$

This change is reflected in the friction factor. The Reynolds number, however, does not change, except that the "modified average" transfer flux now involves still another lumped parameter, the bulk average viscosity $\bar{\mu}$, defined as the viscosity at the bulk average temperature, $\bar{T}$. Actually the viscosity is now a distributed parameter, varying in a way dictated by the variation in fluid temperature. The Reynolds number, therefore, is less of a true measure of conditions in the fluid than with isothermal flow, for it makes no allowance for changes in either the velocity profile or the temperature profile. Furthermore, if $\bar{T}$ changes appreciably with distance along the pipe, μ must be "lumped" along the pipe as well as across it. N_{Re} does not take into account the form of the temperature change along the pipe: it remains a single "average" value.

Since f changes while N_{Re} does not, a correction factor must be included in the equation relating them, to restore kinematic similarity. This Sieder-Tate correction factor is 1.1 $(\bar{\mu}/\mu_w)^{0.25}$ for laminar flow and $(\bar{\mu}/\mu_w)^{0.14}$ for turbulent flow[7]. It is assumed, in applying this factor, that the change in velocity profile is always the same function of this ratio of a lumped parameter $\bar{\mu}$ to the local value of the distributed parameter μ_w. This is unlikely, especially for turbulent flow, and probably the correction factor should also depend on the absolute magnitude of the fluid viscosity. Again, however, the effect would be difficult to establish experimentally.

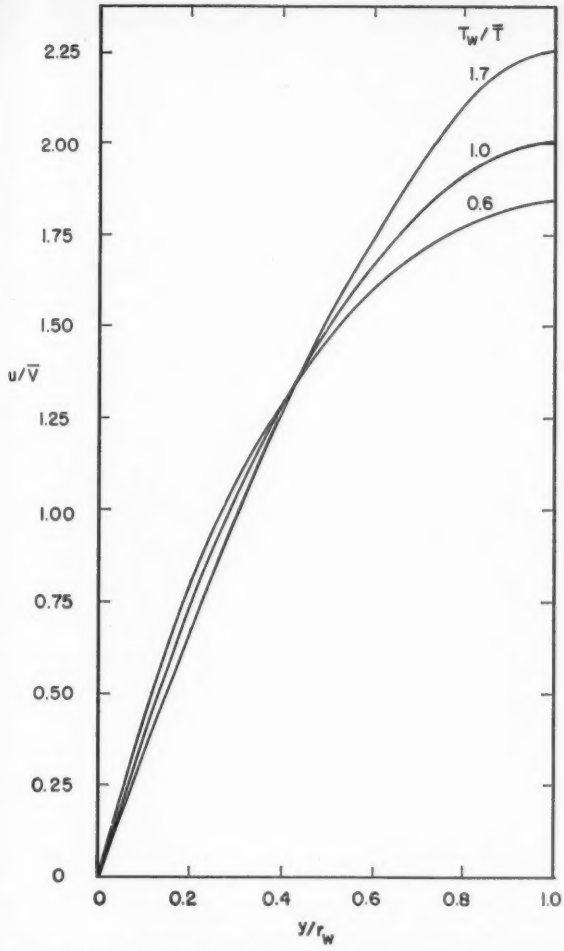

Figure 4 — Effect of temperature gradients on velocity profile.

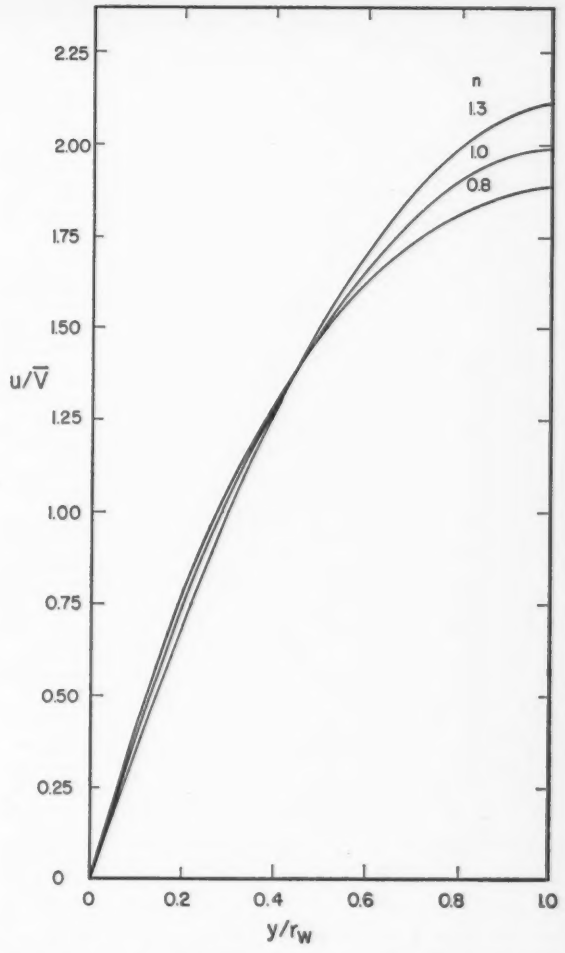

Figure 5 — Velocity profiles in laminar flow of non-Newtonian fluids.

Isothermal Flow of a Non-Newtonian Fluid. In the flow of an incompressible non-Newtonian fluid the apparent viscosity varies across the pipe, since it is a function of the velocity gradient. The shape of the velocity profile therefore differs from that in a Newtonian fluid, as shown in Figure 5. The viscous transfer flux of momentum, for many non-Newtonian fluids, is given by an empirical equation of the form

$$j_{MV} = -K\left(\frac{du}{dy}\right)^n \quad \ldots\ldots\ldots\ldots\ldots\ldots (14)$$

where K and n are constants. The momentum flux at the wall, i_{Mw}, becomes $-K(du/dy)_w^n$, and the "modified average" viscous flux is

$$\bar{j}'_{MV} = K\left(\frac{\bar{V}}{\Delta y}\right)^n\left(\frac{\Delta y}{D}\right)^n = -K\left(\frac{\bar{V}}{D}\right)^n \quad \ldots\ldots\ldots (15)$$

where $\bar{V}/\Delta y$ is the average velocity gradient in the fluid. The overall convective flux, J_M, remains equal to $\rho\bar{V}^2$. The Reynolds number, then, by substitution in Equation (10), is

$$N_{Re} = -\frac{J_M}{\bar{j}'_{MV}} = \frac{D^n\bar{V}^{2-n}\rho}{K} \quad \ldots\ldots\ldots\ldots\ldots (16)$$

This is the Reynolds number $N_{Re}{}^{\circ}$ used by Dodge and Metzner[8]. When flow is laminar the relation between f and N_{Re} for a non-Newtonian fluid is

$$f = \frac{16}{N_{Re}}\,2^{n-3}\left(3+\frac{1}{n}\right)^n = \frac{16}{N_{Re}}\,\phi(n) \quad \ldots\ldots\ldots\ldots (17)$$

Function $\phi(n)$ is analogous to the Sieder-Tate correction factor for the non-isothermal flow of a Newtonian fluid. It restores kinematic similarity by "correcting" the shape of the velocity profile to that obtained in the fully developed laminar flow of a Newtonian fluid.

With turbulent flow the shape of the velocity profile also depends on n, although presumably the "correction factor" would not be the same as that for laminar flow. An equation relating f, N_{Re}, and n has been proposed by Dodge and Metzner[8]. They assumed that the shape of the profile is independent of K in the turbulent region; as with a Newtonian fluid (for which $K = \mu$) it seems probable that this is not quite true.

Heat Transfer

In heat transfer by conduction thermal energy is transferred by virtue of temperature gradient. Since temperature is a scalar the heat fluxes are simple vectors, not tensors as are momentum fluxes (stresses) in fluid dynamics. The situation in heat transfer thus appears simpler, at first glance, than in fluid flow, and the lumped parameters might appear to involve fewer assumptions. Actually the reverse is true. In heat transfer to or from a fluid flowing in a pipe, the transfer flux at wall is nearly always more dependent on the fluid motion, especially in turbulent flow, than on thermal conduction. Heat transfer

is thus influenced by two superimposed and interrelated fields: temperature gradient vectors and the stress tensors.

Distributed Parameters. The important distributed parameters are the temperature and specific enthalpy of the fluid, the thermal diffusivity, and the transfer flux of thermal energy.

Consider the fluid passing through a cross section of the pipe. Let the temperature at the pipe wall, T_w, be used as the datum for calculating the specific enthalpy H. Assume that there is no phase change in the fluid and that its heat capacity c_p is constant. Then

$$H = \int_{T_w}^{T} c_p dT = c_p(T - T_w) \quad \ldots\ldots(18)$$

The enthalpy per unit volume of fluid — the "concentration" of enthalpy — is ρH or $\rho c_p(T - T_w)$. The total transfer flux of thermal energy, j_H, is related to the gradient of this concentration when ρ is constant by

$$j_H = -(\alpha + \epsilon_H)\frac{d(\rho H)}{dy} = -(\alpha + \epsilon_H)\rho c_p \frac{dT}{dy} \quad \ldots\ldots(19)$$

This flux varies from zero at the pipe axis to a maximum value, j_{Hw}, at the pipe wall. If all the transfer is by conduction, ϵ_H is zero and at all points

$$j_{HV} = -\alpha\rho c_p \frac{dT}{dy} = -k\frac{dT}{dy} \quad \ldots\ldots(20)$$

The heat flux at the wall is related to the individual heat transfer coefficient h by the equation

$$j_{Hw} = h(\bar{T} - T_w) \quad \ldots\ldots(21)$$

Lumped Parameters. An important lumped parameter is the average or "mixing-cup" temperature $\bar{T}$, which is related to the average enthalpy $\bar{H}$ of all the fluid in the cross section by the equation

$$\bar{H} = c_p(\bar{T} - T_w) \quad \ldots\ldots(22)$$

The average concentration of enthalpy is $\rho\bar{H}$, and the overall convective flux of enthalpy, J_H, is*

$$J_H = \bar{V}\rho\bar{H} = \bar{V}\rho c_p(\bar{T} - T_w) \quad \ldots\ldots(23)$$

The "modified average" transfer flux of thermal energy, $\bar{j}'_{HV}$, is defined in the same way as the corresponding momentum flux. It is

$$\bar{j}'_{HV} = -k\frac{\Delta T}{\Delta y}\cdot\frac{\Delta y}{D} = -k\frac{\bar{T} - T_w}{D} \quad \ldots\ldots(24)$$

where $(\bar{T} - T_w)/\Delta y$ is the "average" temperature gradient in the fluid indicated in Figure 6.

Flux Ratios. Dimensionless Groups. The ratios of the scalar magnitudes of the several heat fluxes, as thus defined, are proportional to common dimensionless groups. Thus from Equations (21) and (23)

$$\frac{j_{Hw}}{J_H} = \frac{h(\bar{T} - T_w)}{\bar{V}\rho c_p(\bar{T} - T_w)} = \frac{h}{c_p G} = N_{St} \quad \ldots\ldots(25)$$

From Equations (23) and (24)

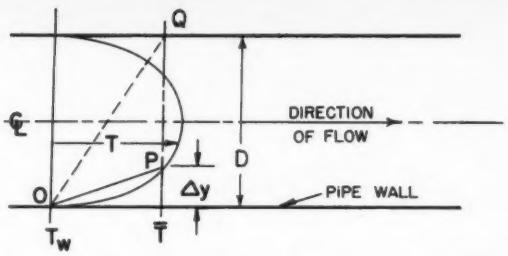

Figure 6—Definition of "average" temperature gradient.

$$-\frac{J_H}{\bar{j}'_{HV}} = \frac{\bar{V}\rho c_p(\bar{T} - T_w)}{k(\bar{T} - T_w)/D} = \frac{DGc_p}{k} = N_{Pe} \quad \ldots\ldots(26)$$

Also,

$$-\frac{j_{Hw}}{\bar{j}'_{HV}} = \frac{h(\bar{T} - T_w)}{k(\bar{T} - T_w)/D} = \frac{hD}{k} = N_{Nu} \quad \ldots\ldots(27)$$

Relationships among Dimensionless Groups. The lumped parameters N_{St} and N_{Pe} are related in the same way as the corresponding parameters for fluid friction, f and N_{Re}. When the thermal transfer flux is essentially all by molecular action, j_{Hw} and $\bar{j}'_{HV}$ are uniquely related and a unique relationship should exist between N_{St} and N_{Pe}, or, since $N_{Nu} = N_{St}\,N_{Pe}$, between N_{Nu} and N_{Pe}. This assumes that the shape of the temperature profile is "fully developed" and is always the same at a fixed value of N_{Pe}. It is apparently a valid assumption for heat transfer to liquid metals, as shown by the empirical equation of Lyon[9]

$$N_{Nu} = 7 + 0.025\,N_{Pe}^{0.8} \quad \ldots\ldots(28)$$

When flow is laminar the heat transfer is essentially all by conduction, but the temperature profile continuously changes with length and never becomes fully developed. The relationship is then of the form

$$N_{Nu} = \phi(N_{Gz}) = \phi(N_{Pe})\left(\frac{\pi D}{4L}\right) \quad \ldots\ldots(29)$$

where N_{Gz} is the Graetz number, which equals $(\pi D/4L)\,N_{Pe}$. The quantity $\pi D/4L$ may be regarded as a correction factor, lumped over the pipe length, which allows for the difference between the changing temperature profile and the steady "fully developed" profile used in the definition of N_{Pe}.

With turbulent flow the temperature profile may be considered fully developed, provided the temperature change along the pipe is small. The shape of the profile, however, is dictated not only by the thermal conductivity of the fluid but also by the fluid motion, and is therefore influenced by the molecular and eddy viscosities. Distance Δy, which may be considered constant for fully developed isothermal fluid flow, is no longer constant. For this reason N_{Pe}, which contains this variable Δy implicit in its definition, is not as generally useful as N_{Re}.

If the temperature and velocity profiles, by chance, have the same shape, so that at any point $u/\bar{V} = T/\bar{T}$, the distance Δy in the definition of N_{Re} and N_{Pe} (Equations (7), (10), (24) and (26)) is the same for both dimensionless groups. The relationships between the overall convective flux and the transfer flux at the pipe wall are also the same. This is to say

$$\frac{j_{Hw}}{J_H} = \frac{j_{Mw}}{J_M} \quad \ldots\ldots(30)$$

This means, from Equations (8) and (25), that

$$N_{St} = f/2 \quad \ldots\ldots(31)$$

Equation (31) is a statement of the Reynolds analogy, and is approximately true for heat transfer to gases.

*As with the convective flux of momentum, this is not quite true. The overall convective flux of enthalpy is rigorously equal to $\rho c_p\overline{V(T - T_w)}$ or $\rho c_p\bar{V}(\bar{T} - T_w)/\beta$, where β is the "convective flux correction factor".

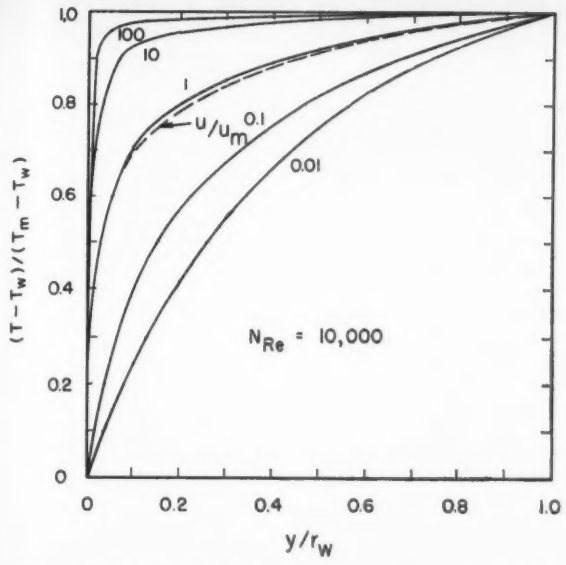

Figure 7—Relationship of N_{Pr} to temperature and velocity profiles.

With most fluids, however, the profiles of temperature and velocity do not have the same shape. Correlations among the dimensionless groups may then be considered to use the fully developed constant-viscosity velocity profile as a standard to which the temperature profiles are "corrected." It is assumed that at a given N_{Re} the velocity profile always has the same shape.

The shape of the temperature profile is "corrected" to that of the velocity profile by using the ratio of the molecular diffusivities of momentum and thermal energy. That is to say, it is assumed that

$$\frac{\Delta y_M}{\Delta y_H} = \phi\left(\frac{\nu}{\alpha}\right) \quad \ldots\ldots\ldots\ldots\ldots\ldots\ldots\ldots (32)$$

Ratio ν/α is the Prandtl number, N_{Pr}. The assumption stated by Equation (32) is somewhat dubious, since ν and α refer only to molecular transfer and ignore any effect of turbulence. Furthermore, ν and α as normally used are themselves lumped parameters, the "bulk average" values for the fluid, and do not consider how the distributed values actually vary across the cross section.

As shown by experiment, however, the shape of the temperature profile varies significantly with N_{Pr}[10]. This is illustrated in Figure 7. Possibly the effect of other variables is too small to establish experimentally. Assuming Equation (32) is valid, Equation (31) is modified to

$$N_{St}\,\psi(N_{Pr}) = f/2 \quad \ldots\ldots\ldots\ldots\ldots\ldots\ldots\ldots (33)$$

For turbulent flow, as found empirically, $\psi(N_{Pr}) = N_{Pr}^{2/3}$, and

$$N_{St}\,N_{Pr}^{2/3} = f/2 \quad \ldots\ldots\ldots\ldots\ldots\ldots\ldots\ldots (34)$$

Since the temperature is not constant the shape of the velocity profile must also be "corrected" to allow for changes from the constant-viscosity profile by using the ratio $\bar{\mu}/\mu_w$, and

$$N_{St}\,N_{Pr}^{2/3} = \frac{f}{2}\left(\frac{\bar{\mu}}{\mu_w}\right)^{0.14}$$

or

$$N_{St}\,N_{Pr}^{2/3}\left(\frac{\mu_w}{\bar{\mu}}\right)^{0.14} = j_C = \frac{f}{2} \quad \ldots\ldots\ldots\ldots\ldots\ldots\ldots\ldots (35)$$

where j_C is the Colburn "j factor". Equation (35) is a statement of the Colburn analogy. Substitution of empirical relations between f and N_{Re} gives equations relating h and N_{Re}.

The form of empirical correlations for turbulent-flow heat transfer may also be established as follows. As previously discussed, if the shape of the temperature profile depended only on N_{Pr}, then N_{Nu} would be a unique function of N_{Pe}. Since this is not true, it is necessary to "correct" the shape of the temperature profile to that of the reference velocity profile. The correction factor is assumed to be a function of N_{Pr}. Then

$$N_{Nu} = \chi(N_{Pe}, N_{Pr}) \quad \ldots\ldots\ldots\ldots\ldots\ldots\ldots\ldots (36)$$

Since $N_{Pe} = N_{Re}\,N_{Pr}$, Equation (36) becomes

$$N_{Nu} = \chi(N_{Re}, N_{Pr}) \quad \ldots\ldots\ldots\ldots\ldots\ldots\ldots\ldots (37)$$

A recent empirical equation in this form is that of Friend and Metzner[11]

$$N_{Nu} = 0.022\,N_{Re}^{0.80}\,N_{Pr}^{0.42} \quad \ldots\ldots\ldots\ldots\ldots\ldots\ldots\ldots (38)$$

Summary and Conclusions

(1) Heat transfer and fluid friction, even in fully developed flow in a cylindrical pipe, involve complex interrelationships among a number of distributed parameters. Engineering correlations are almost always based on lumped parameters. Lumped and distributed parameters for simple cases of heat transfer and fluid friction in a cylindrical pipe are listed in Table 1.

(2) A lumped parameter is equal or proportional to some average value of the corresponding distributed parameter, and like any average gives no indication of the form of the distribution. If a given lumped parameter depends on the form of the distribution, some assumption as to the form of the distribution must be made in defining the lumped parameter.

(3) Common dimensionless groups — f, N_{Re}, N_{Pr}, N_{St}, etc. — are lumped parameters. They may be regarded as being proportional to the ratios of the scalar magnitudes of arbitrarily defined flux vectors. N_{Pr} for heat transfer is the analogue of N_{Re} for momentum transfer.

(4) N_{Re} implicitly depends on the form of the velocity distribution, and its use implies kinematic similarity. N_{Pe} and N_{Nu} similarly depend on the form of the temperature distribution.

(5) When kinematic similarity is assumed, consideration of the flux vectors leads directly to the form of empirical equations relating f and N_{Re}. When the shape of the temperature profile is assumed constant, the same reasoning leads to the form of equations relating N_{St} and N_{Pe}.

TABLE 1

LUMPED AND DISTRIBUTED PARAMETERS IN SIMPLE CASES OF FLUID FRICTION AND HEAT TRANSFER

Assumed Constant	Distributed Parameters	Important Local Values	Lumped Parameters
A. Flow of constant-viscosity incompressible fluid.			
ν ρ	u j_M	j_{Mw}	$\bar{\Gamma}$ $G = \bar{\Gamma}\rho$ $J_M = \bar{\Gamma}G = \rho\bar{\Gamma}^2$ $\bar{j}_{MV}$ $f = -2j_{Mw}/J_M$ $N_{Re} = -J_M/\bar{j}_{MV}$
B. Heat transfer in forced convection of incompressible constant-viscosity fluid.			
ν ρ α $N_{Pr} = \nu/\alpha$	T H j_H j_{HV}	j_{Hw}	$\bar{T}$ $\bar{H} = \rho c_p(\bar{T} - T_w)$ $J_H = \bar{\Gamma}\rho\bar{H} = \bar{\Gamma}\rho c_p(\bar{T} - T_w)$ $\bar{j}_{HV}$ $N_{St} = j_{Hw}/J_H$ $N_{Pe} = -J_H/\bar{j}_{HV}$ $N_{Nu} = -j_{Hw}/\bar{j}_{HV}$

(6) For situations in which the shape of the velocity profile or temperature profile cannot be considered constant, empirical correlations may be considered as being based on standard or reference profiles to which the actual profiles are "corrected".

(7) The standard profiles are the velocity profiles found with steady fully developed flow of a constant-viscosity fluid. Two standards are used: one for laminar and one for turbulent flow. It is assumed that in turbulent flow the shape of the velocity profile depends only on N_{Re}, although this assumption appears somewhat dubious.

(8) The "correction factor" which restores kinematic similarity in the non-isothermal flow of a Newtonian fluid is the Sieder-Tate correction factor. That for the isothermal laminar flow of a non-Newtonian fluid is $\phi(n)$.

(9) The Prandtl number performs a similar function in equations for turbulent heat transfer, "correcting" the shape of the temperature profile to that of the reference velocity profile.

(10) Expressions for heat transfer in laminar flow involve N_{Gz}, which may be regarded as the product of N_{Pe} with a "correction factor", $\pi D/4L$. This factor allows for the difference between the shape of the developing temperature profile and that of the reference profile.

(11) Although adequate for most engineering purposes, some "correction factors" appear to be incomplete measures of changes in profile shape. Empirical correlations should perhaps contain other functions involving fluid properties, but such secondary "correction factors" would be difficult to establish experimentally. More desirable would be better analytical solutions to problems in turbulent transfer. Traditional empirical correlations are based on oversimplifications of highly complex phenomena, and are therefore applicable only to relatively simple systems. This is not to deny their usefulness nor their importance, for they provide solutions to problems which can be solved in no other way. In the longer view, however, they are merely useful expedients which should be discarded when more powerful generalization, have been developed. They are but way-stations along the road to a better understanding of turbulent transfer processes.

Nomenclature

c_p = Heat capacity at constant pressure, B.t.u./lb., °F.
D = Pipe diameter, ft.
f = Fanning friction factor
G = Mass velocity, lb./sec., ft.²
g_c = Newton's-law conversion factor, lb.-ft./lb.$_f$-sec.²
H = Specific enthalpy above T_w as datum, B.t.u./lb.; $\bar{H}$, bulk average value
h = Individual heat transfer coefficient, B.t.u./hr., ft.², °F.
J = Overall convective flux; J_H, flux of enthalpy, B.t.u./sec., ft.²; J_M, flux of momentum, lb./ft., sec.²
j = Transfer flux; j_V, by molecular action; j_H, flux of thermal energy, B.t.u./sec., ft.²; j'_{HV} "modified average" flux of thermal energy, defined by Equation (24); j_M, momentum flux, lb./ft., sec.²; $\bar{j}_{MV}$, "average" momentum flux, defined by Equation (6); $\bar{j}'_{MV}$, "modified average" momentum flux, defined by Equation (7).
j_C = Colburn "j factor"
K = Coefficient of non-Newtonian fluid, (Equation (14))
k = Thermal conductivity, B.t.u./sec., ft.², (°F./ft.)
L = Pipe length, ft.
N_{Gz} = Graetz number
N_{Nu} = Nusselt number
N_{Pe} = Peclet number
N_{Pr} = Prandtl number
N_{Re} = Reynolds number
N_{St} = Stanton number
n = Coefficient of non-Newtonian fluid, (Equation (14))
p = Pressure, lb.$_f$/ft.²
T = Temperature, °F.; $\bar{T}$, bulk average temperature
u = Local fluid velocity, ft./sec.
x = Axial distance
y = Radial distance

Greek Letters

α = Thermal diffusivity, ft.²/sec.
β = Convective flux correction factor
Δy = Distance used in definition of $\bar{j}'_{MV}$ (Equation (6))
ϵ = Eddy diffusivity, ft.²/sec.; ϵ_H, of thermal energy; ϵ_M of momentum
μ = Absolute viscosity, lb./ft., sec.; $\bar{\mu}$, bulk average viscosity
ν = Kinematic viscosity, ft.²/sec.
ρ = Density, lb./ft.³
τ = Shear stress, lb.$_f$/ft.²
ϕ, χ, ψ = "Functions of"

Subscripts

M = For momentum transfer
H = For heat transfer
T = By turbulent action
V = By molecular or viscous action
w = Value at pipe wall

References

(1) Klinkenberg, A., and Mooy, H. H., Chem. Eng. Progr., **44,** 17 (1948).
(2) Ipsen, D. C., "Units, Dimensions and Dimensionless Numbers", McGraw-Hill Book Co., Inc., New York, 1960.
(3) McAdams, W. H., "Heat Transmission", 3rd ed., p. 129 ff, McGraw-Hill Book Co., Inc., New York, 1954.
(4) Ibid., p. 135.
(5) Hanratty, T. J., and Flint, D. L., A.I.Ch.E. Journal, **4,** 132 (1958).
(6) White, R. A., and Churchill, S. W., A.I.Ch.E. Journal, **5,** 354 (1959).
(7) McCabe, W. L., and Smith, J. C., "Unit Operations of Chemical Engineering", p. 73, McGraw-Hill Book Co., Inc., New York, 1956.
(8) Dodge, D. W., and Metzner, A. B., A.I.Ch.E. Journal, **5,** 189 (1959).
(9) Lyon, R. H., Chem. Eng. Progr., **47,** 75 (1951).
(10) Martinelli, R. C., Trans. ASME, **69,** 947 (1947).
(11) Friend, W. L., and Metzner, A. B., A.I.Ch.E. Journal, **4,** 393 (1958).

★ ★ ★

Fundamental Aspects of Solids-Gas Flow

Part VI: Multiparticle Behavior in Turbulent Fluids[1]

L. B. TOROBIN[2] and W. H. GAUVIN[3]

At Reynolds numbers approaching unity the particles in a solids-gas system acquire a turbulent motion in response to the turbulence of the ambient fluid. This regime is of particular importance and a discussion of recent theoretical and experimental attempts to describe it is presented. The reaction of the fluid phase to the presence of the particles is equally important. The extent to which the mean and turbulent properties of the fluid motion are affected by the presence of the solids phase is governed by the particle concentration and the fluid and solids Reynolds numbers. The experimental evidence is as yet inconclusive owing to the difficulty of obtaining reliable data. The theoretical attack is similarly made difficult by the need to employ mixed Eulerian and Lagrangian coordinates. A discussion of electrostatic charging phenomena has also been included and it shows that in some systems it exerts an over-riding influence on the particle motion and momentum transfer.

The various aspects of solids-gas flow which have been discussed in the five previous articles of this series[1] were restricted to the behavior of single particles. Consideration will now be given to multiparticle systems in turbulent fluids in which the inertia of the fluid may be sufficiently large or the particles sufficiently small for the solids to have a turbulent motion of their own. This subject is one of great theoretical and analytical complexity and many of its aspects are still in a very preliminary stage of development. The experimental approach is equally difficult and precise methods of measurement of the physical properties of multiparticle systems are often lacking. The discussion which follows reflects the uncertainties of the theoretical knowledge as well as the paucity of reliable data needed for a sound statistical characterization of the system.

Consideration will first be given to the mechanism of entrainment of solid particles in horizontal streams, and their effect on the fluid velocity profile. This will be followed by a review of the few studies, both theoretical and experimental, which are concerned with the turbulent motion of a small particle in a turbulent fluid. No attempt will be made at this stage to deal with the momentum transfer aspects of dilute-phase pneumatic conveying, as this topic will be treated in a subsequent article. A brief discussion of electrostatic charging phenomena has also been included because of its related interest.

[1]*Manuscript received November 2, 1960; accepted March 25, 1961.*
[2]*Esso Research and Engineering Company, Linden, N.J., U.S.A.*
[3]*McGill University and Pulp and Paper Research Institute of Canada, Montreal, Que. Contribution from McGill University and Pulp and Paper Research Institute of Canada.*

X—MULTIPARTICLE BEHAVIOUR IN HORIZONTAL TURBULENT STREAMS

Phenomena occurring in sediment-carrying horizontal streams should be of direct interest to workers dealing with dilute phase solids-gas flow. Vanoni[2] stressed that although most of the mechanics of the transportation of sediment was investigated in connection with the control and development of natural streams, it is directly applicable to the flow of solids-gas mixtures in industry. The underlying mechanisms of these two fields have much in common, but sediment transport theory has generally been ignored in investigations of solids-gas flow.

When a bed of solids is submerged in a horizontal fluid stream of gradually increasing velocity, four succeeding types of behavior may be discerned: (a) initially there is no solids motion; then (b) individual grains in isolated random areas of the bed begin a rolling or sliding intermittent motion in short steps; (c) some grains are actually lifted into the stream and they eventually settle out, colliding with particles which are thus dislodged from the bed and are in turn carried into the stream; this phenomenon which is referred to as *saltation* results in the transport of the material along the bed mainly in the form of continuously changing ripples so that saltation is best described by statistical methods; (d) in the final stage the grains are lifted and suspended by the cross-component of the fluid turbulence — their trajectories increasing in length as the fluid velocity increases. The critical fluid shear stress on the bed surface that will just start particle motion is designated by the symbol τ_c. The solids movement in the horizontal solids-gas systems will exhibit a similar behavior if the particle concentration exceeds a characteristic value.

Fluid Velocity Required to Initiate Motion

White[3] investigated the equilibrium of grains on the bed of a stream, and found that for spherical particles, fluid turbulence may reduce the required value of τ_c by more than 40%. Rubey[4] in an analysis similar to that of White, found the minimum drag required to be given by:

$$R_{min} = C_D' d^2 \rho_c U_c^2/2 \quad \ldots\ldots\ldots\ldots\ldots\ldots (1)$$

where U_c is the fluid velocity at the grain and is less than the average stream velocity. This expression is similar to the general resistance equation in which C_D' would correspond to the drag coefficient. This relationship was not successful for beds made up of fine grains, however.

Vanoni[5] showed that since τ_c is approximately proportional to U_c^2 it would account for the rule of thumb long used by geologists that the mass of the largest particles that can be moved by a stream is proportional to the sixth power of the stream velocity.

Shields[6] recognized that the fluid velocity at the grains was lower than the stream velocity, and he applied the Karman-

Nikuradse statement of the velocity distribution in a fluid stream to obtain the relationship:

$$\tau_c/(\rho - \rho_o)\, gd = \Phi(U_\tau d/\nu) \quad \ldots\ldots (2)$$

Shields found that τ_c tends towards a minimum when the particle Reynolds number, defined by $(U_\tau d/\nu)$ was equal to 10 while White[3] found that it was smaller for $(U_\tau d/\nu) > 3.5$ than for $(U_\tau d/\nu) < 2$.

Bed Load Transport

"Bed Load" transportation theories have been presented to enable the calculation of the total sediment carried on or near the bottom of an horizontal stream. DuBoys[7] proposed the expression:

$$w = B\, \tau_o(\tau_o - \tau_c) \quad \ldots\ldots (3)$$

where w = mass flow rate of solids carried per unit width;
B = sediment parameter.

Values of B and τ_c have been correlated and listed by Brown[8] but the applicability of the expression has been found to be limited.

Einstein[9], on the other hand, disputed this concept of a critical hydraulic quantity, and felt that the phenomenon is one that involves probability. He assumed the particles to migrate in jumps of length L proportional to the particle diameter. The number of particles migrating would be proportional to the number of grains in the surface layer and also to the probability that the local drag on the particles is sufficient to lift them into the stream.

Einstein defined two dimensionless parameters Φ_p and Φ_f which reflected the energy of particle and fluid movement respectively. These were given as:

$$\Phi_p = (w/\rho)\,[\rho_o/(\rho - \rho_o)]^{1/2}/[g_c d^3]^{1/2} \quad \ldots\ldots (4)$$

and

$$\Phi_f = [(\rho - \rho_o)/\rho_o]\,[d/a'S] \quad \ldots\ldots (5)$$

and Einstein was able to show an experimental and analytical interrelationship between the two functions in support of his model. Einstein found that his relationship seemed to account for observations obtained from a system involving sand with a wide particle-size distribution. Vanoni[2], however, found it to be inaccurate when applied to systems of uniformly-sized particles.

Kalinske[10,11] proposed similar expressions, which gave fair agreement for systems of the latter type, of the form:

$$w = [(\rho d)\sqrt{\tau_o/\rho_o}]\,[\Phi_k \tau_c/\tau_o] \quad \ldots\ldots (6)$$

where Φ_k is a function which is related to the fluid turbulence.

Solids Concentration Gradients in Horizontal Fluid Flow

The solid phase of a horizontally-flowing solid-fluid system will often exhibit a concentration gradient which in the case of solids-gas flow may determine the flow characteristics and energy requirements of the system. An equation for the concentration of sedimenting particles in a still fluid was proposed by Schmidt in 1925[12] and re-stated by O'Brien[13,14] in 1933. It has the form:

$$cv_t + D_p(dc/dy) = 0 \quad \ldots\ldots (7)$$

where D_p = a diffusion coefficient;
y = the vertical distance from the lower boundary of the system;
c = the concentration of solids;
v_t = the free-fall velocity of the particles.

v_t would be more strictly defined as the fall velocity of the particles in a system whose turbulence parameters are equivalent to those existing in the system to which the expression is being applied. This statement of dynamic equilibrium balances the settling rate of cv_t, with $D_p(dc/dy)$ the upward rate of movement of the solids due to the turbulent fluctuations of the fluid. D_p was found experimentally to be a function of y, and it was measured by Kalinske[11].

Rouse[15] derived an expression for the solids distribution in the following manner:

By definition for a solids-free flow

$$\tau = \rho_o D_f(dU/dy) \quad \ldots\ldots (8)$$

He then introduced two simplifying assumptions by saying that $D_f = D_p$ and by assuming τ to be a linear function of y, i.e.

$$\tau/\tau_o = 1 - (y/h) \quad \ldots\ldots (9)$$

From the von Karman Law

$$dU/dy = [\sqrt{\tau_o/\rho_o}]/ky = U_\tau/ky \quad \ldots\ldots (10)$$

so that

$$D_f = ky\, U_\tau[1 - (y/h)] \quad \ldots\ldots (11)$$

By substituting 7 into 11 and integrating, Rouse obtained:

$$c/c_1 = \left[\left(\frac{h - y}{y}\right)\left(\frac{y_1}{h - y_1}\right)\right]^{a_1} \quad \ldots\ldots (12)$$

where c_1 = concentration at level y_1; and

$$a_1 = v_t/(kU_\tau) \quad \ldots\ldots (13)$$

where v_t is the settling velocity of the solids at level y_1.

Also, since $\tau_o = \rho_o ghS \quad \ldots\ldots (14)$

$$U_\tau = (ghS)^{1/2} \quad \ldots\ldots (15)$$

and

$$a_1 = v_t/[k(ghS)^{1/2}] \quad \ldots\ldots (16)$$

Vanoni[16] and Ismail[17] have experimentally verified the general form of this expression, but the experimental a_1 referred to as $(a_1)_{exp.}$ was smaller than the theoretical value. In addition, the suspended matter was more evenly distributed than was predicted by the theoretical expression.

Data subsequently obtained by Vanoni[5] showed agreement with Equation (13) when (a_1) was adjusted to a proper value. Vanoni felt that $(a_1)_{exp.}$ was not equal to the theoretical value because the assumption that $D_p = D_f$ did not take into consideration the smaller inertia of the fluid compared with that of the solids. He corrected for this by putting:

$$D_p = a_2 D_f \quad \ldots\ldots (17)$$

Experiment showed a_2 to vary from 1.0 to 1.5, and it seemed to be affected by the size of the particles.

Ismail[17] obtained the empirical relation $D_p = 1.5\ D_f$ for 0.10-mm. sand particles in water, and $D_p = 1.3\ D_f$ for 0.16-mm. particles all in the same system. Carstens[18] however doubted that a_2 could be greater than unity, since D_f is really the diffusion coefficient of the fluid. Since the density of the the fluid was at all times less than the density of the solids, D_f should always be bigger than D_p. Carstens cited evidence to this effect in his work and in that of Wagenschein[19].

In reply to Carstens, Ismail claimed that the work of Sherwood and Woertz[20] and also that of Corcoran[21] showed in effect that a_2 could be greater than 1. Nevertheless the results discussed in Part III of this series, dealing with the resistance of a spherical particle in a fluctuating flow make it very difficult to uphold this argument. Ismail's apparent observations may suggest that the model employed is erroneous and the mixing length analogy cannot be applied to this system.

The Effect of the Suspended Solids on the Fluid Friction Factor

The effect of the suspended solids on the flow characteristics of the fluid was investigated by Vanoni[5] and he found that the value of the Von Karman universal constant k was decreased in a fluid-solid system. In his experimental study, the flow rate and the depth of the channel were kept constant (i.e., the shear remained constant) and the solids content of the stream was increased. From Equations (8), (10) and (11), if τ_o (and therefore $U\bar{\tau}$) is kept constant, decreasing k would cause

(dU/dy) to increase so that D_f would decrease. Vanoni found that k would decrease to as low as 0.2 with an increase in stream loading.

Vanoni noted that increasing (dU/dy) will tend to increase the mean velocity, and the friction factor for the channel will tend to decrease, a behavior which was confirmed by experimental observation. He attempted to explain the decrease in k by assuming that the presence of the suspended matter damps the turbulence since it must supply the energy per unit mass of fluid per unit time to prevent the solids from settling, and this would be proportional to the solids concentration and settling velocity. Results obtained with sedimenting systems have shown D_f to increase with particle concentration, but Vanoni admitted that the process by which this occurred was not clear. In his observations the energy which would be required to suspend the solids amounted to only 3% of the amount required to overcome the friction in the channel, whereas the alterations to the friction factor were of a much larger magnitude.

In a solids-liquid system the velocity of the particles with respect to the fluid, i.e., their slip velocity, is very small relative to the values encountered in solids-gas systems. In systems with low slip velocities, the turbulence generated by this relative motion may be negligible in comparison to the turbulent energy being used up to suspend the solids phase, and the net effect of the solids is to exert a damping action on the fluctuating velocity of the conveying medium. In a solids-gas system, the finite relative velocity could generate turbulence which will be discharged from the wake of the solids in much the same manner as in the production of turbulence by the placement of a wire mesh over the cross sectional area of the moving stream. It may very well be that in this case the turbulence generated by the particles would exceed that which is withdrawn from the system in the process of the suspension of the solid phase. Other aspects of the problem of the reaction of the fluid phase to the presence of the solids will be taken up in discussions which follow.

XI—ALTERATION OF FLUID VELOCITY PROFILES DUE TO PRESENCE OF PARTICLES

Laminar Flow

The presence of solids particles in a laminar stream flowing through a pipe will cause an alteration in the characteristic parabolic velocity distribution. Brinkman[22] deduced an expression for the flow pattern in a vertical column by analogy with Poiseuille's law to give:

$$U = \frac{P_m}{\mu}\left(g_c\frac{dp}{dx} - \rho g\right)\left\{\frac{I_o[(y/P_m - 1]}{I_o\, a/\sqrt{P_m}}\right\} \quad \ldots\ldots\ldots(18)$$

where I_o = Bessel function of zero order and first kind and of imaginary argument;
y = distance from the axis;
and P_m is the permeability of the system defined by:

$$P_m = (r^2/18)\,\{(3 + 4/\phi_v - 3\,[(8/\phi_v) - 3]^{1/2}\} \quad \ldots\ldots\ldots(19)$$

Plots of the velocity profile for different values of ϕ_v showed that the distribution becomes less elongated as ϕ_v is increased so that it is almost uniform at $P_m = 10^{-2}$ ft.^{2} This result has not as yet been confirmed by experiment.

If the particles become sufficiently small, the multiparticle system will begin to assume the properties of a non-Newtonian fluid, and the results of the investigations of these systems is not of direct interest to the solids-gas flow problem.

Turbulent Flow

The results obtained with sedimenting streams give some indication of the alterations in the velocity profile of the stream caused by the presence of the solids. A better analysis of Vanoni's data than had originally been given by Vanoni himself was suggested by Hunt[23] who showed the velocity distribution in a particle-laden stream to be given by:

$$\frac{U_{max} - U}{(ghS)^{1/2}} = -\frac{1}{k}\left\{(1-y/h)^{1/2} + k_2 ln\left[\frac{k_2 - (1-y/h)^{1/2}}{k_2}\right]\right\} \ldots(20)$$

where k_2 = constant of integration:
U_{max} = maximum velocity of the stream:
y = distance along the y axis, i.e., the axis transverse to the flow;
h = total depth of flow.

The particle concentration effect acts by altering the value of k, and this must be determined by experiment.

Laursen and Lin[21] felt that bed conditions alone govern the variation of k_3 which is used in defining the velocity profile as:

$$U \propto y^{1/k_3} \quad \ldots\ldots\ldots(21)$$

They believed that the suspended sediment has no effect on the production or distribution of turbulence, and that the phenomenon is similar to that noted by Nikuradse in connection with the change of the velocity distribution in a pipe with the roughening of the pipe wall.

In a communication to Laursen and Lin, Ismail[17] noted that their conclusion was based on values of the function k_3 and on the contention that as the velocity increases, k_3 tends to the value for solids-free fluid. Ismail reported detailed experimental observations which suggested that this was not correct.

Very little is quantitatively known about the effects of the solids phase on the velocity profile of a gas flow other than that the pressure drop in two-phase flow which is contributed by the gas phase cannot be determined from the conventional friction factor plots for solids-free flow. No method has as yet been presented for the calculation of this quantity, and this has hindered the development of a general theory for solids-gas flow. Coulson and Richardson[25] pointed out that small concentrations of solids in solids-liquid pipe flow have caused a reduction in the overall pressure drop encountered. Experimental measurement of the effects of model fibres in the flow characteristics of fibre suspensions carried out in this laboratory[26] have shown that for short fibres (less than one millimeter in length) no flocculation occurred and the reduction in pressure drop (below the value for water alone) increased as the fibre concentration increased. For longer fibres, flocculation did occur, which was accompanied by a marked increase in pressure drop over the value for water alone, owing to the establishment of a laminar regime of flow. Turbulent conditions at higher velocities caused the disruption of the flocs, and the pressure drop fell once more below the water value.

Knowledge of the velocity profile of a solids-fluid system would allow the measurement of the pressure drop due to the fluid phase. However, velocity profile data for solids-gas systems are lacking, mainly because of the difficulty in employing a pitot tube in two-phase flow. Dussard and Shapiro[27] have recently designed a modified form of the pitot tube for the measurement of the velocity profiles of particle-laden streams, and this instrument may become an important tool for the investigation of solids-gas systems.

Zenz[28], in a study of solids-gas flow in pipes found that in the case of one material there was no appreciable difference in the pressure drop for the flow of the solids-gas mixtures and the flow of solids-free air. This suggests that the presence of the solids altered the turbulence characteristics of the fluid so as to lower the frictional retardation which it encountered at the pipe wall.

Segler[29] recorded the velocity distribution in a 9-in. pneumatic grain conveying tube through which varying concentrations of wheat grains were being transmitted. The velocity profiles, shown in Figure 1, were found to vary with the solids concentration and the greatest change occurred in the vicinity of the pipe wall. Increased loading elongated the profile and *decreased* the velocity gradient at the wall. No attempt was made to calculate the pressure drop due to the movement of the gas phase with an increase in solids concentration. This observation,

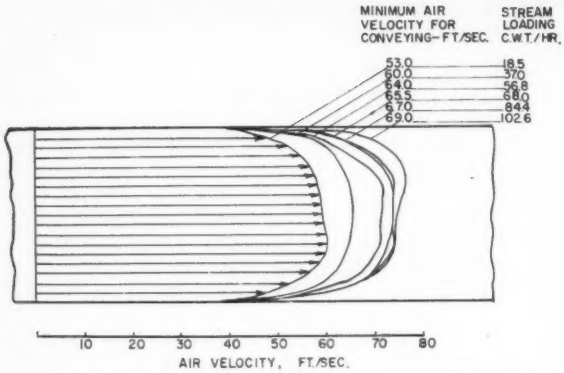

Figure 1—Velocity profiles of air stream containing solids.

if correct, would be of great assistance in interpreting and explaining data obtained in investigations of dilute phase solids-gas flow, since it suggests that the fluid pressure drop is at times almost half of what would be obtained with solids-free flow.

XII—THE TURBULENT MOTION OF A SMALL PARTICLE IN A TURBULENT FLUID

The previous discussion has shown that the alterations in the mean and turbulent characteristics of a flow by entrained solids will be related to the motion of the constituent solid particles. Three particle regimes occur in solids-gas systems. If the velocity of the particle is such that its mean relative Reynolds number is in excess of say 100, its motion will be essentially linear, and its effect on the free-stream turbulence will be similar to the action of a screen placed normal to the flow. The investigations of Schwarz[30] and those of the present authors[31], discussed in Part V of this series, were performed in this region. At the lower Reynolds numbers of this regime, the wake turbulence contributed to the flow will be associated with high wave numbers, and it will hasten the dissipation of the fluid turbulence. At higher Reynolds numbers, the wave numbers will become sufficiently low so that there will be a general increase in the stream turbulence level. Even when the gross level of turbulent energy is reduced, the vorticity shed by a particle would have frequencies which would be the most effective in accelerating the spectral momentum transfer in the wake of the neighbouring downstream particles.

A second particle regime occurs when the particle Reynolds number is less than unity. Here the particle mean velocity is essentially equal to that of the free-stream, and the particle acquires a turbulent motion which is a response to the fluid turbulence in its immediate vicinity. Intuitively it would be expected that as the size of the particle decreases or its density approaches that of the fluid, the particle motion will follow more faithfully the motion of the fluid which it displaces. The discussion in this section will deal with this second regime.

Separating regime 1 and 2 will be a third intermediate state of motion where the particle has both a mean velocity with respect to the fluid, i.e., a finite mean Reynolds number, and a turbulent motion which is a response to the ambient fluid turbulence. The theoretical description of this regime will have to await further mathematical progress with mixed Lagrangian and Eulerian statistics.

The simplest model from which the problem of the turbulent motion of a particle can be broached is a stationary one in which the particle is suspended in an infinite fluid element which is oscillating with a periodic sinusoidal motion, and a description is sought of the particle fluctuation frequency and amplitude. The theoretical and experimental treatment of this system has been discussed in Part III of this series[1]. This stationary model has been adapted to the turbulent fluid case by giving the coordinates of the stationary system the velocity of the particle being considered. A solution of this type was obtained by Tchen[32] who assumed the particle to be in a periodic field defined by:

$$u_f = Ae^{i\omega\theta} \quad \ldots\ldots(22)$$

A similar solution was obtained by Liu[33] who used a generalized harmonic approach in which the velocity of the particle is represented by a Fourier integral. This allowed him to obtain an expression of the function $\psi(\omega)$ which denotes the ratio of the sinusoidal component of the velocity of the spherical particle to the corresponding component velocity of the fluid element at the position of its centre, when the spherical particle is absent. In other words, $\psi(\omega) = \overline{u'_p{}^2}/\overline{u'_f{}^2}$. The function is simplified for the following special cases:

(1) Non-viscous fluid: If the viscous effect is negligible compared to the inertia effect:

$$\psi(\omega) = 3\rho_o/(2\rho + \rho_o) \quad \ldots\ldots(23)$$

(2) If $(r\omega^{1/2})/(\nu^{1/2}) \ll 1$

$$\psi(\omega) = 1 - (1)/[1 - (9/2)\,(i\rho_o\nu)/(\rho - \rho_o)\omega r^2)] \quad \ldots\ldots(24)$$

and if $(\omega r^2)/(\nu) \gg (\rho_o)/(\rho - \rho_o)$

$\psi(\omega)$ becomes very small and the particles remain nearly at rest as the turbulent flow beats on them.

(3) As the sphere radius r decreases to a very small value, $\psi(\omega)$ tends to 1 and this will occur when:

$$r^2 \ll (9/2)\,[(\rho_o)/(\rho - \rho_o)\,(\nu/\omega)] \quad \ldots\ldots(25)$$

Solutions of this type require that the particle diameter be much smaller than the Eulerian microscale, and that the particle always remain associated with a given packet of fluctuating fluid. Even then it is doubtful whether one can assume that Stokes' Law applies since a fluid element in a turbulent field will be undergoing continual distortion. Corrsin and Lumley[34] have shown that a further weakness in the derivation develops when it is applied to a turbulent fluid. If the coordinates are fixed to the particle, the inhomogeneity of the particle movement will be related to time alone, but the fluid velocity inhomogeneity will still remain a function of space as well as time. Lumley[35] has elaborated on the extreme mathematical difficulties which occur when this factor is incorporated into an attempted solution.

Friedlander[36] has used a mathematical approach similar to that used in the calculation of Brownian movement to obtain a relationship between $\overline{u'_r{}^2}$ and $\overline{u'_f{}^2}$. Here again it was necessary to assume that $Re \to o$, and that the particle diameter was much smaller than the fluid Eulerian microscale. In addition, $(d\sqrt{\overline{u'_r{}^2}}\,\rho_o/\mu)$ was restricted to being less than 1, and the Stokesian drag was assumed to be valid for the fluctuating resistance. For very small particles entrained in a liquid, Friedlander assumed that the Lagrangian velocity correlation would suffice (i.e., the particle would remain associated with a given packet of fluid so that correlations as a function of time only could be employed) and an approximate expression for $\overline{u'_r{}^2} = \overline{u'_p{}^2} - \overline{u'_f{}^2}$ was found to be given by:

$$\overline{u'_r{}^2} \simeq 2(1 - \rho_o/\rho)^2\,\overline{u'_f{}^2}/\lambda^2\beta^2 \quad \ldots\ldots(26)$$

where λ is the Lagrangian microscale, in sec.

and
$$\beta = 3\pi\mu d/m \quad \ldots\ldots(27)$$

For the case of solid particles of unit specific gravity in a gas flow, Friedlander applied the simultaneous experimental measurements of the Eulerian and Lagrangian correlations given by Mickelsen[37] for an eight-inch duct which were discussed in Part I[1]. This led to an approximate expression:

$$\overline{u'_r{}^2}/\overline{u'_f{}^2} = z/(z + \beta) \quad \ldots\ldots(28)$$

where z is an experimental constant. A plot of $\overline{u'_r{}^2}/\overline{u'_f{}^2}$ as a

function of the particle diameter for a mean air velocity of 75 ft./sec. in the 8-in. pipe at 20°C. ($z = 200$ sec.$^{-1}$) showed the former to rise from zero at $d = 0$ to 0.2 at $d = 20$ microns. The ratio approached 1, i.e., $\overline{u'_p{}^2} \to 0$ as d approached 100 microns. The solution was not suggested for use above 10 microns however, since there would be a mean relative velocity between the particle and the fluid, and the particle would have a finite mean Reynolds number. In addition, a plot of Nu', the Nusselt number for mass transfer, was shown simultaneously against d. Nu' rose from a value of 2 at $d = 0$ to a value of about 4.2 at $d = 100$ microns. Friedlander commented concerning the latter finding that the assumption sometimes made of $Nu = 2$ (stagnant case) for particles carried along by a turbulent fluid may be in error. Recent studies by Dlouhy[38,39], on the other hand, have shown that small droplets (from 10 to 40 microns) will evaporate in turbulent streams with $Nu = 2$. It should be noted, however, that the Mickelsen's data, on which Friedlander based his calculations, may be unreliable[40].

By using similar simplifying arguments and restrictions and by neglecting the effects of acceleration Soo[41] obtained solutions of the particle turbulence parameters as a function of those of the fluid. The solutions were given as a family of curves showing the ratios of the intensities, scales and diffusivities of the particles to those of the fluid as a function of:

$$\Phi_s = \left(\frac{\overline{Re}}{9}\right)\left(\frac{d}{\lambda}\right)\left(\frac{\rho}{\rho_o}\right) \quad \ldots\ldots\ldots\ldots\ldots\ldots (29)$$

where

$$\overline{Re} = d\sqrt{\overline{u'^2}}\,\rho_o/\mu \quad \ldots\ldots\ldots\ldots\ldots\ldots (30)$$

and λ is the Lagrangian microscale of turbulence.

The relationships which he obtained were not applicable to real systems, and Soo decided that because of the difficulties involved in obtaining adequate solutions the interrelationships would have to be obtained experimentally.

In what is perhaps the most sophisticated investigation of solids-gas flow to date, Soo developed experimental and computational methods which allowed him to measure the statistical properties of both the particulate and entraining fluid motion[42,43]. The experimental system consisted of a 3-in. square duct with a 10-ft. horizontal plexiglass test section. Glass beads, 105 to 210 microns in diameter, were fed at rates up to 0.5 lb./min. into the air stream which was varied up to 85 ft./sec. A thin vertical sheet of light was used to illuminate the system and the particle motion was recorded by stroboscopic photography. By drilling equal-sized holes through the sequence of particle images on the photographic plates, Soo used an optical autocorrelation technique to measure the Lagrangian scale and intensity of the particle motion. The average Lagrangian properties in the central core of the fluid phase were estimated with the particles present by using a helium diffusion technique.

The particle Reynolds number was in all cases less than 10, and there was no significant alteration of the average fluid turbulence properties by the presence of the solids. Two remarkable results were obtained. In the first place, although the fluid turbulence would be expected to be roughly isotropic in the central third of the duct in which the measurements were taken, the particle intensity in the y direction $\sqrt{\overline{v'_p{}^2}}$ was considerably smaller than the particle intensity $\sqrt{\overline{u'_p{}^2}}$ in the axial direction. Soo feels that this is a direct result of the energy required to overcome the gravitational forces tending to cause the particles to settle out. This could have been confirmed by using a horizontal sheet of light and measuring the z component of the particle intensity.

The comparison of the particle intensities with the fluid intensities provided an even more startling result in that the former were in general considerably *greater* than the stream turbulence. The theoretical solutions obtained by Soo had shown the ratio:

$$T = (\overline{u'^2} - \overline{u'_p{}^2})/(\overline{u'^2}) \quad \ldots\ldots\ldots\ldots\ldots\ldots (31)$$

to increase from zero at $\Phi_s < 0.1$ and then increase to 1 at $\Phi_s > 50$. The experimental results all showed *negative* values for this ratio, at times going as low as -12. Using a more valid set of starting equations, than in his original solution, Soo attempted to obtain an approximate solution for the particle turbulence parameters for varying particle distance from the duct wall[44]. This showed that the effect of the wall was to displace the T versus Φ_s curves *upwards* rather than downwards, and at no time were there any negative values of T predicted.

Soo then attempted to explain the results as being caused by the increase in fluid turbulence, with increasing distance from the duct centre, discussed in Part I[1]. If a particle was in an off-centre region where the ratio of the fluid turbulence at that point to the turbulence at the duct centre was say 2, and if T was actually zero, the value of T which would be calculated using the central fluid intensity would be -3. Soo's observations were taken in the central third of the pipe so that it is difficult to see how the higher particle intensities could be transported into this region by particles which were in the vicinity of the wall. Even if this argument is granted, however, it still does not explain the large particle intensities which were observed at the centre. For example, the experimental data at a mean fluid Reynolds number of 40,000 and $\Phi_s = 10$ show T values of -11 whereas the largest negative value of T which could be attributed to the maximum intensity in the whole duct cross-section (i.e., the sharp rise near the wall) would only give a value of -1.

The reason for the particle intensities being higher than the fluid is difficult to explain, since Soo's careful experimental techniques leave little doubt that this behavior actually occurs. It must be that the particle velocity fluctuations are a response to forces other than the fluid turbulence. The generation of static charges, which is to be discussed in the following section, is very difficult to avoid in solids-gas systems, even when elaborate grounding and humidifying procedures are employed, and mutual particle repulsion would perhaps contribute to the fluctuating motion. A second possibility could be that the drag forces on the particle in a turbulent packet of fluid are more complicated than those given by the Stokesian solution employed and that they themselves may act in an unsymmetrical and unsteady manner. In spite of the difficulty of offering a plausible explanation for the results which he obtained, Soo's researches are representative of the type of investigations which will eventually provide a scientific understanding of dilute-phase flow.

Peskin[44,45,46,47] has raised the possibility that fluctuating pressure forces are exerted on each particle in a solids-fluid system by its neighbors, similar to those predicted by potential flow theory. Konig[48] for example has shown that two particles moving in a ficticious inviscid fluid will exert a force $\bar{F}$ on each other given by:

$$\bar{F} = (3/2)\,(\rho_o/m)\,U^2\pi^2\,(r^6/|l|^5)\bar{l} \quad \ldots\ldots\ldots\ldots (32)$$

where $\bar{l}$ is the displacement vector between the particles.

Peskin assumed that this force term can be extended to non-steady motion and can be applied to particles which are in turbulent motion in a turbulent velocity field. In order to proceed, he assumed that the solids will not affect the fluid turbulence, and that the fluid drag on the particles is Stokesian. The extremely difficult task then becomes to evaluate the total interparticle pressure force acting on a particle due to its neighbors. If the assumptions made are granted, the force is given by:

$$\overline{F(t)} = \frac{3}{2}\frac{\rho_o}{m}\pi^2 r^6\,(u')^2 \sum_{i=i}^{N} \frac{\bar{l}_i}{|l_i|^5} \quad \ldots\ldots\ldots\ldots (33)$$

where u' is the intensity of fluid motion relative to the particles. An important consequence of the solution of (33) is that there is a particle diffusivity due to the random pressure forces, but that these are felt only by slow particles, and can be ignored as the particle velocity is increased. Heavy particles will, of course, tend to have very low diffusivities.

The method of dealing with random interparticle forces presented by Peskin should be directly applicable to the case of electrostatic repulsion in charged systems.

The Effect of the Solids on the Fluid Turbulence Level

Measurements cannot be taken with a hot-wire anemometer in a particle-laden stream so that indirect turbulence measurements must be obtained from diffusion experiments. The information which is available from these results is interesting, but they are limited as to detail since they provide intensity and scale values which are the average across the diffusion breadth. Particles with sufficiently high Reynolds numbers would be expected to contribute turbulent energies in a wave number range which may have a maximum effect on the downstream particles, and yet their contribution to the overall level of the stream could be insignificant. Spectral density measurements would in addition provide an insight into the energy consumed in suspending the particles but the development of instruments to obtain this information will be extremely difficult.

The tracer diffusion technique has been employed by Hanratty, Latinen and Wilhelm[49] to obtain turbulence measurements in fluidized beds. Their results with water-fluidized 3-mm. glass spheres show that the intensity decreased steadily with increasing voidage, and the intensity values at a voidage of 90% were essentially equal to the particle-free case. The scale value from 70% voids upwards also decreased steadily to the empty tube result.

Kada and Hanratty[50] have recently extended the use of the tracer technique to study the effect of solids on the fluid turbulence of cocurrent solids-liquid systems. Here the difference between the solids and fluid velocities is very small and would be extremely difficult to measure. The authors estimated it by assuming that the free-stream turbulence would not affect the particle boundary layer and wake structure, and the particle Reynolds number range calculated by this means was 0.66 to 18.3. The product of the square of the relative intensity and the particle Reynolds number was in all cases much less than 45 so that the turbulence effect should be small[31]. At the lower particle Reynolds numbers, the solids did not affect the fluid turbulent diffusion coefficient up to a solids concentration of 1%. With a particle Reynolds number of 18.1 however, there was a 20% increase in the diffusion coefficient with a solids concentration of only 0.15%. Up to the limiting concentration of this study (2.5% solids) the turbulent diffusion coefficient increased sharply for low fluid Reynolds numbers, but increased very gradually with a Reynolds number of 50,000. The accumulation of data of this type is very important for an understanding of solids-fluid systems, particularly since the results are not complicated by electrostatic effects.

The only results available in dilute-phase solids-gas flow are the ones discussed previously given by Soo[43]. Unfortunately these were taken at particle Reynolds numbers less than 10, where there would not be any contribution from the wake, nevertheless they indicate that any damping action if present was restricted to the low energy, high frequency end of the spectrum.

XIII—ELECTROSTATIC CONSIDERATIONS

Solids-gas systems differ from their solids-liquid counterparts in that they tend to generate static electricity. This effect may play a significant role in obscuring data by introducing force terms which are not accounted for in the theoretical equations being tested.

Coulson and Richardson[25] noted that electrostatic charge accumulation in a solids-gas system may increase the pressure drop by a factor of 10. They feel that considerable further research is needed for a better understanding of the phenomenon. Lewis, Gilliland and Bauer[51] found that fluidized particles which were treated so as to minimize electrostatic charging gave characteristic curves which differed in shape from those obtained with untreated particles.

Mehta[52] studied the flow of glass spheres suspended in an air stream moving through pyrex pipe. He observed extensive charging between the particles and the air, and the particles and the pipe wall. Long axial arcs were formed every few minutes and these were succeeded by pressure waves which caused error in the manometer readings. The discharge caused the combustion of traces of oil entrained in the air, depositing carbon on the pipe walls. Mehta noticed that the pattern of flow, i.e., the distribution of the solids phase over the flow cross-section could be altered at will by altering the position of the grounding wires, and no amount of grounding was able to mitigate the charging action.

Mitlin[53] referred to the "anomalous behavior" of sand particles in a *metal* pipe. The pressure drops encountered would gradually increase with time to a constant value. It reverted to its initial value after the flow had been discontinued for a lengthy period of time. Mitlin felt that this could be explained by the electrostatic charge residing on a very fine dust layer on the inside surface of the tube. This phenomenon is held to account in part for the increase of pressure drop with solids concentration. In their study of the elutriation of fine particles from dense-phase fluidized beds, Chin-Yung Wen and Hashinger[54] recently found that reproducible data could be obtained after "the electrostatic charge was sufficiently eliminated from the column" by wrapping grounding wires around it and also introducing a grounding wire into the bed. They questioned the validity of a previous study[55] on the basis of the possible existence of electrostatic charges.

Culgan[56] found that in a short time the metal wall of a conveying system carrying plastic particles will become coated with a hard layer of this material. This could result in a system similar to the one noted by Mitlin, and it would be difficult to define the electrostatic generation components without knowledge of the actual surface composition of the pipe.

Richardson and McLeman[57] have recently reported a very detailed investigation of the development of electrostatic forces in solids-gas systems which reflects an increased awareness of the importance of this phenomenon. The solids were conveyed in a horizontal 1-in. diameter brass pipe which was 114-ft. long. When 0.05-in. sand particles were recirculated through the test loop, the relative velocity between the solids and the conveying gas gradually increased to an equilibrium value. The charge buildup was not associated with the particles since the substitution of fresh sand had no effect. Oddly enough cleaning the pipe surface, grounding or charging it produced no visible effect. Correlations were obtained between the pressure drop and the relative velocity increase, but no attempt was made to relate their variations with the time of conveying. Surprisingly, no correlation was found between the charges on the particles and pipe surface on the one hand and the relative velocity and pressure drop on the other. Richardson and McLeman feel that this supports the existence of a charged dust layer at the tube wall. With the sand system, the dust required an opposite charge to the particles, and the resulting attraction for the wall region retarded the particle motion. When Perspex particles were used, the pressure drop *decreased* with time, and in this situation the charged dust layer was felt to have acquired a similar charge to the particles which caused them to move near the axis of the duct.

Khudiakow and Chukhanov[58] found that electrostatic retardation of particle movement could become large enough to completely halt the flow of the solids phase in a vertical solids-gas system. High speed photographs had indicated that lesser amounts of charging had caused the particle motion to be "rather drastically changed".

Electrostatic discharge is sometimes a hazard which prevents materials such as sulphur from being conveyed pneumatically. Sinha[59] as well as Gasterstadt[60] reported the generation of large sparks in industrial solids-gas systems.

There has been no attempt at a quantitative evaluation of the effect and extent of electrostatic charging occurring with motion of particles in a pipe.

Green[61] developed an equation for the motion of a charged smoke particle introduced into a stream of gas moving with laminar flow between two vertical plates maintained at a potential gradient E_o:

v = velocity of movement of the particle to one of the plates

$$= (E_o n_e e)/(6\pi\mu r) \quad (34)$$

This indicates the type of expression which may have to be incorporated into the momentum equations defining solids-gas systems.

It would be advantageous to be able to predict the electrostatic generation qualities of the various combinations of solids-phase and pipe wall materials encountered. This would however, necessarily involve a better understanding than is presently available of the mechanism by which friction generates static electricity.

Thomson[62] held that frictional electricity is really merely contact electricity, the contact being made good by considerable pressure. Vieweg[63] cited the Helmholtz theory of frictional electricity which postulated that the fundamental cause is a contact difference of potential which exists between any two materials. When two *unlike* surfaces are brought together, there is a concentration of charge at the surface of contact. On separation, if either is a nonconductor, the contact potential is greatly magnified and both surfaces are charged. If both surfaces are conducting, the charges are said to neutralize on separation in the last instant of charging.

A more recent paper by Harper[64] showed that it is erroneous to think that no rubbing potential will occur if both components of the system are *conductors*. The charging of metal powders by blowing against metal surfaces is found to be comparable to that obtained when insulating powders are used. Experiments indicated that one cause for the electrification of metal — metal surfaces is a manifestation of their contact potential, and Harper felt that these must always be present. The magnitude of the charge generated may be calculated from the contact potential and the *topography* of the surface involved by the use of a quantum-mechanical theory based on the original Volta-Helmholz hypothesis. Subsequent experiments by Harper[65] seem to show that for *light* contact with *metals*, hydrophylic surfaces such as glass acquire a considerable charge, whereas hydrophobic surfaces such as polythene, amber, polystyrene, nylon, Perspex, silicone and Teflon do not.

The mechanisms of the frictional electrification of particles on dispersion into a solids-gas system are still little understood[66] and the data obtained are not reproducible and are often inconsistent and even contradictory.

The charges on sprays of electrified particles were studied by Sachsse[67] and Loeb[68] for systems of dust particles, and by Chapman[69] for atomized liquid droplets. These indicate positive and negative charges to be present in equal numbers. In some cases the charge was proportional to the surface area, whereas in others it was found to vary as the particle radius.

Kunkel[66] observed photographically the trajectory of charged solid particles in an air stream. It was found that if a mass of particles were separated to form a cloud, practically all the particles would become charged, but the cloud as a whole would be neutral. If the cloud would come into contact with a surface, an asymmetry of charge might or might not occur. Asymmetry was usually observed in systems of metals in combination with insulators where the insulator usually received the negative charge. Kunkel found that in some cases, i.e., talc particles on a metal, a highly charged dust coating would cling to the metal. A surprising conclusion of the trials was that humidity does not affect separation charging. No change was observed as the relative humidity was increased to a value of 90% at a room temperature of 20°C. Also, fluid turbulence was found to have little effect on the charging of the particles.

CONCLUSIONS

Progress is being made with attempts to predict theoretically the turbulent behavior of solid particles as a function of the fluid turbulence. These researches have uncovered such difficulties that experimental observations will have to be relied on for any useable information. Ingenious empirical methods are being developed and preliminary results suggest that the starting equations used in the theoretical derivations may not take full account of the various forces acting on the particle.

Acknowledgements

The authors wish to express their appreciation for the continued assistance given to them by Librarians A. Finnemore and L. Lefebvre of the Pulp and Paper Research Institute of Canada, and P. Keir of McGill University, in obtaining the many papers reviewed in this series. L. B. Torobin is indebted to the Scientific Research Bureau, Trade and Commerce Department, Province of Quebec for three consecutive fellowships in support of his research program.

Nomenclature

Any consistent set of units may be employed. Those given are merely illustrative.

a = tube radius, ft.
a' = hydraulic radius of stream, ft.
A = amplitude, ft.
B = sediment parameter, ft.^{2} sec.^{3}/lb. mass.
c = solids concentration, lb./ft.^{3}
C_D = drag coefficient, dimensionless.
$C_{D'}$ = coefficient of minimum drag to initiate motion, dimensionless.
d = particle diameter, ft.
D_f = diffusion coefficient for fluid, ft.^{2}/sec.
D_p = diffusion coefficient for solids, ft.^{2}/sec.
e = electrical charge, coulombs.
E_o = potential gradient, volts/ft.
E = energy gradient in direction of flow, ft.-lb./ft.
F_1, F_2 = experimental factors defined in text, dimensionless.
$\overline{F}$ = interparticle force between two moving particles, poundals
h = total depth of flow, ft.
g = local acceleration of gravity, ft./sec.^{2}
g_c = dimensional constant, (ft.) (lb. mass)/(sec.)^2 (lb. force)
I_o = Bessel function, Equation (18)
k = von Karman constant, dimensionless
k_1, k_2, k_3, etc. = experimental constants, dimensionless
L = length, ft.
l = interparticle distance, ft.
m = particle mass, lb.
Nu = Nusselt number, dimensionless
Nu' = Nusselt number for mass transfer, dimensionless
n_e = number of electrical charges, dimensionless
p = pressure, lb. force/ft.^{2}
P_m = permeability of system, ft.^{2}
r = sphere radius, ft.
R = fluid drag force on particle (lb. mass)/(ft./sec.^{2})
Re = particle Reynolds number based on mean motion, dimensionless
$\overline{Re}$ = turbulent Reynolds number ($d\sqrt{\overline{u'^2}}\rho_o/\mu$), dimensionless
S = slope of stream bottom, dimensionless
T = ratio defined by Equation (31)
u_f = fluid element velocity, ft./sec.
u'_f = fluid fluctuating velocity, ft./sec.
u'_p, v'_p = particle fluctuating velocities, ft./sec.
u'_r = relative particle fluctuating velocity, ft./sec.
U = mean fluid velocity relative to particle, ft./sec.
U_c = critical fluid velocity required to initiate particle motion, ft./sec.
U_o = mean fluid velocity, ft./sec.
U_τ = friction velocity = $(\tau_o/\rho_o)^{1/2}$, ft./sec.
v = particle velocity, ft./sec.
v_t = free-fall velocity of solids, ft./sec.
w = mass flow rate of solids carried per unit width, (lb. mass)/(sec.) (ft.)
y = distance along axis transverse to flow, ft.
z = experimental constant, sec.$^{-1}$
$\alpha_1, \alpha_2, \alpha_3$, etc. = experimental factors defined in text
β = $3\pi\mu d/m$, sec.$^{-1}$
θ = time, sec.
λ = microscale of turbulence, ft. or sec.
μ = fluid viscosity, lb./(sec.) (ft.)
ν = kinematic viscosity, ft.^{2}/sec.
ρ_o = fluid density, lb./ft.^{3}
ρ = particle density, lb./ft.^{3}
ρ_b = bulk density, lb./ft.^{3}

τ = fluid shearing stress in solids-free flow, (lb. mass) (ft./sec.²)/(ft.²)
τ_c = fluid shearing stress required to initiate particle motion, (lb. mass) (ft./sec.²)/(ft.²)
τ_o = fluid shearing stress at bed surface, (lb. mass) (ft./sec.²)/(ft.²)
Φ_f = fluid movement parameter, Equation (5), dimensionless
Φ_k = Kalinske function, Equation (6), dimensionless
Φ_p = particle movement parameter, Equation (4), dimensionless.
Φ_s = Soo parameter, Equation (29), dimensionless
ϕ_v = volume concentration of solids, ft.³ of solids per ft.³
$\psi(\omega)$ = ratio of $\overline{u'_p{}^2}$ to $\overline{u'_f{}^2}$, dimensionless
ω = angular frequency, radians/sec.

References

(1) Torobin, L. B., and Gauvin, W. H. Can. J. Chem. Eng., Part I, **37:** 129 (1959); Part II, id., 167 (1959); Part III, id., 224 (1959); Part IV, **38:** 142 (1960); Part V, id., 182 (1960).
(2) Vanoni, V. A., Proc. Third Midwestern Conf. on Fluid Mechanics, Univ. of Minn. (1953).
(3) White, J. T., and Broadhurst, P. H., Trans. Inst. Mining Engrs. (London), **111:** 920 (1952-53).
(4) Rubey, W. W., U.S. Geol. Survey Profess. Paper 189-E (1938).
(5) Vanoni, V. A., Proc. Fifth Iowa Hydraulics Conf., (June 1952).
(6) Segler, G., "Pneumatic Grain Conveying", Braunschweig, Germany (1951).
(7) Duboys, P., Ann. Ponts et Chaussées (5), **18:** 141 (1879).
(8) Brown, C. B., "Engineering Hydraulics", ed. by H. Rouse, John Wiley & Sons, Inc., New York (1950).
(9) Einstein, H. A., Trans. Am. Soc. Civil Engrs. **107:** 561 (1942).
(10) Kalinske, A. A. and Pien, C. L., Trans. Am. Geophys. Union, **2:** 530 (1943).
(11) Kalinske, A. A., Trans. Am. Geophys. Union, **28:** 615 (1947).
(12) Schmidt, W., "Probleme der Komischen Physik", Jensen and Schwassman Publications, Hamburg (1925).
(13) O'Brien, M. P., Trans. Am. Geophys. Union, 487 (1933).
(14) O'Brien, M. P., Trans. Am. Geophys. Union, **14:** 481 (1933).
(15) Rouse, H., Proc. 5th Intern. Congr, Appl. Mech., Cambridge (1939).
(16) Vanoni, V. A., Trans. Am. Soc. Civil Engrs. **111:** 67 (1946).
(17) Ismail, H. M., Trans. Am. Soc. Civil Engrs., **117:** 409 (1952).
(18) Carstens, M. R., Trans. Am. Soc. Civil Engrs. **117:** 443 (1952).
(19) Wagenschein, M., Ann. Physik, Series 4, **65:** 461 (1921).
(20) Sherwood, T. K., and Woertz, B. B., Ind. Eng. Chem. **31:** 1034 (1939).
(21) Corcoran, W., Ph.D. Thesis, Calif. Inst. Techn. (1948).
(22) Brinkman, H. C., Appl. Sci. Research (London), **A-2:** 190 (1949).
(23) Hunt, H. N., Proc. Roy. Soc. (London), **224 A:** 323 (1954).
(24) Laursen, E. M., and Lin, P. N., Trans. Am. Soc. Civil Engrs. **117:** 435 (1952).
(25) Coulson, J. M. and Richardson, J. F., "Chemical Engineering". McGraw-Hill Book Co., Inc., New York (1954).
(26) Schieck, R. R., Ph.D. Thesis, McGill Univ., Montreal, Canada (1959).
(27) Dussard, J. L., D. Sc. Thesis, M.I.T. (1954).
(28) Zenz, F. A., "Fluidization", ed, by D. F. Othmer, Reinhold Publishing Corp., New York (1956).
(29) Nat. Inst. Agr. Engrs. Record of Trial No. 47 (1947).
(30) Schwarz, H. W., Dr. Eng. Thesis, Johns Hopkins Univ. Baltimore (1957).
(31) Torobin, L. B., and Gauvin, W. H., A.I.Ch.E. Journal (In press).
(32) Tchen, C. M., "Mean Value and Correlation Problems Connected with the Motion of Small Particles Suspended in a Turbulent Fluid", Martinus Nijhoff, The Hague (1947).
(33) Liu, V. C., "Turbulent Dispersion of Dynamic Particles". Univ. Mich., Eng. Research Inst., Ann Arbor (1955).
(34) Corrsin, S., and Lumley, J. L., Appl. Sci. Research, **114** (1956).
(35) Lumley, J. L., Ph.D. Thesis, John Hopkins Univ., Baltimore (1957).
(36) Friedlander, S. K., A.I.Ch.E. Journal, **3:** 381 (1957).
(37) Mickelsen, W. R., Nat. Advisory Comm. Aeronaut. Tech. Notes, 3570 (1955).
(38) Dlouhy, J., and Gauvin, W. H., A.I.Ch.E. Journal, **6:** 29 (1960).
(39) Dlouhy, J., and Gauvin, W. H., Can. J. Chem. Eng., **38:** 113 (1960).
(40) Baldwin, L. V., Private Communication.
(41) Soo, S. L., Chem. Eng. Sci., **5:** 57 (1956).
(42) Soo, S. L., Tien, C. L., and Kadamb, V., Rev. Sci. Instr., **30:** 821 (1959).
(43) Soo, S. L., Ihrig, H. K. Jr., and El Kouh, A. F., 1959 Annual Mtg. Am. Soc. Mech. Engrs., (Atlantic City, N.J., 1959) Paper No. 59-A-59.
(44) Soo, S. L., and Tien, C. L., J. Appl. Mechanics, **27E,** 5 (1960).
(45) Peskin, R. L., Project Squid Report, PP-97-TR (ONR) (1959).
(46) Peskin, R. L., Project Squid Report, PR-92-P (ONR) (1959).
(47) Peskin, R. L., Proceedings of the 1960 Heat and Fluid Mechanics Institute, Stanford Univ., June 1960. Published by Stanford University Press.
(48) Konig, W., Ann. Phys. Leipzig., **42:** 43 (1891).
(49) Hanratty, T. J., Latinen, G., and Wilhelm, R. H., A.I.Ch.E. Journal, **2:** 372 (1956).
(50) Kada, H., and Hanratty, T. J., A.I.Ch.E. Journal, **6:** 624 (1960).
(51) Lewis, W. K., Gilliland, E. R. and Bauer, W. C., Ind. Eng. Chem. **41:** 1104 (1949).
(52) Mehta, N. G., Ph.D. Thesis, Purdue Univ. (1955).
(53) Mitlin, A., Ph.D. Thesis, Univ. London (1954).
(54) Chin-Yung Wen and Hashinger, R. F., A.I.Ch.E. Journal, **6:** 220 (1960).
(55) Osberg, G. L. and Charlesworth, D. H., Chem. Eng. Progr., **47:** 566 (1951).
(56) Culgan, J. M., Ph.D. Thesis, Georgia Inst. Techn. (1952).
(57) Richardson, J. F., and McLeman, M., Trans. Inst. Chem. Engrs., **38:** 257 (1961).
(58) Khudiakow, G. N., and Chukhanov, Z. F., Doklady Akad. Nauk. S.S.S.R. **78:** 681 (1951).
(59) Sinha, K. N., Mining Geol. Met. Inst. India, 123-144 (Discussion), 145 (1950).
(60) Gasterstadt, J., Diss. Techn. Hochsch. Dresden (1922).
(61) Green, H. L., In "Flow Properties of Dispersive Systems", Ed. by J. J. Hermans, North Holland Publishing Co., Amsterdam (1953).
(62) Thomson, I., Gen. Elec. Rev., **25:** 418 (1922).
(63) Vieweg, E., J. Phys. Chem., **30:** 865 (1926).
(64) Harper, J., Proc. Roy. Soc. **A205:** 83 (1951).
(65) Harper, J., Proc. Roy. Soc. **A218:** 111 (1953).
(66) Kunkel, M., J. Appl. Phys., **21:** 820 (1950).
(67) Sachsse, H., Ann. Physik. **14:** 396 (1934).
(68) Loeb, L. B., Science **102:** 573 (1945).
(69) Chapman, S., Physics **5:** 150 (1934).

★ ★ ★

Optimal Bypass Rates for Sequences of Stirred Tank Reactors[1]

RUTHERFORD ARIS[2]

A general method of finding the optimal volumes, temperatures and bypass rates for a sequence of stirred tank reactors is developed. After a discussion of the method of dynamic programming, the example of a sequence of adiabatic reactors of equal volume with a single reaction is used as an illustration. A simple graphical construction for determining the optimal bypass rates is given for this case. The limiting cases of the optimal control of a batch reaction by addition of cold feed is also solved.

We propose to consider several design problems for sequences of stirred tank reactors which arise when we require the operation to be optimal. It is well known that for certain reactions a higher yield may be attained by using two reactors at slightly different temperatures[1,2,3]. Denbigh[1] has given a very striking illustration of this for a system of four reactions and while so dramatic an increase in yield (25% with one reactor, 57% with two) is rare, even small increases in efficiency can represent considerable gains in profitability. The problems we wish to take up here are concerned with optimal bypass rates; other problems with stirred tanks have been dealt with elsewhere[3,4].

The general method to be used is that of dynamic programming which may briefly be described as follows. Consider a sequence of R stirred tanks (shown schematically in Figure 1) which we will number from the end to the beginning, so that the feed enters reactor R, passes to reactor $R-1$ and so on, leaving as product from reactor 1. At each stage we have certain design or control variables such as the temperature, pressure or holding time, which must be chosen in some sense optimally. The choice of design variables at stage r affects the course of the reaction in that reactor, and so the transformation of the state of the process stream that this reactor effects. The state of the stream may be specified by the concentrations, temperature etc. and we denote the set of values of these quantities in reactor r and in the stream leaving it by p_r. Thus the state of the feed is denoted p_{R+1} and that of the product by p_1. If the design variables at stage r are denoted by q_r the equations governing the behavior of the reactor may be written

$$p_r = S(p_{r+1}; q_r) \qquad (1)$$

This is perhaps a little abstract but the definite equations will be given later and for the moment this formula only means that when we have chosen the design variables q_r we know what the product state of the reactor r, p_r, will be for any feed state, p_{r+1}. This knowledge may be through a thorough understanding of the kinetics of the reaction and behavior of the stirred tank, or it may be purely empirical, a summary of operating experience.

Let us define a profit function $P(p_1; q_1, \ldots q_R)$ which expresses our estimate of the gain acruing from the reaction. In its simplest form P might simply be the yield of one particular species, but at a more realistic level it would take into account the cost associated with the design variables, q_r. In any case, given the feed state p_{R+1}, the profit P can be evaluated by means of Equation (1) as soon as the design variables $q_1, \ldots q_R$ have been specified. We want to find the optimal design policy, that is the set of values $q_1, \ldots q_R$ that make P as large as possible. There will normally be restrictions on these design variables, as for example when the temperature must be beneath some upper limit, and a design which satisfies these restrictions is called admissible. When the admissible policy that maximizes P has been found, this maximum value is a function only of the feed state and number of stages, so that we may write

$$f_R(p_{R+1}) = \text{Max } P \qquad (2)$$

We must also emphasise that the optimal policy is a function of R and p_{R+1} and this we do by referring to it, where necessary, as the optimal R-stage policy with respect to the feed state p_{R+1}.

We will consider a special form of the profit function that suffices for all our applications, namely

$$P = V(p_1) - V(p_{R+1}) - C(q_1) - \ldots C(q_R)$$
$$= \sum_1^R \{V(p_r) - V(p_{r+1}) - C(q_r)\} \qquad (3)$$

Here $V(p_r)$ represents the value of the process stream in the state p_r and $C(q_r)$ represents the cost of operating with conditions q_r. Each term of the sum in Equation (3) represents the net profit from one reactor as it increases the value of the stream from $V(p_{r+1})$ to $V(p_r)$ at a cost $C(q_r)$.

Let us build up the optimal R-stage policy a stage at a time. If $R = 1$ then

$$f_1(p_2) = \text{Max } \{V(p_1) - V(p_2) - C(q_1)\}, \qquad (4)$$

where this maximum has to be obtained by a right choice of q_1 and p_1 is given by

$$p_1 = S(p_2; q_1) \qquad (5)$$

This problem presents little difficulty for the number of design variables in q_1 is quite small. Now let this one stage be the second of two stages from which the profit will be

$$\{V(p_2) - V(p_3) - C(q_2)\} + \{V(p_1) - V(p_2) - C(q_1)\} \qquad (6)$$

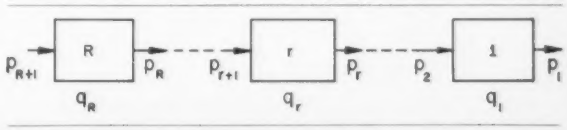

Figure 1—The general stage-wise process.

[1]*Manuscript received November 1, 1960; accepted February 27, 1961.*
[2]*Department of Chemical Engineering, University of Minnesota, Minneapolis, Minn., U.S.A.*

But whatever choice of q_2 is made we certainly cannot do better than to make the optimal choice of q_1 with respect to the state p_2 that results from the choice of q_2, for p_2 is the feed state to the final stage. Thus for any choice of q_2 the greatest value of (6) will be

$$\{V(p_2) - V(p_3) - C(q_2)\} + f_1(p_2)$$

and by varying our choice of q_2 we shall find the maximum of this namely,

$$f_2(p_3) = \text{Max}\{V(p_2) - V(p_3) - C(q_2) + f_1(p_2)\} \quad \ldots\ldots\ldots\ldots (7)$$

Again this is no great burden since only a few design variables have to be simultaneously chosen. Proceeding in this way we make the two stages, whose optimal policy and profit we now know, the last two of three stages, and in seeking the optimal three stage policy vary only the conditions in the first stage and always use the optimal two stage policy with respect to the state this produces. Thus in general

$$f_R(p_{R+1}) = \text{Max}\{V(p_R) - V(p_{R+1}) - C(q_R) + f_{R-1}(p_R)\} \quad \ldots\ldots (8)$$

and the maximization is attained by correct choice of q_R.

To see how vast an economy this can introduce consider a six stage process with two design variables, q, at each stage and two variables, p, specifying the state. Suppose that a search over ten values of each of the variables in q is sufficient to determine the maximum then if the conditions in all six stages were varied simultaneously in the search for the maximum 10^{12} calculations would be needed. By dynamic programming only 10^2 calculations are needed in determining the maximum at any one stage but f_{R-1} has to be done for a sufficient range of values of the feed state p_R to allow of its being used for the next step in Equation (8). Suppose this also requires ten values of each variable in p, then $10^2 \times 10^2 = 10^4$ calculations will be needed at each of the first five stages and so a total of 50,100 calculations are needed for all six stages. The undirected search would thus take at least ten million times longer than the dynamic program. This is the ratio of some 20 years to one minute! Of course the unorganized simultaneous variation of all 12 design variables is about the least intelligent way of tackling the problem and it will immediately be suggested that a steepest ascent would be much better. This is indeed true but even if it reduced the number of calculations to that of the dynamic program it would still produce far less information. For the dynamic program produces the optimal r-stage policies $r = 1, 2, \ldots R-1$ for a whole range of feed states, whereas a direct search can at best only provide them for a few, rather arbitrary states, and in an intelligent design all such information is needed.

To conclude this general introduction let us see how the results of a dynamic programming calculation can be presented. Table 1 is constructed with R major sections and, given the feed state p_{R+1}, we enter the table in section R at this value. Corresponding to it we can read of from the succeeding columns the optimal policy for stage R, the resulting state and the maximum value of the profit function. But the remaining stages use the optimal $(R-1)$-stage policy with respect to their feed state p_R, so that the conditions in stage $R-1$ can be found by entering section $R-1$ at p_R as shown. This course is pursued all the way up the table and the complete optimal policy extracted. Notice that it could have been found equally easily for any fewer number of stages. We also notice that the algorithm (8) is ideally suited to the digital computer for it is completely recursive and makes minimal demands on storage capacity. "0" denotes the relevant entry in the table.

TABLE 1

No. of stages	Feed state	Optimal policy	Product state	Optimal profit function
1	p_2	q_1	p_1	f_1
	0	0	0	
2	p_3	q_2	p_2	f_2
	0	0	0	
$R-1$	p_R	q_{R-1}	p_{R-1}	f_{R-1}
	0	0	0	
R	p_{R+1}	q_R	p_R	f_R
	0	0	0	0

The Adiabatic Sequence of Stirred Tanks

It is well known that a reversible exothermic reaction goes most rapidly if the temperature is made to decrease as the reaction proceeds. At any composition there is an optimal temperature at which the reaction rate is greatest and this is the temperature that should be used[3, 5]. A rather simple method of attaining this by bypassing cold feed suggests itself and is illustrated in Figure 2. Of the total flow q a fraction $\lambda_R q$ is preheated to a temperature T_{R+1} and fed to reactor R. The product is now mixed with a bypass flow of the unreacted feed at its original temperature T_o to make up a flow of $\lambda_{R-1}q$ to reactor $(R-1)$. This mixing with cold feed takes place before (or, since they are well mixed, equivalently in) each reactor, until finally all of the original flow passes to the last reactor (reactor 1) and emerges as product. Each stage is insulated and the only heat added to the system is in the preheater so that it should be possible to achieve an optimal sequence of temperatures by rightly choosing T_{R+1}, λ_R, $\lambda_{R-1}, \ldots \lambda_2$, subject to $\lambda_R \leqslant \lambda_{R-1} \leqslant \ldots \leqslant \lambda_2 \leqslant \lambda_1 = 1$. But these quantities will have to be very nicely chosen for too little bypass will not decrease the temperature sufficiently, whereas too much will retard the reaction.

If the single reaction $\sum_1^n a_i A_i = 0$ is taking place between the n chemical species $A_1, \ldots A_n$, the concentration c_i of A_i at any time can be written

$$c_i = c_{io} + a_i c \quad \ldots\ldots\ldots\ldots\ldots\ldots\ldots\ldots (9)$$

Here c is the extent of reaction and c_{io} the concentration of A_i in the original feed. The state of the process stream in and leaving reactor r can thus be described by two quantities, the extent of reaction, c_r, and the temperature, T_r. The cold unreacted feed is in the state $c = 0$, $T = T_o$. The problem we will consider is that of obtaining the greatest extent of reaction in the final product (i.e. maximizing c_1) in a sequence of tanks of equal volume, V. Now since $\lambda_1 = 1$ and $c_{R+1} = 0$ we can write this

$$c_1 = \lambda_1 c_1 - \lambda_{R+1} c_{R+1} = \sum_1^R (\lambda_r c_r - \lambda_{r+1} c_{r+1}), \quad \ldots\ldots\ldots\ldots (10)$$

where $\lambda_{R+1} = \lambda_R$ as there is no bypassing before the first stage.

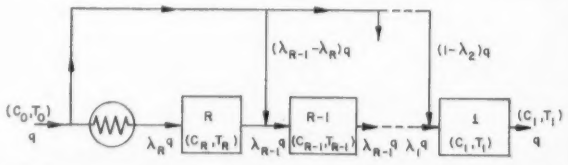

Figure 2—The sequence of adiabatic stirred tanks with bypassing.

The rate of reaction, namely the rate of change of c by reaction, is a known function of the concentrations and temperature and so, by (9), of c and T; we write it as $r(c,T)$. A mass balance of A_i over reactor r and a heat balance yield the equations

$$\lambda_r q c_{ri} - \lambda_{r+1} q c_{i,r+1} - (\lambda_r - \lambda_{r+1}) q c_{io} = \alpha_i V r(c_r, T_r) \quad \ldots\ldots\ldots (11)$$

and

$$\lambda_r q T_r - \lambda_{r+1} q T_{r+1} - (\lambda_r - \lambda_{r+1}) q T_o = H V r(c_r, T_r), \quad \ldots\ldots\ldots (12)$$

where

H = heat of reaction/mean molar heat of reagents

By means of Equation (9) all the Equations (11) $i = 1, \ldots n$ become a single equation

$$\lambda_r c_r - \lambda_{r+1} c_{r+1} = V r(c_r, T_r)/q \quad \ldots\ldots\ldots (13)$$

If we make a slight change of temperature variable and write

$$t = (T - T_o)/H \quad \ldots\ldots\ldots (14)$$

and

$$R(c,t) = (V/q) r(c,T) \quad \ldots\ldots\ldots (15)$$

then (12) and (13) can be written

$$\lambda_r t_r - \lambda_{r+1} t_{r+1} = \lambda_r c_r - \lambda_{r+1} c_{r+1} = R(c_r, t_r) \quad \ldots\ldots\ldots (16)$$

It is necessary now to distinguish between the first stage reactor R with its associated preheater and the remaining stages for the first is not truly adiabatic and involves a cost of heating that the others do not. Let

$$f_r(c_{r+1}, t_{r+1}) = \text{Max} \sum_1^r (\lambda_s c_s - \lambda_{s+1} c_{s+1}), \; r = 1, \ldots R-1, \quad \ldots\ldots (17)$$

be the maximum value of the profit function attained in the r adiabatic stages terminating with reactor 1. For this maximization the bypass ratios $\lambda_{r+1}, \lambda_r, \ldots \lambda_2$ have to be chosen optimally. Applying the principle of optimality embodied in Equation (8)

$$f_r(c_{r+1}, t_{r+1}) = \text{Max} \{\lambda_r c_r - \lambda_{r+1} c_{r+1} + f_{r-1}(c_r, t_r)\} \quad \ldots\ldots\ldots (18)$$

where now only λ_{r+1} has to be chosen since λ_r is known from the $(r-1)$-stage policy. The choice of λ_{r+1} is restricted only by

$$0 \leqslant \lambda_{r+1} \leqslant \lambda_r \quad \ldots\ldots\ldots (19)$$

For the whole process we should take account of the cost of preheating to a temperature $T_{R+1} (= T_o + H t_{R+1}/c_p)$. Let this be expressed as a fraction of the value of a unit extent of reaction by the function $h(t_{r+1})$. Then the final choice of preheat temperature will be the value of t_{R+1} that maximizes

$$\lambda_R c_R + f_{R-1}(c_R, t_R) - h(t_{R+1}) \quad \ldots\ldots\ldots (20)$$

where

$$\lambda_R c_R = \lambda_R (t_R - t_{R+1}) = R(c_R, t_R) \quad \ldots\ldots\ldots (21)$$

Equations (16), (18) and (19) can be solved for $r = 1,2, \ldots R-1$ to give $\lambda_2, \ldots \lambda_R$ and then Equations (20) and (21) can be solved for t_{R+1}. This is a simple enough matter on the computer and little more could be said were it not that a rather simple graphical construction illuminates the whole problem.

We observe first that by Equation (16) we can write $c_1 = \sum_1^R R(c_r, t_r)$, so that we have to maximize the sum of the reaction rates at each stage. Now in a plane with coordinates c and t the curves of constant R are as shown by the full lines in Figure 3, the upper curve corresponding to a smaller value of R. Consider first the determination of

$$f_1(c_2, t_2) = \text{Max}(c_1 - \lambda_2 c_2) = \text{Max } R(c_1, t_1) \quad \ldots\ldots\ldots (22)$$

The point $(\bar{c}_1, \bar{t}_1) = (\lambda_2 c_2, \lambda_2 t_2)$ lies on the line from the origin through (c_2, t_2) and represents the state of the stream after mixing with a fraction $(1 - \lambda_2)$ of cold unreacted feed. Indeed by Equation (16) which can be written

$$t_1 - \bar{t}_1 = c_1 - \bar{c}_1 = R(c_1, t_1) \quad \ldots\ldots\ldots (23)$$

we see that it is the feed state to reactor 1. We also see by this

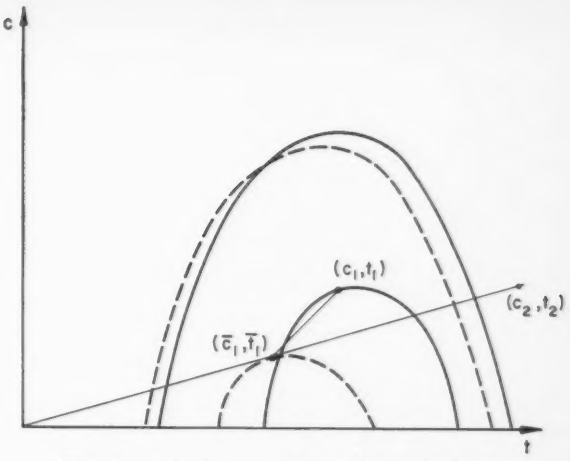

Figure 3—Optimal conditions for a single stage.

equation that in the c, t-plane the feed state $(\bar{c}_1, \bar{t}_1)$ lies below and to the left of the product state (c_1, t_1) by a distance $R(c_1, t_1)$. We may thus draw a set of loci of $\bar{c}_1, \bar{t}_1$ for which the reaction rate $R(c_1, t_1)$ is constant; these are shown as broken lines in Figure 3. Now for any given (c_2, t_2) it is evident that $(\bar{c}_1, \bar{t}_1)$ should be chosen to be the point where one of the broken curves is tangent to the ray through (c_2, t_2), for this will give the largest value of R and so by (22) of the increased yield. Evidently this point $(\bar{c}_1, \bar{t}_1)$ is the same for all points (c_2, t_2) on the same ray (i.e., having the same value of the ratio c_2/t_2), though the value of λ_2 required to attain it varies with the point (c_2, t_2), for $\lambda_2 = \bar{c}_1/c_2$. However it is easily possible to draw the locus, $\bar{\Gamma}_1$, of the tangent points $(\bar{c}_1, \bar{t}_1)$ and the locus, Γ_1, of corresponding points (c_1, t_1) given by Equation (23). With these two loci the construction is immediate. Given any state (c_2, t_2) we join this point to the origin and draw a line of unit slope from the intersection of this ray with $\bar{\Gamma}_1$ to Γ_1. λ_2 is the ratio of the distance from the origin to the intersection with $\bar{\Gamma}_1$ to the distance from the origin to (c_2, t_2) and f_1 is the difference in ordinate between $\bar{\Gamma}_1$ and Γ_1. Evidently $f_1(c_2, t_2) = 0$ if (c_2, t_2) lies to the left of $\bar{\Gamma}_1$, whilst if (c_2, t_2) is to the right of $\bar{\Gamma}_1$, $f_1(c_2, t_2) = \phi(c_2/t_2)$ is a function only of the ratio c_2/t_2.

Consider now two stages for which by (16) and (18)

$$f_2(c_3, t_3) = \text{Max}\{R(c_2, t_2) + f_1(c_2, t_2)\}.$$

In looking for this maximum we might as well look for it in the easiest way possible, namely along a ray from the origin since f_1 is constant on this. But R is greatest if (c_2, t_2) is a point of tangency of the ray with a curve of constant R. The locus Γ_2 of optimal states (c_2, t_2) can thus be drawn immediately and the locus $\bar{\Gamma}_2$ of states representing the optimal feed is obtained by taking a point a distance $R(c_2, t_2)/\lambda_2$ below and to the left of (c_2, t_2) for

$$c_2 - (\lambda_3/\lambda_2) c_3 = t_2 - (\lambda_3/\lambda_2) t_3 = R(c_2, t_2)/\lambda_2$$

and λ_2 is known from the one stage policy. Thus for any point (c_3, t_3) the point $(\bar{c}_2, \bar{t}_2) = (\lambda_3 c_3, \lambda_3 t_3, \lambda_2)$ lies on $\bar{\Gamma}_2$ and we see again how λ_3 and f_2 can be found graphically. It is again clear that $f_2(c_3, t_3)$ is zero to the left of $\bar{\Gamma}_2$ and a function only of the ratio c_3/t_3 to the right. It follows that in seeking Γ_3 the locus of optimal conditions (c_3, t_3) we shall be led to the same curve as Γ_2, the locus of points of contact of rays with curves of the family R = constant.

In this way a system of curves can be drawn $\Gamma_1, \Gamma_2, \ldots \Gamma_{R-1}$, $\bar{\Gamma}_1, \bar{\Gamma}_2, \ldots \bar{\Gamma}_{R-1}$, where by coincidence $\Gamma_2, \Gamma_3, \ldots \Gamma_{R-1}$ are coincident. It is illustrated in Figure 4 for $R = 4$. A is the point (c_4, t_4) and this joined to the origin 0 intersecting $\bar{\Gamma}_3$ at B. BC is the line of unit slope with C on $\Gamma_3 \equiv \Gamma_2$ and D the intersection of DC and $\bar{\Gamma}_2$. We proceed in this way up to G on Γ_1, and have immediately that $f_3(c_4, t_4)$ is the difference

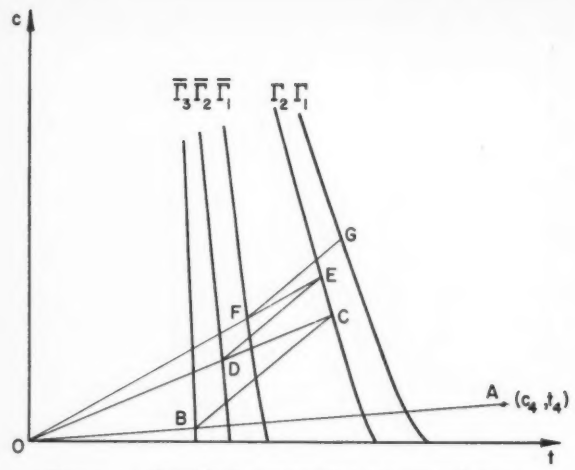

Figure 4—Graphical construction for several stages.

in ordinates of G and B. The bypass ratios are given by $\lambda_2 = OF/OE$, $\lambda_3/\lambda_2 = OD/OC$ and $\lambda_4/\lambda_3 = OB/OA$.

For the final stage, reactor R, we will take a simple form for the preheating cost and assume that it is proportional to the amount of heat supplied, $h = \alpha\lambda_R t_{R+1}$. Then by Equation (20) we have to maximize

$$\lambda_R c_R + f_{R-1}(c_R, t_R) - \alpha\lambda_R t_{R+1}$$

This is a simple direct calculation in which any point $(0, t_{R+1})$ is taken and the point (c_R, t_R) on the line of unit slope through it which satisfies Equation (21) is found by trial and error. Then the quantity $c_R + f_{R-1}/\lambda_R$ can be plotted as a function of t_{R+1}. For any given α the optimal t_{R+1} is the point where this curve has slope α. Thus the t-axis could be graduated in values of α and the curve Γ_R drawn and the construction would be immediate.

Needless to say the whole calculation would be a matter of seconds on a digital computer, which would be very suitable for controlling the reactor. Suppose that the preheater is a heat exchanger dependent on some other part of the factory and so liable to uncontrolled variation. Then a measurement of t_{R+1} could be fed to a computer and the computer activate the valve adjustment mechanisms to keep the bypass rates optimal. It would not be much harder, though the calculation would have to be rather differently formulated, to control for variations in the total flow rate or in the basic feed temperature. If the function $r(c, T)$ were sufficiently well established it might be that the computer should be used to calculate a set of tables from which these adjustments would be made by hand.

The General Bypass Design Problem

The problem we have used in the previous paragraph to exhibit the method of dynamic programming is a particularly simple one. We now give a general algorithm which allows us to determine the size and rate of heat removal, as well as the bypass rate, at each state which will maximize a very general expression for the profit.

Let m independent simultaneous reactions $\sum_{i=1}^{n} a_{ij}A_i = 0$, $j = 1, \ldots m$, be taking place between the n species, $A_1, \ldots A_n$. Then in place of Equation (9) we have to write for the concentration of A_i

$$c_i = c_{io} + \sum_{j=1}^{m} a_{ij}c^j,\ i = 1, \ldots n, \quad \ldots\ldots(24)$$

where c^j is the extent of the j^{th} reaction and c_{io} the concentration of A_i in the feed. The time rate of change of c^j by reaction is r^j, a known function of composition and temperature and so by (24) a known function of the extents $c^1, \ldots c^m$ and T. Then a mass balance for A_i gives

$$\lambda_r q c_{ir} - \lambda_{r+1} q c_{i,r+1} - (\lambda_r - \lambda_{r+1}) q c_{io} = V_r \sum_{j=1}^{m} a_{ij} r^j(c^1, \ldots c^m, T)$$

or by substitution from (24)

$$q \sum_{j=1}^{m} a_{ij} \{\lambda_{r+1} c^j_{r+1} - \lambda_r c^j_r + \theta_r r^j(c^1_r, \ldots c^m_r, T_r)\} = 0, \quad \ldots\ldots(25)$$

where $\theta_r = V_r/q$ and c^j_r is the extent of reaction in reactor r. But in saying that the reactions $\Sigma a_{ij}A_i = 0$ were independent we meant that the only set of numbers $\beta_1, \ldots \beta_m$ such that $\sum_1^m a_{ij}\beta_j = 0$ is the trivial set $\beta_1 = \beta_2 = \ldots = \beta_m = 0$. It follows therefore that the bracketed expressions in (25) must be zero and we have m equations

$$\lambda_{r+1} c^j_{r+1} - \lambda_r c^j_r + \theta_r r^j(c^1_r, \ldots c^m_r, T_r) = 0, \quad \ldots\ldots(26)$$

$$j = 1, \ldots m$$

A heat balance will give an equation

$$\lambda_{r+1} T_{r+1} - \lambda_r T_r - (\lambda_r - \lambda_{r+1}) T_o + \theta_r \sum_{j=1}^{m} H_j r^j - Q_r = 0 \quad \ldots\ldots(27)$$

where the H_j are the heats of reaction divided by the mean molar heat of the reactants and Q_r is proportional to the rate of heat removal from reactor r.

In the optimal design problem we now have $3R$ quantities to choose for R reactors, $\theta_1 \ldots \theta_R$, $Q_1, \ldots Q_R$, $\lambda_2, \ldots \lambda_R$ and T_{R+1}. Because of the non-linear way in which T enters the equations it is probably more convenient to choose $T_1, \ldots T_R$ and use Equation (27) to calculate $Q_1, \ldots Q_R$. The profit function may be constructed quite generally. Let $v(c^1, \ldots c^m)$ be the value of a unit volume of the process stream when the reactions have proceeded to the extents $c^1, \ldots c^m$. Then the gain in value by the reaction is,

$$q\{v(c^1_1, \ldots c^m_1) - v(0, \ldots 0)\} =$$

$$q \sum_{1}^{R} \{\lambda_r \bar{v}(c^1_r, \ldots c^m_r) - \lambda_{r+1} \bar{v}(c^1_{r+1}, \ldots c^m_{r+1})\} \quad \ldots\ldots(28)$$

where $$\bar{v}(c^1, \ldots c^m) = v(c^1, \ldots c^m) - v(0, \ldots 0) \quad \ldots\ldots(29)$$

The cost of constructing and operating a reactor of volume $V_r = q\,\theta_r$ at temperature T_r will be a function $C(V_r, T_r, \lambda_r q) = c_r$ and the cost of preheating to a temperature T_{r+1} can be absorbed into the expression for this cost in reactor R. We therefore have a net profit

$$P_R = \sum_{1}^{R} p_r = \sum_{1}^{R} [q\{\lambda_r \bar{v}_r - \lambda_{r+1} \bar{v}_{r+1}\} - C_r], \quad \ldots\ldots(30)$$

where $\bar{v}_r$ denotes $\bar{v}(c^1_r, \ldots c^m_r)$.

When the design variables are chosen and the feed state $c^1_{R+1}, \ldots c^m_{R+1}$, T_{R+1} is specified Equations (26) and (27) can be solved and the net profit P_R calculated. Its maximum value is thus a function only of the feed state,

$$f_R(c^i_{R+1}, T_{R+1}) = \text{Max } P_R \quad \ldots\ldots(31)$$

Applying the principle of optimality we are led to the sequence of equations

$$f_r(c^i_{r+1}, T_{r+1}) = \text{Max}\{p_r + f_{r-1}(c^i_r, T_r)\},\ r = 1, \ldots R-1, \quad \ldots\ldots(32)$$

where the maximization is by suitable choice of V_r, T_r and λ_{r+1}. This maximization will reveal whether or not a bypass is needed ($\lambda_r = \lambda_{r+1}$ for no bypass) or if the reactor should be adiabatic ($Q_r = 0$). The design variables will be subject to certain restrictions probably of the form

$$V_r \leqslant V^*,\ T_* \leqslant T_r \leqslant T^*,\ 0 \leqslant \lambda_{r+1} \leqslant \lambda_r, \quad \ldots\ldots(33)$$

but this makes the search easier for it limits the region within which the maximum must be found.

In the final step with feed composition $c^i = 0$ $T = T_o$ we have

$$f_R(0,T_o) = \text{Max}\{p_R + f_{R-1}(c^i{}_R, T_R)\}, \quad \ldots\ldots\ldots (34)$$

where p_R involves the cost of the arrangements for preheating, if these are economic.

A Limiting Case

It is interesting to consider the batch reaction as the limiting case of an infinite number of infinitesimal stirred tanks. We cannot take over the model of section 2 with tanks of equal volume, for the actual holding time in stage r is $V/\lambda_r q$. Thus letting $V \to 0$ would lead to infinitesimal time intervals of varying length and the limit would not describe the batch reaction. Rather we must let the volume V_r of the stage vary so that the holding time is constant, i.e., $V_r = \lambda_r V$, where V is the volume of stage 1. Then Equation (16) become

$$\lambda_r t_r - \lambda_{r+1} t_{r+1} = \lambda_r c_r - \lambda_{r+1} c_{r+1} = \lambda_r \, Vr(c_r,t_r)/q \quad \ldots\ldots\ldots (35)$$

Defining $f_r(c_{r+1}, t_{r+1})$ in the same way as before we have the same general Equation (18) and the same one stage policy. However the equation for two stages now reads

$$\begin{aligned} f_2(c_3,t_3) &= \text{Max}\{\lambda_2 c_2 - \lambda_3 c_3 + f_1(c_2,t_2)\} \\ &= \text{Max}\{\lambda_2 \, Vr(c_2,t_2)/q + f_1(c_2,t_2)\} \end{aligned}$$

If we look for this maximum along a ray of constant c_2/t_2, f_1 is constant as before and λ_2 is inversely proportional to c_2. This time therefore we do not look for the maximum value of r (the point of tangency with curves r = constant) but for the maximum value of r/c_2. But on the ray $c_2 = \beta t_2$, $r/c_2 = r(c_2, c_2/\beta)/c_2$ and this has a maximum where

$$c_2{}^2 \frac{d}{dc_2}\left(\frac{r(c_2,c_2/\beta)}{c_2}\right) = c_2 \frac{\partial r}{\partial c_2} + t_2 \frac{\partial r}{\partial t_2} - r = 0$$

This defines a fixed locus in the (c, t) plane, which is the projection on to the (c, t) plane of the line along which a straight line from the origin would touch the three dimensional surface $r(c, t)$. The locus of corresponding inlet points $\bar{c}_2 = (\lambda_3/\lambda_2)c_3$ and $\bar{t}_2 = (\lambda_3/\lambda_2)t_3$ is now given by

$$c_2 - \bar{c}_2 = t_2 - \bar{t}_2 = Vr(c_2,t_2)/q,$$

and since V/q is constant this also is a fixed locus in the c, t plane. These two loci can be labelled Γ_2 and $\bar{\Gamma}_2$ respectively in accordance with the preceding example, but this time we see that as the construction proceeds all the Γ_r curves will coincide with Γ_2 and all the $\bar{\Gamma}_r$ with $\bar{\Gamma}_2$. What is more as $V \to 0$ these two curves will approach one another, so that for a very large number of very small stages the system would be described by a line zig-zagging between two adjacent curves $\bar{\Gamma}_2$ and Γ_2. In the limit $V = 0$ these coincide in a single curve Γ whose equation is $cr_c + tr_t - r = 0$.

Now the limiting form of Equation (35) can be obtained by letting $\tau = rV/q$ be the current time measured from the end of the process and $\theta = RVq$ be the total time. Now let $V \to 0$ and $R \to \infty$ so that θ is constant, then λ_r, c_r and t_r are replaced by $\lambda(\tau)$, $c(\tau)$ and $t(\tau)$ and

$$\frac{d}{d\tau}(\lambda c) = \frac{d}{d\tau}(\lambda t) = -\lambda r(c,t)$$

Since in a batch reaction the quantity that is directly controllable is the rate of addition of cold reagents, namely $d\lambda/d\tau$, we might write the equations

$$\frac{d\lambda}{d\tau} = -\mu, \quad \ldots\ldots\ldots (36)$$

$$\frac{dc}{d\tau} = -r(c,t) + \frac{\mu c}{\lambda} \quad \ldots\ldots\ldots (37)$$

$$\frac{dt}{d\tau} = -r(c,t) + \frac{\mu t}{\lambda} \quad \ldots\ldots\ldots (38)$$

λ is the fraction of the final volume that is there at time τ and since this is increasing as τ decreases to zero, μ is positive.

It would appear then that if the batch process controlled by the addition of cold reagent is indeed the limit of the stagewise process then it should be induced to proceed along the curve Γ. Two questions then arise: in the first place how is μ to be controlled to keep on Γ and secondly if the state of the system is not on Γ how can it most rapidly be brought there?

The first question may be quickly answered. If $t = \gamma(c)$ is the equation of Γ elimination of r between (37) and (38) and integration gives

$$\{\gamma(c) - c\} = \lambda_1 \{\gamma(c_1) - c_1\} \quad \ldots\ldots\ldots (39)$$

where c_1 is the value of c when $\lambda = \lambda_1$. The required value of μ is

$$\mu = \lambda r[c,\gamma(c)] \{[1 - \gamma'(c)]/[\gamma(c) - c\gamma'(c)]\} \quad \ldots\ldots\ldots (40)$$

The second question requires rather a different approach. Let $c(\theta)$, $t(\theta)$ and $\lambda(\theta)$ be given and let us ask for the control action $\mu(\tau)$, $\theta \geqslant \tau \geqslant 0$, that will maximize the net conversion $\lambda(0)c(0) - \lambda(\theta)c(\theta)$. Let this maximum conversion be

$$f(u,v,w,\theta) = \text{Max} \int_o^\theta \lambda r(c,t) \, d\tau \quad \ldots\ldots\ldots (41)$$

where c, t and λ satisfy the Equations (36)–(38) and the initial conditions

$$c(\theta) = u, \quad t(\theta) = v, \quad \lambda(\theta) = w \quad \ldots\ldots\ldots (42)$$

Now if σ is a positive quantity less than θ

$$f(u,v,w,\theta) = \text{Max}\left[\int_{\theta-\sigma}^{\theta} \lambda r \, d\tau + \int_o^{\theta-\sigma} \lambda r \, d\tau\right]$$

The maximization is still by choice of μ, $\theta \geqslant \tau \geqslant 0$, but if in the second integral we do not make an optimal choice of μ, $\theta - \sigma \geqslant \tau \geqslant 0$, with respect to the initial conditions $c(\theta - \sigma)$, $t(\theta - \sigma)$, $\lambda(\theta - \sigma)$, we shall certainly not attain the maximum. Thus Bellman's principle of optimality leads us to write

$$f(u,v,w,\theta) = \text{Max}\left[\int_{\theta-\sigma}^{\theta} \lambda r d\tau + f[c(\theta-\sigma), t(\theta-\sigma), \lambda(\theta-\sigma), \theta-\sigma]\right] \quad \ldots (43)$$

and in this maximization μ has only to be chosen in the interval $\theta \geqslant \tau \geqslant \theta - \sigma$. In the limit $\sigma \to 0$ only $\mu(\theta)$ has to be chosen and the limit of Equation (43) is the partial differential equation

$$f_\theta = \text{Max}[r(u,v)\{w + f_u + f_v\} + \mu\{f_w - (uf_u + vf_v)/w\}] \quad \ldots (44)$$

Here the maximization is by choice of $\mu = \mu(\theta)$ and this choice is obvious. If

$$\Delta = f_w - (uf_u + vf_v)/w \quad \ldots\ldots\ldots (45)$$

is positive μ should be as large as possible; if Δ is negative μ should be as small as possible. There will be a limit to the rate at which cold reagents can be added so that

$$0 \leqslant \mu \leqslant \nu, \quad \ldots\ldots\ldots (46)$$

then $\mu = 0$ if $\Delta < 0$ and $\mu = \nu$ if $\Delta > 0$.

This type of control in which the controlled variable is at one or the other of its extreme positions has been variously styled on-off, relay or bang-bang. Δ is evidently a discriminating function saying when adding more reagent is worthwhile ($\Delta > 0$) and when it is not ($\Delta < 0$). The nature of the situation is such that when it is worthwhile to add more it should be added at the greatest possible rate and that when it is not worthwhile it should be cut off altogether. The curve along which $\Delta = 0$ is a switching boundary between these two extremes and on it μ can take any value. We should be inclined to identify

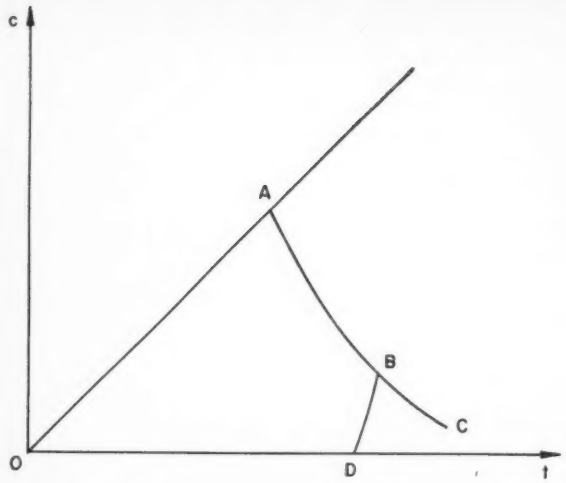

Figure 5—Optimal control of batch reaction by the addition of cold reagents.

this switching boundary with the curve Γ obtained as the limit of the stagewise process. This identification can be established from Equation (44) by considering the characteristic equations of this partial differential equation. We find first of all that the characteristics are reaction paths, so that Γ is a characteristic. Then by differentiating the discriminant function Δ along a characteristic we find

$$d\Delta/d\theta = -\{1 + (f_u + f_v)/w\}\,(ur_u + vr_v - r),$$

so that Δ is constant on Γ since its equation is $ur_u + vr_v = r$. But this constant can only be zero for were it not μ would be either zero or ν and the reaction path would not stay on Γ.

We should also consider the possibility that the value of μ given by Equation (40) exceeds the upper bound ν on Γ. In Figure 5 the curve *ABC* is Γ and on *AB* the value of μ given by (40) is less than ν but on *BC* it is greater. Let *BD* be the reaction path through *B* on which $\mu = \nu$, then in this case the switching boundary should be *ABD*. The optimal policy can be stated as follows: if the state of the system is represented by a point lying in the sector *OABD* the reaction should be allowed without addition of cold reagents: if the state of the system lies to the right of *ABD* or on the boundary *BD* cold reagents should be added as rapidly as possible: for states on *AB* the rate of addition is given by Equation (40).

Nomenclature

A_i	=	chemical species, $i = 1,\ldots n$
$C(q)$	=	cost of operating under conditions q
c	=	extent of a single reaction
c_i	=	concentration of A_i
c_{i_0}	=	initial concentration of A_i
c^j	=	extent of j^{th} reaction
$f_R(p_{R+1})$	=	maximum profit from R stages with feed state p_{R+1}
H	=	heat of reaction/mean molar heat of reagents
$h(t)$	=	cost of preheating to temperature t
P	=	profit function
p_r	=	state vector for stream leaving stage r
Q_r	=	rate of heat removal from stage r
q_r	=	control variable vector for stage r
q	=	flow rate
R	=	number of reactors or stages
$R(c,t)$	=	$(V/q)r(c,t)$
$r(c,t)$	=	rate of reaction in the case of a single reaction
r^j	=	rate of j^{th} reaction.
$S(p_{r+1}; q_r)$	=	transformation of state effected in stage r
T	=	temperature
T_o	=	temperature of cold reagents
T_*, T^*	=	lower and upper bounds on temperature
t	=	reduced temperature, $c_p(T - T_o)/(-\Delta H)$
u	=	initial value of c
V_r	=	volume of reactor r
V^*	=	upper bound on reactor volume
$V(p)$	=	value of stream in state p
v	=	initial value of t
$v(c^j)$	=	value of stream when reactions are at extents c^j
w	=	initial value of λ
α_i, α_{ij}	=	stoichiometric coefficients
β	=	proportionality constant
$\gamma(c)$	=	equation of the curve Γ
Δ	=	$uf_u + vf_v - wf_w$
θ	=	total time of process
θ_r	=	holding time of r^{th} reactor
λ	=	amount of reagent present
λ_r	=	fraction of total flow through stage r
μ	=	rate of addition of reagents
ν	=	upper bound of μ
τ	=	time from the end of the process

Suffix Notation:

i	=	value belonging to i^{th} chemical species
j	=	value associated with j^{th} reaction
R	=	value in stage R, the first stage of an R-stage process
r	=	value in stage r, the r^{th} stage from the end of the process
1	=	value in stage 1, the last stage of the process

References

(1) Denbigh, K. G., Chem. Eng. Sci., **8,** 125-131 (1958).
(2) Aris, R., Chem. Eng. Sci., **12,** 56-64 (1960).
(3) Aris, R., The optimal design of chemical reactors, New York, Academic Press (1961).
(4) Aris, R., Chem. Eng. Sci. in the press (1960).
(5) Denbigh, K. G., Trans. Faraday Soc., **40,** 352-373 (1944).

★ ★ ★

The Effect of Intraparticle Temperature Distribution on the Catalytic Effectiveness Factor of a Porous Catalyst[1]

T. AKEHATA[2], S. NAMKOONG[2], H. KUBOTA[2] and M. SHINDO[2]

The effect of intraparticle temperature distribution on the catalytic effectiveness factor is derived, and its magnitude is estimated using an approximate solution. These calculations show that for the several cases examined the term containing the effect of temperature is less than 10% of that due to the concentration effect.

In reaction kinetic studies dealing with porous catalysts, the effect of intraparticle diffusion on reaction rate is taken into account by "a catalytic effectiveness factor" which was first introduced by Thiele[1]. Methods of calculating this factor have been presented by Thiele[1] and Wagner[2] for first order or pseudo first order reactions, and by Kubota and Shindo et al[3,4] for other than first order reactions. In all these cases, however, the temperature distribution within the catalyst pellet has been considered uniform.

Recently Prater[5] has pointed out that the temperature and concentration within a pellet are simply related, and that occasionally the temperature difference between the centre and the outer catalyst surface may be rather large. Methods of calculating the effect of intraparticle temperature distribution on the catalytic effectiveness factor are presented, along with illustrative calculations for a few commercially important reactions.

Fundamental Equations and their Solutions

Assuming a steady state, and that a catalyst having any shape can be replaced by an equivalent spherical form, the concentration distribution of a particular component within the pellet may be obtained from the solution of the following equation;

$$D_i\left(\frac{d^2c}{dr^2}+\frac{2}{r}\frac{dc}{dr}\right)+v_i(c,t)=0 \qquad (1)$$

and the temperature distribution from the solution of

$$\lambda_i\left(\frac{d^2t}{dr^2}+\frac{2}{r}\frac{dt}{dr}\right)+v_i(c,t)Q=0 \qquad (2)$$

with boundary conditions

$$\begin{aligned} dc/dr &= dt/dr = 0 && \text{at } r=0\\ c &= c_s,\ t=t_s && \text{at } r=d_p/2 \end{aligned} \qquad (3)$$

where v_i is reaction rate, defined as moles increase of the particular component per unit time per unit volume of catalyst pellet.

[1]*Manuscript received June 30; accepted February 10, 1961.*
[2]*Tokyo Institute of Technology, Tokyo, Japan.*

Equations (1) and (2) may be combined to relate concentration and temperature, as indicated by Prater[5].

$$t=\left(\frac{D_iQ}{\lambda_i}\right)(c-c_s)+t_s=g(c) \qquad (4)^*$$

Substitution of Equation (4) into Equation (1) yields

$$D_i\left(\frac{d^2c}{dr^2}+\frac{2}{r}\frac{dc}{dr}\right)+v_i[c,g(c)]=0 \qquad (5)$$

Numerical Solution: Equation (5) may be solved by a numerical method as indicated by Kubota and Shindo[3] even when the reaction rate is not first order, or is given in graphical or in tabular form. The catalytic effectiveness factor defined as

$$E_f=\frac{\int_0^{d_p/2}4\pi r v_i[c,g(c)]\,dr}{(1/6)\pi d_p^3\,v_i(c_s,t_s)} \qquad (6)$$

is found as a function of c_s and t_s.

Approximate Solution: The numerical method above is rather tedious, so that an approximate method simplifying the calculations is desirable.

Consider first the case when the temperature within the pellet is uniform. Equation (1) may be converted into Equation (7), by assuming a Taylor expansion of the reaction rate term using only the first order term. Thus,

$$D_i\left(\frac{d^2c}{dr^2}+\frac{2}{r}\frac{dc}{dr}\right)+v_{is}+v_s'(c-c_s)=0 \qquad (7)$$

v_{is} is the reaction rate at the catalyst surface, and $v_s'=dv_i/dc$ at $c=c_s$. This approximation of reaction rate assumes a pseudo first order reaction, but differs from the first order approximation given by Wagner[2] and Hoogschagen[6]. Schematically, the two approximations are illustrated in Figure 1.

Equation (7) may be solved analytically, as Thiele[1] has done, and the catalytic effectiveness factor is given by

$$E_f=\frac{3}{m}\left(\frac{1}{\tanh m}-\frac{1}{m}\right) \qquad (8)$$

*Addition of Equation (1) multiplied by (Q/λ_i) and Equation (2) multiplied by $(-1/\lambda_i)$ produces

$$d^2(rf)/dr^2=0$$

where $f=(D_iQ/\lambda_i)c-t$. From the boundary conditions, f should be equal to $(D_iQ/\lambda_i)c_s-t_s$, and Equation (4) is thus obtained.

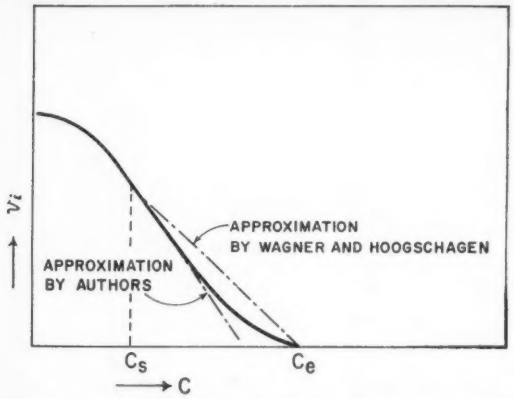

Figure 1—Approximation of general reaction rate to a first order equation.

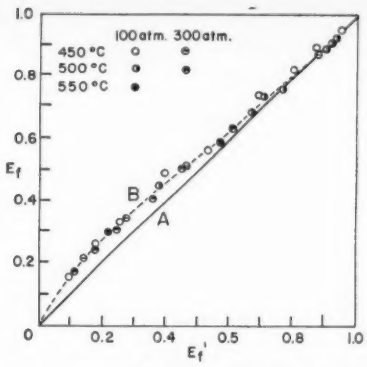

Figure 2—Relation between E_f, calculated numerically and E_f', calculated by the approximate method for ammonia synthesis reaction.

where

$$m = \frac{d_p}{2}\sqrt{-\frac{v_s'}{D_i}} \quad \ldots\ldots\ldots\ldots\ldots\ldots\ldots\ldots (9)$$

m is regarded as a modified Thiele modulus.

A comparison of calculated effectiveness factors by the numerical method and the approximate method has been made for the ammonia synthesis reaction[4]. The result is shown in Figure 2, where the relation between the value of E_f' calculated by the approximate method and E_f calculated numerically is given by curve B, which is fairly close to the line A expressing $E_f = E_f'$.

Assuming now this pseudo first order approximation, consider the effect of temperature distribution within the pellet.

$$D_i\left(\frac{d^2c}{dr^2} + \frac{2}{r}\frac{dc}{dr}\right) + v_{is} + v_{cs}'(c - c_s) + v_{ts}'(t - t_s) = 0 \quad \ldots\ldots (10)$$

where v_{is} is the reaction rate at the outer catalyst surface,

$$v_{cs}' = (dv_i/dc)_s = c_s,$$
$$v_{ts}' = (dv_i/dt)_t = t_s.$$

Substitution of Equation (4) into equation (10) leads to Equation (11).

$$\frac{d^2c}{dr^2} + \frac{2}{r}\frac{dc}{dr} + \frac{v_{is}}{D_i} + \left(\frac{v_{cs}'}{D_i} + \frac{v_{ts}'Q}{\lambda_i}\right)(c - c_s) = 0 \quad \ldots\ldots\ldots (11)$$

Equation (11) is a first order linear equation with respect to c and easily solved. The catalytic effectiveness factor can be calculated from Equation (8), if m is modified to

$$m = \frac{d_p}{2}\sqrt{-\left(\frac{Qv'_{ts}}{\lambda_i} + \frac{v'_{cs}}{D_i}\right)} \quad \ldots\ldots\ldots\ldots\ldots (12)$$

TABLE 1

CALCULATED EFFECTIVENESS FACTORS FOR A FEW INDUSTRIAL REACTIONS

Assumption; d_p = 6mm, ϵ = 0.5

Reaction System	Reaction Conditions	Q (cal./mol.)	D_i[a] (cm.²/sec.)	λ_i[a] $\left(\frac{\text{cal.}}{\text{cm.sec.°C.}}\right)$	$\frac{v_{cs}'}{D_i}$	$\frac{Qv_{ts}'}{\lambda_i}$	m or m^*	E_f
ammonia synthesis on industrial iron catalyst[6]	inlet H_2. 75%, N_2. 25% 500°C., 300 atm $Z_{NH_3\,S}=0$	12,800	1.02×10^{-3}	4.07×10^{-3}	−39,200	242	59.2	0.054
SO_2 oxidation on industrial vanadium catalyst[9]	inlet SO_2; 8%, O_2; 12%, N_2; 80% 450°C., 1 atm $xSO_{2\,S}=0$	23,200	5.53×10^{-2}	7.62×10^{-4}	−81.7	6.95	2.6	0.71
naphthalene oxidation on vanadium catalyst[10]	inlet $C_{10}H_8$; 0.9% air; 99.1% 350°C., 1 atm $xC_{10}H_{8\,S}=0$	520,000**	5×10^{-2}	5×10^{-4}	−6,080	435	22.5	0.13
ethylene oxidation on silver catalyst[11]	inlet C_2H_4; 3% air; 97.0% 218°C., 1 atm $xC_2H_4 = 0.5$	$32.9 \times 10^3 N$ +337.28 $x(1-N)$***	5×10^{-2}	5×10^{-4}	−62	2.5	2.3	0.65
CO conversion[12]	inlet CO; 11.7% 350°C., 1 atm $xCO_S=0$	10,000	5.5×10^{-3}	8×10^{-4}	−7.9	0.28	0.83	0.92
Cumene cracking on silica-alumina catalyst[13]	510°C., 1 atm $xC_S=0$	−23,700	2.0×10^{-3}	8×10^{-4}	−1,470	−52.6	32.7	0.092

[a]assumed values

Nomenclature; Z; mole fraction, x; conversion,

** No side reaction is assumed, i.e., $C_{10}H_8 + 4.5\ 0_2 = C_8H_4O_3 + 2H_2O + 2CO_2 + 520{,}000$ cal.

***Two parallel reactions proceed as: $\begin{cases} C_2H_4 + 0.5\ O_2 = C_2H_4O + 32{,}900 \text{ cal.} \\ C_2H_4 + 3\ O_2 = 2CO_2 + 2H_2O + 337{,}280 \text{ cal.} \end{cases}$

and selectivity $N = k_1/(k_1 + k_2)$

If the experimental reaction rate value v_i^* includes the effect of mass and heat transfer within the pellet, the effectiveness factor can be obtained from the relationship † between E_f and m^* which is given by Wagner[2] and Hoogschagen[5], where m^* is defined as

$$m^* = \frac{d_p}{2}\sqrt{-\left(\frac{Qv_{is}'^*}{\lambda_i} + \frac{v_{cs}'^*}{D_i}\right)} \quad \ldots\ldots\ldots\ldots\ldots\ldots (13)$$

Illustration

In order to calculate the effectiveness factor, values of λ_i and D_i must be known. Few reliable data are available, however, so that for these illustrative calculations λ_i and D_i are assumed from the works of Hoogschagen[6] and Sehr[7], and others. Calculated results for a few reactions at particular conditions are summarized in Table 1. It may be noted that the term containing the temperature effect Qv_{is}'/λ_i is less than 10% of the concentration term v_{cs}'/D_i. Thus it is concluded that the effect of temperature distribution within a catalyst pellet is not important.

$$v_{is}^* = E_f v_{is}', \; v_{cs}'^* = E_f v_{cs}',$$

then

$$m^* = \frac{d_p}{2}\sqrt{E_f\left(-\frac{Qv_{is}'}{\lambda_i} + \frac{v_{cs}'}{D_i}\right)}$$

Therefore

$$m^{*2} = E_f m_2^2$$

m is expressed by a function of E_f from Equation (8), so that a relation between m^* and E_f is obtained.

† *As* $v_i^* = E_f V_i$,

Nomenclature

c = Concentration of a particular component
D_i = Effective diffusion coefficient in catalyst
d_p = Effective particle diameter
E_f, E_f' = Catalytic effectiveness factor
m = Modified Thiele modulus
Q = Heat of reaction
r = Distance from centre of spherical catalyst
t = Temperature
t_s = Temperature of surface of catalyst particle
v_i = Reaction rate, moles increase per unit time per unit volume of catalyst particle ($= v/(1 - \epsilon)$, where v is reaction rate for packed bed of catalyst, and ϵ is void fraction of catalyst bed,
v_s' = $\frac{dv_i}{dc}$, neglecting the effect of temperature distribution
v_{cs}' = $\left(\frac{\partial v_i}{\partial c}\right)_c = c_s$
v_{ts}' = $\left(\frac{\partial v_i}{\partial t}\right)_t = t_s$
λ_i = Thermal conductivity of catalyst particle

References

(1) Thiele, E. W., Ind. Eng. Chem., **31,** 916 (1939).
(2) Wagner, C., Z. Physik. Chem., **A193,** 1 (1943).
(3) Kubota, H. and Shindo, M., Chem. Eng. (Japan), **20,** 11 (1956).
(4) Kubota, H., Shindo, M., Akehata, T., and Lin, A., ibid., **23,** 284 (1959).
(5) Hoogschagen, J., Ind. Eng. Chem., **47,** 906 (1955).
(6) Prater, C. D., Chem. Eng. Sci., **8,** 284 (1958).
(7) Sehr, R. A., ibid., **9,** 145 (1958).
(8) Kubota, H. and Shindo, M., Chem. Eng. (Japan), **23,** 242 (1959).
(9) Kubota, H., Ishizawa, M., and Shindo, M., J. Sulphuric Acid Assoc. Japan, **12,** 243 (1959).
(10) Joffee, I. I. and Sherman, Yu. G., Zhur. Fiz. Khim., **28,** 2095 (1954).
(11) Kurilenko, A. I., Rĭbakova, N. A., Kulĭkova, N. V., and Temkin, M. I., Zhur. Fiz. Khim., **32,** 797 (1958).
(12) Konoki, K., Chem. Eng. (Japan), **21,** 408 (1957)
(13) Corrigan, T. E., Garver, J. C., Rase, H. F., and Kirk, R. S., Chem. Eng. Progr., **49,** 603 (1953).

★ ★ ★

A Design Parameter for Multicomponent Tray Design Estimates[1]

ALFRED J. SUROWIEC[2]

This report develops computational techniques that are useful in multicomponent distillation. A design parameter, $(\partial n/\partial N)_s$, is introduced which is numerically equal to the number of theoretical plates required to do the work of one total reflux tray at the bottom of the enriching section. For a minimum sized tower, $(\partial n/\partial N)_s$ is less than 3.5. Economic conditions may permit values as high as 6.

The ratio of the number of theoretical trays, n, to the minimum number, N, for the combined enriching and stripping sections, including reboiler and condenser, and the ratio of the reflux leaving the enriching section, L_s, to the minimum reflux, L_{M_s}, can be found from:

$$n/N = \frac{2.303(\partial n/\partial N)_s \log_{10}(\partial n/\partial N)_s}{(\partial n/\partial N)_s - 1}$$

$$L_s/L_{M_s} = \frac{(\partial n/\partial N)_s}{(\partial n/\partial N)_s - 1}$$

A total of 36 sets of minimum reflux data in multicomponent systems were correlated with an average error of −4% in the ratio n/N by these equations.

Since $(\partial n/\partial N)_s$ is related to the relative volatility and the compositions of the counterflowing liquid and vapor streams at the bottom of the enriching section, the reflux L_s can be found from a feed tray balance. A procedure is provided for evaluating L_s after a value for the design parameter has been selected.

When a designer has selected a reflux ratio and made a tray calculation, he frequently has little idea of the kind of selection he has made and may be forced into an involved economic balance in order to find out. Even when such a balance has been made, he still has little idea where he stands in relation to the distillation process itself. A logical measure of the desirability of a design choice is to compare it with the minimum number of trays and the minimum reflux for the same separation. A more convenient and flexible measure is to introduce a design parameter which gives the number of theoretical operating trays required to do the work of one total reflux tray at any point in the tower.

Basic Equations To compare the number of operating trays with the number of total reflux trays it is useful to place the operating line equations in the same form as the equilibrium relationship by introducing a composition ratio ϕ, such that[1]

$$Y_{n+1} = \phi_n X_n \quad \ldots\ldots(1)$$

Then, along with the equilibrium relationship

$$Y_n = \alpha_n X_n \quad \ldots\ldots(2)$$

there results for a single tray

$$Y_n/Y_{n+1} = \alpha_n/\phi_n \quad \ldots\ldots(3)$$

In logarithmic form

$$\log Y_n - \log Y_{n+1} = \log(\alpha_n/\phi_n) \quad \ldots\ldots(4)$$

For differential numbers of trays, the following procedure is a short cut to the lengthy derivation of Equation (71) in Appendix B. Differential trays are discussed under Mathematical Conventions in Appendix C.

Using Taylor's series for the finite difference in Equation (4),

$$\log(\alpha/\phi)_n = \sum_{k=1}^{\infty} \frac{(-)^k d^k \log Y_{n+1}}{k!\, dn^k} \quad \ldots\ldots(5)$$

Differentiating,

$$\frac{d}{dn}\log(\alpha/\phi)_n = -\sum_{k=2}^{\infty} \frac{(-)^k k d^k \log Y_{n+1}}{k!\, dn^k} \quad \ldots\ldots(6)$$

Combining,

$$\log(\alpha/\phi)_n + \tfrac{1}{2}\frac{d}{dn}\log(\alpha/\phi)_n + \frac{d}{dn}\log Y_{n+1} = \sum_{k=3}^{\infty} \frac{(-)^k(1 - k/2)d^k \log Y_{n+1}}{k!\, dn^k} \quad \ldots\ldots(7)$$

Rearranging and neglecting third order and higher terms,

$$\log(\alpha/\phi)_n\, dn + \tfrac{1}{2} d \log(\alpha/\phi)_n + d \log Y_{n+1} = 0 \quad \ldots\ldots(8), (71)$$

At total reflux, ϕ is equal to unity and the minimum number of trays is given by

$$\log \alpha_N dN + \tfrac{1}{2} d \log \alpha_N + d \log Y_{N+1} = 0 \quad \ldots\ldots(9)$$

Equations (8) and (9) were found to have an error less than 4% in the number of trays. (See discussion of Equation (76) in Appendix B.)

The component distribution at total reflux is different from that at some other reflux ratio. However, for the keys, α_N can be taken equal to α_n when Y_{N+1} equals Y_{n+1}. Equations (8) and (9) then yield

$$dn = \frac{\log \alpha_n}{\log(\alpha/\phi)_n} dN + \tfrac{1}{2}\frac{d \log \phi_n}{\log(\alpha/\phi)_n} \quad \ldots\ldots(10)$$

Equation (10) holds for any pair of components where there is little difference between α_n and α_N. In what follows it will be written only for the key components.

Equation (10) shows that the differential of n has been written as a function of N and ϕ, i.e.,

$$dn = (\partial n/\partial N)dN + (\partial n/\partial \phi)d\phi \quad \ldots\ldots(11)$$

[1]*Manuscript received October 16, 1960; accepted March 15, 1961.*
[2]*Chemical Engineer, 78 Midland Boulevard, Maplewood, N.J., U.S.A.*

Inspection shows that

$$(\partial n/\partial N) = \frac{\log \alpha_n}{\log(\alpha/\phi)_n} \quad \ldots\ldots(12)$$

Rearranging,

$$\frac{\log \alpha_n}{\log \phi_n} = \frac{(\partial n/\partial N)}{(\partial n/\partial N) - 1} \quad \ldots\ldots(13)$$

Differentiating and neglecting a term in $d \log \alpha$ which is not justified by subsequent approximate methods of integration,

$$d \log \phi_n = \frac{\log \alpha_n}{(\partial n/\partial N)^2} d(\partial n/\partial N) \quad \ldots\ldots(14)$$

Making the substitutions in Equation (10)

$$dn = (\partial n/\partial N) dN + \tfrac{1}{2} d \log(\partial n/\partial N) \quad \ldots\ldots(15)$$

Integration of Equations (8) and (15) can be accomplished by taking $\log Y_n - \log Y_{n+1}$ linear in $\log Y_{n+1}$[2], and by setting $1/(\partial n/\partial N)$ proportional to N. Then,

$$-\Delta n \cdot \frac{\Delta \log(Y_n/Y_{n+1})}{\Delta \log \log(Y_n/Y_{n+1})} = \Delta \log Y_{n+1} + \tfrac{1}{2} \Delta \log(Y_n/Y_{n+1}) \quad \ldots\ldots(16)$$

and,

$$\Delta n \cdot \frac{\Delta\left(\frac{1}{(\partial n/\partial N)}\right)}{\Delta \log\left(\frac{1}{(\partial n/\partial N)}\right)} = \Delta N - \tfrac{1}{2} \Delta \left(\frac{1}{(\partial n/\partial N)}\right) \quad \ldots\ldots(17)$$

where

$$-\Delta N \cdot \frac{\Delta \log \alpha_N}{\Delta \log \log \alpha_N} = \Delta \log Y_{N+1} + \tfrac{1}{2} \Delta \log \alpha_N \quad \ldots\ldots(18)$$

At first glance, there would appear to be no particular advantage of Equation (17) over (16). However, the differential coefficient defined by Equation (12) is a useful design parameter which gives the ratio of the operating trays to the total reflux trays at any point in the tower. The linear approximation used in arriving at Equation (16) was found to yield accuracies of from 5 to 10% in the number of trays. The equations are applicable to the stripping or enriching sections but require a feed plate match before they can be applied to the overall tower.

Feed Plate Match A feed plate match can be made by reducing the multicomponent system to an equivalent binary system and by introducing feed at the intersection of the operating lines. In the new basis, the operating line in the enriching section takes the form

$$V_{n+1}(y_l + y_h)_{n+1}(Y/1 + Y)_{n+1} = L_n(x_l + x_h)_n (X/1 + X)_n + D(x_l + x_h)_D (X/1 + X)_D;$$
$$0 \leqq n \leqq e \quad \ldots\ldots(19)$$

where

$$(Y/1 + Y)_{n+1} = (\phi X/1 + \phi X)_n \quad \ldots\ldots(20)$$

$$(Y/1 + Y)_n = (\alpha X/1 + \alpha X)_n \quad \ldots\ldots(21)$$

Similar expressions can be written for the stripping section for $n \geqq (f-1)$.

For a partially vaporized feed, a component balance gives

$$F(z_l + z_h)(Z/1 + Z) = F_L(x_l + x_h)_F (X/1 + X)_F + F_V(y_l + y_h)_F (Y/1 + Y)_F \quad \ldots\ldots(22)$$

$$Y_F = \alpha_F X_F \quad \ldots\ldots(23)$$

The operating lines for stripping and enriching are coupled by

$$L_{f-1}(x_l + x_h)_{f-1} - L_e(x_l + x_h)_e = F_L(x_l + x_h)_F \quad \ldots\ldots(24a)$$

$$V_{e+1}(y_l + y_h)_{e+1} - V_f(y_l + y_h)_f = F_V(y_l + y_h)_F \quad \ldots\ldots(24b)$$

The intersection of the operating lines is defined by

$$\phi_s = Y_{s+1}/X_s \quad \ldots\ldots(25)$$

Rearranging Equations (24a & b) with the aid of a component balance and allowing e or $f-1$ to approach the intersection,

$$\frac{-F_L(x_l + x_h)_F}{F_V(y_l + y_h)_F}\left[\frac{(X/1 + X)_F - (X/1 + X)_s}{(Y/1 + Y)_F - (Y/1 + Y)_{s+1}}\right] = \frac{L_e(x_l + x_h)_e}{V_{e+1}(y_l + y_h)_{e+1}}\left[\frac{(X/1+X)_s - (X/1+X)_e}{(Y/1+Y)_{s+1} - (Y/1+Y)_{e+1}}\right]_{s=f-1} \quad \ldots(26a)$$

$$= \frac{L_{f-1}(x_l + x_h)_{f-1}}{V_f(y_l + y_h)_f}\left[\frac{(X/1+X)_s - (X/1+X)_{f-1}}{(Y/1+Y)_{s+1} - (Y/1+Y)_f}\right]_{s=e} \quad \ldots\ldots(26b)$$

The right hand sides of Equations (26a & b) tend toward unity so that

$$\frac{-F_L(x_l+x_h)_F}{F_V(y_l+y_h)_F} = \frac{(Y/1+Y)_F - (Z/1+Z)}{(X/1+X)_F - (Z/1+Z)} \cong \frac{(Y/1+Y)_{s+1} - (Z/1+Z)}{(X/1+X)_s - (Z/1+Z)} \quad \ldots\ldots(27)$$

Equation (27) also applies when feed is flashed on an equilibrium feed tray, and

$$X_f = X_{e+1} = X_F; \quad Y_f = Y_{e+1} = Y_F \quad \ldots\ldots(28)$$

For an all liquid feed at its bubble point,

$$X_s = X_e = X_{f-1} = X_F; \quad F_V = 0; \quad Z = X_F \quad \ldots\ldots(29)$$

For an all vapor feed at its dew point,

$$Y_{s+1} = Y_{e+1} = Y_f = Y_F; \quad F_L = 0; \quad Z = Y_F \quad \ldots\ldots(30)$$

Using these feed conventions, and setting $(\partial n/\partial N)$ equal to unity at X_D and X_B, Equation (17) takes the form, for the overall tower: (See Appendix D.)

$$(n/N) = \frac{(\partial n/\partial N)_s \log(\partial n/\partial N)_s}{(\partial n/\partial N)_s - 1} \quad \ldots\ldots(31)$$

It is assumed in the above that

$$\alpha_{f-1} = \alpha_s = \alpha_e$$

so that, for a saturated liquid or vapor feed,

$$(\partial n/\partial N)_e = (\partial n/\partial N)_s = (\partial n/\partial N)_{f-1}$$

Figure 1 shows the intersection of the operating lines.

A certain amount of caution should be exercised in the use of Equation (31). Refluxing of excessive light and heavy components about the feed tray may cause a reverse fractionation which can result in the operating lines intersecting on the opposite side of the equilibrium curve with $\phi > \alpha$. This situation frequently occurs at minimum reflux[3]. Theoretically, refluxing of heavy non-product components in the fractionation section can be carried out until all of the overhead product components have been displaced from the reflux. Then, since $V = L + D$, the product components appear in the vapor stream in the same ratio as in the overhead product. Inspection of the particular case at hand will show if it is advantageous to assume in (31) that all non-product components are absent from the enriching and stripping sections when the design parameter is determined and then to allow for the refluxing effect around the feed tray[4].

Effect of Reflux Ratio When the design parameter is constant, the ratio of the actual number of trays to the minimum number of trays for the overall tower is equal to the parameter itself. To obtain, for example, a system requiring three times the minimum number of trays with $(\partial n/\partial N)$ constant at 3, it is only necessary to draw in the total reflux steps on a McCabe-Thiele diagram in the equivalent binary system, and then, between the first and second steps on the 45° diagonal, begin two more total reflux constructions. The diagram is now composed of three interlacing total reflux steps with compositions given by their intersections. (Note that $X_n = Y_{n+3}$.) The operating line is now a curve drawn nearly one third the way from the equilibrium curve to the 45° diagonal, as in Figure 2.

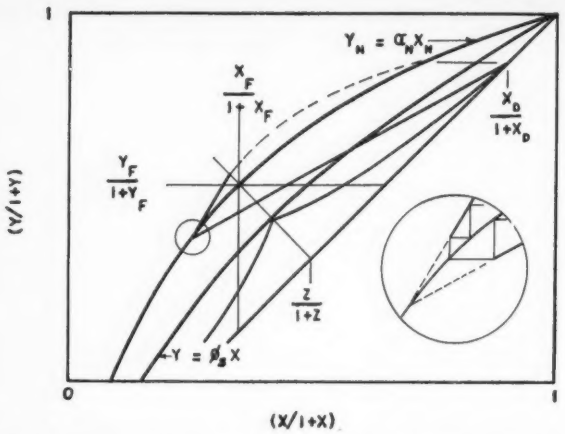

Figure 1—Intersection of the operating lines and extrapolation of minimum reflux in the equivalent binary system.

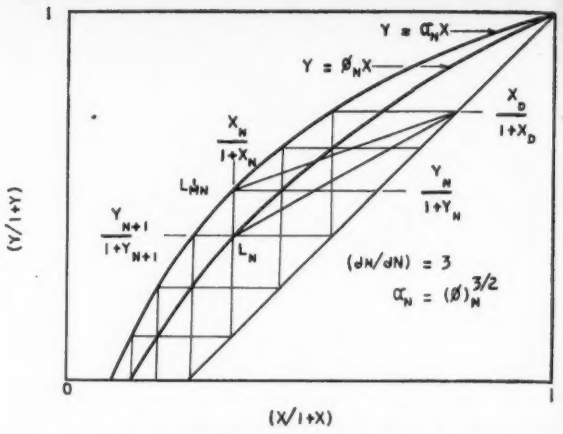

Figure 2—McCabe-Thiele diagram in the equivalent binary system when $(\partial n/\partial N)$ equals 3.

This type of construction can be repeated for any rational value of n/N equal to $(\partial n/\partial N)$. The geometry of the problem is such that the distance between the equilibrium curve and the 45° diagonal is broken up into nearly equal parts totalling $(\partial n/\partial N)$ in number. The distance between the equilibrium curve and the 45° diagonal is given by

$$(Y/1+Y)_{n+1} - (X/1+X)_{n+1} \;\&\; (Y/1+Y)_n - (X/1+X)_n$$

while the distance from the operating line to the 45° line is in turn

$$(Y/1+Y)_{n+1} - (X/1+X)_n$$

The ratio of the two distances is then

$$\left[\frac{(\partial n/\partial N)}{(\partial n/\partial N)-1}\right]_Y = \frac{(Y/1+Y)_{n+1} - (X/1+X)_{n+1}}{(Y/1+Y)_{n+1} - (X/1+X)_n} \quad \ldots\ldots(32a)$$

$$\left[\frac{(\partial n/\partial N)}{(\partial n/\partial N)-1}\right]_X = \frac{(Y/1+Y)_n - (X/1+X)_n}{(Y/1+Y)_{n+1} - (X/1+X)_n} \quad \ldots\ldots(32b)$$

A little manipulation gives

$$\left[\frac{(\partial n/\partial N)}{(\partial n/\partial N)-1}\right]_Y = \frac{\phi_n + Y_{n+1}}{\alpha_{n+1} + Y_{n+1}} \cdot \frac{\alpha_{n+1} - 1}{\phi_n - 1} \quad \ldots\ldots(33a)$$

$$\left[\frac{(\partial n/\partial N)}{(\partial n/\partial N)-1}\right]_X = \frac{1 + \phi_n X_n}{1 + \alpha_n X_n} \cdot \frac{\alpha_n - 1}{\phi_n - 1} \quad \ldots\ldots(33b)$$

Equations (33a) and (33b) are at best approximations. They yield the same value for the design parameter when lines of constant ϕ and α are parallel. For small values of relative volatilities they reduce to Equation (13). They will be useful in determining the effect of reflux ratio on the design parameter.

Define L'_{Mn} as the reflux that obtains when the operating line in the enriching section intersects the equilibrium curve. L'_{Mn} is not a true minimum reflux but a pseudo minimum reflux that is obtained from a geometrical construction with an equilibrium curve that has already been established and not from material and equilibrium balances.

When L'_{Mn} intersects the equilibrium curve at $Y = Y_{n+1}$, a condition analagous to an all vapor feed at its dew point, Equation (19) yields

$$\frac{L_n(x_l+x_k)_n}{L'_{Mn}(x'_l+x'_k)_{Mn}} = \frac{(Y/1+Y)_{n+1} - (X/1+X)_{n+1}}{(Y/1+Y)_{n+1} - (X/1+X)_n} \quad \ldots\ldots(34)$$

$$= \left[\frac{(\partial n/\partial N)}{(\partial n/\partial N)-1}\right]_Y \quad \ldots\ldots(35)$$

When L'_{Mn} intersects the equilibrium curve at $X = X_n$, a condition analagous to an all liquid feed at its bubble point, then

$$\frac{L_n(x_l+x_k)_n}{L'_{Mn}(x'_l+x'_k)_{Mn}} = \frac{(X/1+X)_D - (Y/1+Y)_{n+1}}{(X/1+X)_D - (Y/1+Y)_n} \cdot \frac{(Y/1+Y)_n - (X/1+X)_n}{(Y/1+Y)_{n+1} - (X/1+X)_n} \quad \ldots\ldots(36)$$

$$= \frac{(X_D - \phi_n X_n)(1 + \alpha_n X_n)}{(X_D - \alpha_n X_n)(1 + \phi_n X_n)} \left[\frac{(\partial n/\partial N)}{(\partial n/\partial N) - 1}\right]_X \quad \ldots\ldots(37)$$

In the fractionation section, components lighter than the light key component soon reach constant compositions[5], and

$$y_{in+1} = y_{in} = K_{in}x_{in} \quad \ldots\ldots(38)$$

$$= (L_n/V_{n+1})x_{in} + (D/V_{n+1})x_{iD} \quad \ldots\ldots(39)$$

and

$$L_n x_{in} = \frac{Dx_{iD}}{\left[\frac{K_{in}}{(L_n/V_{n+1})} - 1\right]}; \quad n \leqq e \quad \ldots\ldots(40)$$

During the refluxing of heavy components in the fractionation section, the heavy key component goes through a maximum. A maximum implies a region of constant composition, however small. Assume Equation (38) applies. Designating u as the tray at which the maximum occurs and making use of the fact that the overhead product is small for the heavy key component, Equation (40) reduces to

$$K_{hu} \geqq L_u/V_{u+1}; \quad u < e \quad \ldots\ldots(41)$$

A similar treatment in the stripping section for the components heavier than the heavy key component yields

$$L_n x_{jn} = \frac{Bx_{jB}}{\left[1 - \frac{K_{jn}}{(L_n/V_{n+1})}\right]}; \quad n \leqq f - 1 \quad \ldots\ldots(42)$$

while for the light key component at its point of maximum concentration

$$K_{lw} \leqq L_w/V_{w+1}; \quad w > f - 1 \quad \ldots\ldots(43)$$

Relative volatilities can be substituted in Equation (40) and in Equation (42) when they are written for n equal to u and n equal to w.

Correlation of Minimum Reflux Except for $n = e$, all values of the true minimum reflux, L_{Mn}, are essentially the same as the pseudo minimum reflux. Since heavy components are fractionated out as n grows large, and lighter components reach

TABLE 1

COMPARISON OF RESULTS OF EQUATIONS (31) & (44)

Source of Data	Test No.	Feed Cond.	N	$(L/D)_M$	L/L_M	n/N	Calculated n/N	Actual $n/N \div$ Calc.
(A)	Ex. 2	B.P.	8.64	0.937	1.25	2.11	2.00	1.06
	3	60% Vap.	,,	*	,,	2.00	,,	1.00
	5	B.P.	,,	*	,,	2.06	,,	1.03
	6	,,	,,	*	,,	2.08	,,	1.04
	7**	,,	,,	*	,,	1.99	,,	0.996
(B)	Ia	8% Vap.	26.85	5.32	6.08	1.11	1.09	1.02
	b	,,	,,	,,	3.57	1.19	1.17	1.02
	c	,,	,,	,,	2.50	1.29	1.28	1.01
	IIa	,,	25.65	4.37	5.50	1.14	1.10	1.04
	b	,,	,,	,,	3.04	1.27	1.21	1.05
	c	,,	,,	,,	2.06	1.47	1.37	1.07
	III	72% Vap.	,,	3.25	2.77	1.33	1.24	1.07
	IV	B.P.	18.4	1.83	2.06	1.47	1.37	1.07
	V	,,	10.44	2.54	2.89	1.34	1.22	1.10
	VI	50% Vap.	13.3	0.942	3.18	1.28	1.20	1.07
	VII	B.P.	29.45	7.00	1.36	1.77	1.80	0.983
(C)	II	B.P.	19	5.2	1.92	1.42	1.41	1.01
		B.P.	,,	,,	1.35	1.84	1.82	1.01
	III	,,	11.2	0.98	2.04	1.52	1.38	1.10
	IV-A	***	9.4	0.53	3.77	1.38	1.15	1.20†
	IV-B	***	11.2	0.76	2.63	1.52	1.26	1.21†
	VII	B.P.	9.0	1.25	1.28	2.00	1.94	1.03
		,,	,,	,,	1.68	1.67	1.52	1.10
		,,	,,	,,	4.11	1.22	1.14	1.07
	VIII	,,	43.1	6.0	2.0	1.35	1.39	0.97
		,,	,,	,,	3.16	1.21	1.21	1.00
	IX	,,	29.0	7.0	2.86	1.21	1.22	0.99
		,,	,,	,,	5.00	1.10	1.15	0.96
	X	,,	20.2	2.3	2.17	1.43	1.34	1.07
		,,	,,	,,	6.52	1.09	1.09	1.00
	XI	,,	11.8	2.26	1.14	2.35	2.4	0.98
	XII	,,	7.7	1.5	3.78	1.23	1.16	1.06
		,,	,,	,,	6.00	1.14	1.09	1.05
	XIII	,,	8.6	1.85	4.86	1.22	1.12	1.09
	XIV	,,	13.0	0.9	3.33	1.31	1.19	1.09
	XV	68% Vap.	3.4	0.78	1.15	2.94	2.32	1.27†
		,,	,,	,,	2.56	1.65	1.27	1.30†
	XVI	B.P.	19.7	3.3	1.21	2.09	2.11	0.99
		,,	,,	,,	1.82	1.59	1.45	1.09
		,,	,,	,,	3.03	1.30	1.22	1.06

* Not reported.
** Reverse fractionation in the stripping section[4].
*** Cold feed.
† Rejected.

(A) Murdoch, P. G., Holland, C. D., Chem. Eng. Progr., **48,** 254 (1952).
(B) Brown, G. G., Martin, H. Z., Trans. Am. Inst. Chem. Engrs., **35,** 679 (1939).
(C) Gilliland, E. R., Ind. Eng. Chem., **32,** 1220 (1940).

constant compositions, the sum of the combined keys obtained by the intersection of the operating line and equilibrium curve on the equivalent binary McCabe-Thiele diagram differs slightly from the result calculated from an equilibrium balance because of changes in relative volatility. The component distributions at the operating and minimum refluxes are not the same. The essential difference at $n = e$ between the pseudo minimum reflux and the true minimum reflux is the quantity of heavy material that enters the enriching section from the feed tray. The sum of the combined keys remains nearly the same. Further, a feed tray analysis will reveal if there is any appreciable difference between the percentages of combined keys at the true minimum reflux and the operating reflux. As a first approximation, Equations (35) and (37) can be written as

$$(L/L_M)_n = (\partial n/\partial N)/[(\partial n/\partial N) - 1];\ n = e, s \ldots\ldots\ldots\ldots (44)$$

Table 1 shows the results obtained with Equations (31) and (44).

Design Procedure To arrive at a tower design, select a value of $(\partial n/\partial N)_s$ for use in Equation (31). From Equation (13), obtain ϕ_s and then by means of Equations (22) through (30), find

$$X_s = L_s x_{ls}/L_s x_{ks}$$

Since Y_{s+1} and X_s are known, the sum of the combined keys,

$$L_s(x_{ls}+x_{ks}) = V_{s+1}(y_{ls+1}+y_{ks+1}) - D(x_{lD}+x_{kD})$$

can be readily found from Equation (19), by eliminating the vapor term.

The sum of a distributed component and the heavy key component can be obtained in the same manner using a value of the design parameter equal to that used for the light and heavy key components. Components lighter than the light key and heavier than the heavy key can be found from Equations (40) and (42) and a feed tray balance. Sufficient information is now available to arrive at L_s. (See Appendix E).

Relative volatilities can be used as a first trial in Equations (40) and (42). If a trial value of L_s is used, it can be set equal to L_n in (41). Using the same value of the design parameter and the same value of n at the intersection of the operating lines when fractionating between the distributed component and the heavy key component is equivalent to saying that n/N is the same as it is for the light and heavy key components. If desired, the feed tray balance can be reworked and $(\partial n/\partial N)_s$ can be calculated and compared with that originally used.

Design Conditions In an economic study with the aid of a computer, Albright[6] found that reflux ratios of 1.20 to 1.30 times the minimum were optimum for his conditions, while Happel[7] presents a correlation which prescribes reflux ratios that are close to the minimum. Substituting these reflux factors in Equations (44) and (31) yields the following:

$(L/L_M)_s$	n/N	$(\partial n/\partial N)_s$
1.2	2.14	6.0
1.25	2.00	5.0
1.3	1.9	4.33

These values should be compared with those employed in the sample problems.

In this connection it is interesting to note that when the relative volatility is sufficiently small, then Equation (44), or (53), predicts the results of Cohen[8]: An enriching section has a minimum size, or volume, when the reflux ratio is twice the minimum at all points and when twice the minimum number of trays are employed. Going a step further, an enriching section with a constant reflux ratio has a minimum size when:

$(\partial n/\partial N)_e$	3.5	3.4	3.0	1.0
n/N	1.75	1.73	1.65	1.00
N_e	∞	8.73	1.54	0
$(L/L_M)_e$	1.4	1.42	1.50	∞

The combined enriching and stripping sections is a minimum when $(\partial n/\partial N)_s$ is less than 3.5.

Discussion

The design parameter introduced herein has certain advantages:

(1) It permits a rapid estimate of the total number of trays from the minimum number of trays.

(2) It permits an estimate of the required reflux ratio from a feed tray balance and eliminates the need for a minimum reflux calculation.

(3) It allows the designer to select a set of design conditions which, if not the optimum, are none the less desirable.

The use of the pseudo minimum reflux is based upon the geometry of the McCabe-Thiele diagram[9] alone. It supposes that the equilibrium curve has been determined by the separation under consideration.

Conventional methods are employed in making a feed tray balance[6]. Location of the feed tray is a free choice and for computational convenience it is taken at the intersection of the operating lines in the equivalent binary system. The question of optimum feed tray location is left to the consideration of the particular case at hand. For "normal" systems, the optimum location occurs at the intersection of the operating lines in the equivalent binary system.

The use of Equation (44) in the optimization studies in the Appendix A is, admittedly, an over simplification. Its use was felt justified because of the results obtained in Table 1. The data of Table 1 could be represented with an average error of -4% in the ratio (n/N), by means of Equations (44) and (31). For the systems represented in Table 1, the key components have relative volatilities of 3.0 or less. Binary systems are not included in the data of Table 1.

Referring to Figure 1, it should be noted that crossing the equilibrium curve during the refluxing of non-product components, particularly at minimum reflux, forces the operating line to change direction within a single step. With an infinite number of steps at the crossing during minimum reflux, this results in a discontinuity of slope of the operating line. An infinity of steps at or near equilibrium at the point of crossing suggests that the operating line becomes tangent to the equilibrium curve at this point. Thus, if the intersection of the operating lines in the equivalent binary system is known for the minimum reflux, the pinch points in the fractionating and stripping sections can be found approximately, simply by drawing tangents to the equilibrium curve from the point of intersection.

Use of the linear approximation in the integration of Equations (8) and (15) follows from the fact that the operating line for enriching can be put into the form

$$[V(y_l+y_h)(Y-1)/(Y+1)]_{n+1} = [L(x_l+x_h)(X-1)/(X+1)]_n + D(x_l-x_h)_D$$

In terms of logarithms,

$$\log Y_{n+1} = \frac{L_n(x_l+x_h)_n \log X_n + 2D(x_l-x_h)_D}{V_{n+1}(y_l+y_h)_{n+1}} + 2g$$

where

$$g \equiv \sum_{k=1}^{\infty} \frac{1}{1+2k}\left[\left(\frac{Y-1}{Y+1}\right)_{n+1}^{1+2k} - \frac{L_n(x_l+x_h)_n}{V_{n+1}(y_l+y_h)_{n+1}}\left(\frac{X-1}{X+1}\right)_n^{1+2k}\right].$$

When $Y_{n+1} < 2$ and $X_n > \frac{1}{3}$, then g becomes small.

When the operating lines in the equivalent binary system are straight, then the slope of the $\log Y_{n+1}$ vs. $\log X_n$ curve goes through a maximum in the enriching section and use of the linear approximation in the integration of Equations (8) and (15) can result in values of n somewhat larger than actual. Usually, $L_n(x_l+x_h)_n$ increases with increasing n for $n < e$, and then decreases as the heavy components begin to appear. If the intersection of the operating lines is determined from the maximum flows, then the linear approximation will yield values of n less than actual. At constant total molal downflow, the maximum flows for the combined keys are given by:

$$L_n(x_l+x_h)_{n,\max} \leqq L_e(x_l+x_h)_e + \sum_{i>h} V_{e+1}\, y_{i,e+1}\,;\ n<e \quad \ldots\ldots\ldots (45)$$

$$\leqq L_{f-1}(x_l+x_h)_{f-1} + \sum_{i<l} L_{f-1}\, x_{i,f-1};\ n>f-1$$

A straight operating line in the equivalent binary sytem permits the use of the coordinate transformation of Stoppel[10] in Equation (9) by replacing Y_{N+1} with

$$\frac{(Y/1+Y)_{n+1} - (\underline{Y}/1+\underline{Y})}{(\overline{Y}/1+\overline{Y}) - (Y/1+Y)_{n+1}} = \frac{(X/1+X)_n - (\underline{X}/1+\underline{X})}{(\overline{X}/1+\overline{X}) - (X/1+X)_n}$$

where $(\underline{X}, \underline{Y})$ and $(\overline{X}, \overline{Y})$ are the left-hand and right-hand intersections of the operating line and equilibrium curve.

Intersections of the operating line and the equilibrium curve are obtained by assuming α to be constant outside the region of immediate interest. Such regions should not include irregular variations of volatility such as that which may occur across a condenser. Thus, in the enriching section, for example:

$$\overline{Y} = \alpha_1 \overline{X};\ \underline{Y} = \alpha_s \underline{X};\ 1 \leqq n \leqq s$$

$$\frac{L_n(x_l+x_h)_n}{V_{n+1}(y_l+y_h)_{n+1}} =$$

$$\frac{(\underline{Y}/1+\underline{Y}) - (X/1+X)_D}{(\underline{X}/1+\underline{X}) - (X/1+X)_D} = \frac{(\overline{Y}/1+\overline{Y}) - (X/1+X)_D}{(\overline{X}/1+\overline{X}) - (X/1+X)_D}$$

It should be noted that $\overline{X}$ can be negative, passing from $+\infty$ to $-\infty$ when $\overline{X}/1+\overline{X}$ is unity.

If the relative volatility is constant, then α_N can be replaced by

$$\frac{1 + (\alpha_n - 1)(\overline{X}/1+\overline{X})}{1 + (\alpha_n - 1)(\underline{X}/1+\underline{X})}$$

If α_N is not constant, then the transformed volatility is calculated in the obvious way from known quantities. With suitable

assumptions, a final form for n, analagous to Equation (18), is obtained.

Nomenclature

B = Bottoms product, moles
D = Overhead product, moles
e = Theoretical plate number at the bottom of the enriching section
$f-1$ = Theoretical plate number at the top of the stripping section
F = Total feed, moles
F_L = Liquid portion of the feed, moles
F_V = Vapor portion of the feed, moles
k = Index of demarkation
K_{in} = Equilibrium constant for component i at the temperature and pressure of plate n
log = Natural logarithm
L_{Mc} = Minimum reflux leaving the bottom tray of the enriching section obtained from a feed tray balance, moles
L_{Mn} = Minimum reflux leaving plate n obtained from an equilibrium balance, moles
L_{Ms} = Minimum reflux leaving the enriching section at the intersection of the operating lines given by Equation (44), moles
L_n = Reflux leaving plate n, moles
L_s = Reflux leaving the enriching section at the intersection of the operating lines, moles
L'_{Mn} = Pseudo minimum reflux leaving plate n obtained by a geometrical construction, moles; $n<e$
n = Theoretical plate number counting from the top of the distillation tower. A partial condenser with condensate to reflux is taken as the first plate, and an equilibrium reboiler as the last. See Appendix D
N = Total reflux trays for the key components computed in terms of vapor compositions
$(\partial n/\partial N)_s$ = Differential coefficient defined by Equations (11) and (12) and evaluated at the intersection of the operating lines in Equation (31)
s = Value of n at the intersection of the operating lines
u = Theoretical plate in the enriching section where the heavy key component reaches its maximum concentration
V_{n+1} = Vapor stream entering plate n, moles.
V_{s+1} = Vapor entering the enriching section at the intersection of the operating lines, moles
w = Theoretical plate number in the stripping section where the light key component is at its maximum concentration
x_{iF} = Mole fraction of component i in the liquid portion of the feed
x_{in} = Mole fraction of component i in the liquid leaving plate n
X = Mole ratio: moles of light key component per mole of heavy key in the liquid
X_B = Mole ratio in the bottoms product
X_D = Mole ratio in the overhead product
X_F = Mole ratio in the liquid portion of the feed
X_n = Mole ratio in the liquid leaving plate n
X_s = Mole ratio in the liquid at the intersection of the operating lines
y_{iF} = Mole fraction of component i in the vapor portion of the feed
y_{in+1} = Mole fraction of component i in the vapor entering plate n
Y = Mole ratio: moles of light key component per mole of heavy key in the vapor
Y_F = Mole ratio in the vapor portion of the feed
Y_{n+1} = Mole ratio in the vapor entering plate n
Y_{s+1} = Mole ratio in the vapor at the intersection of the operating lines
z_i = Mole fraction of component i in the total feed
Z = Moles of light key component per mole of heavy key component in the total feed

Greek Letters

α_{ijn} = Volatility of component i relative to the volatility of component j at the temperature and pressure of plate n
Δ = Final value minus the initial value of the quantity to which it is applied over the region of interest concerned
ϕ_{ijn} = Composition ratio defined by Equation (1)

Superscripts

$'$ = Pseudo minimum reflux
$''$ = Maximum flows

Subscripts

h = Heavy key component
l = Light key component
M = Minimum reflux

In general the subscripts l and h are not used unless it is necessary to distinguish between components other than the light and heavy keys.

References

(1) Gilliland, E. R., Ind. Eng. Chem., **27,** 260 (1935).
(2) Surowiec, A. J., Petrol. Refiner, **38,** 247 (1959).
(3) Colburn, A. P., Trans. Am. Inst. Chem. Engrs., **37,** 805 (1941).
(4) Hengstebeck, R. J., Schubert, D. W., Chem. Eng. Progr., **55,** 243 (1957).
(5) Jenny, F. J., Trans. Am. Inst. Chem. Engrs., **35,** 635 (1939).
(6) Albright, M. A., Petrol. Refiner, **37,** 111 (1958).
(7) Happel, J., Chem. Eng., **65,** No. 14, 144 (1958).
(8) Cohen, K., "Theory of Isotopic Separations", McGraw-Hill Book Co., New York, 1951.
(9) McCabe, W. L., Thiele, E. W., Ind. Eng. Chem., **17,** 605 (1925).
(10) Stoppel, A. E., Petrol. Eng., **18,** No. 7, 189 (1947).
(11) Weinstock, R., "Calculus of Variations", McGraw-Hill Book Co., New York, 1952.
(12) Surowiec, A. J., Ind. Eng. Chem., **53,** 280 (1961).
(13) Boole, G., "Calculus of Finite Differences", p. 18, Chelsea Publishing Co., New York, 1958.

APPENDIX A: OPTIMIZATION STUDIES

Since the reflux loading in a tower determines to a large extent the diameter, the size of an enriching section can be taken as proportional to the integral

$$P = \int_0^s (L_n/D)dn$$

To find a minimum sized plant it is necessary to determine the conditions under which the integral P is stationary.

Variable Reflux Case. Inspection of Figure 2 shows that the reflux loading $L_n(x_{ln} + x_{hn})$ can be gotten in terms of $(\partial n/\partial N)$ and Y_{n+1}, or with Equations (9) and (15), in terms of n and $(\partial n/\partial N)$. In a region where Equations (40) and (41) are applicable, the percentage of combined keys has a value which depends only upon L_n when α does not vary. The functional dependence of the reflux can then be indicated by

$$(L_n/D) = L/D\,[(\partial n/\partial N), n] \quad \ldots\ldots\ldots\ldots (46)$$

According to the Calculus of Variations[11], the integral P will be stationary when

$$\frac{\partial(L_n/D)}{\partial(\partial n/\partial N)} - \frac{d\left(\dfrac{\partial(L_n/D)}{\partial p}\right)}{dn} = 0 \quad \ldots\ldots\ldots\ldots (47)$$

Reference to (46) shows that $p \equiv \dfrac{d(\partial n/\partial N)}{dn}$ does not appear and Equation (47) reduces to

$$\frac{\partial(L_n/D)}{\partial(\partial n/\partial N)} = 0 \quad \ldots\ldots\ldots\ldots\ldots\ldots (48)$$

Equation (48) requires that the design parameter remain constant, hence,

$$dn = (\partial n/\partial N)dN \quad \ldots\ldots\ldots\ldots\ldots\ldots (49)$$

Rewriting the integral P

$$P = (\partial n/\partial N)\int_0^{N_e} (L_n/D)dN \quad \ldots\ldots\ldots\ldots (50)$$

Differentiating with respect to the design parameter and setting the result equal to zero

$$\frac{dP}{d(\partial n/\partial N)} = 0 = \int_0^{N_e}\left(\frac{L_n}{D}\right)dN + (\partial n/\partial N)\int_0^{N_e}\frac{\partial(L_n/D)}{\partial(\partial n/\partial N)}\,dN \quad \ldots\ldots\ldots (51)$$

Making use of Equation (1) and the fact that $(x_1'/x_h')_{Mn} = X_{n+1}$ in Equations (35) and (33a) results in

$$\frac{L_n}{L'_{Mn}} = \frac{\alpha_{n+1} - 1}{\phi_n - 1}\cdot\frac{x'_{1Mn}}{x_{ln}} \quad \ldots\ldots\ldots\ldots (52)$$

with $x'_{tMn} \geqq x_{ln+1}$. With α sufficiently small and of little variation, Equations (52) and (13) yield

$$\frac{L_n}{L'_{Mn}} \cong \frac{(\partial n/\partial N)}{(\partial n/\partial N) - 1} \quad \ldots\ldots(53)$$

Substituting (53) in (51) results in

$$\left[\frac{(\partial n/\partial N)}{(\partial n/\partial N) - 1} - \frac{(\partial n/\partial N)}{[(\partial n/\partial N) - 1]^2}\right] \int_0^{N_e} (L'_{Mn}/D)dN = 0 \quad \ldots(54)$$

Equation (54) reduces to

$$(\partial n/\partial N) = 2$$

and

$$(L/L_M)_n \cong (L/L'_M)_n = 2; \quad n < e$$

Constant Reflux. Setting L_n equal to L_e in the integral P,

$$P = nL_e \quad \ldots\ldots(55)$$

Rewriting Equation (55) for $n = e$ with the aid of (44) and (17), differentiating with respect to $(\partial n/\partial N)_e$ and setting the result equal to zero,

$$N_e = \frac{\frac{1}{2}(\log m - m + 1)}{(m/m - 1)(m - 1 - 2\log m)}; \; m \equiv (\partial n/\partial N)_e \quad \ldots\ldots(56)$$

The solution of (56) yields the following for a minimum sized enriching section with constant reflux:

N_e	$(\partial n/\partial N)_e$
0.00	1.00
1.00	2.82
1.54	3.00
2.02	3.10
8.73	3.40
16.10	3.45
∞	3.50

For the stripping section, P is equal to $(n - s)(L_s + F_L)$, while for the combined enriching and stripping sections, P is given by $nL_s + (n - s)F_L$. The overall tower is a minimum when $L_{Ms}N/F_L$ is equal to

$$\frac{(m-1)^2(1/2m) + (N - N_s)(\log m - m + 1)}{(m/m - 1)(m - 1 - 2\log m)}; \; m \equiv (\partial n/\partial N)_s$$

In order for P to be a minimum for the overall tower, $(\partial n/\partial N)_s$ has a maximum value of 3.5.

APPENDIX B: DERIVATION OF EQUATIONS

The basic differential equations of multicomponent distillation have been arrived at by resorting to a standard technique and employing Taylor's formula. To find the differential change in n, expand n at the point $\log Y_{n+1}$, $\log X_n$, and $\log\alpha_n$, by the Taylor formula, retaining only first order terms. Then,

$$dn = (\partial n/\partial \log X_n)_{Y,\alpha} d\log X_n + (\partial n/\partial \log Y_{n+1})_{X,\alpha} d\log Y_{n+1} \quad \ldots(57)$$
$$+ (\partial n/\partial \log\alpha_n)_{X,Y} d\log\alpha_n$$

Making the substitutions

$$d\log X_n = d\log Y_{n+1} - d\log\phi_n \quad \ldots\ldots(58)$$

and

$$d\log\alpha_n = d\log(\alpha/\phi)_n + d\log\phi_n \quad \ldots\ldots(59)$$

Equation (57) becomes

$$dn = [(\partial n/\partial \log X_n)_{Y,\alpha} + (\partial n/\partial \log Y_{n+1})_{X,\alpha}] d\log Y_{n+1} \quad \ldots\ldots(60)$$
$$+ [\partial n/\partial \log\alpha_n)_{X,Y} - (\partial n/\partial \log X_n)_{Y,\alpha}] d\log\phi_n$$
$$+ (\partial n/\partial \log\alpha_n)_{X,Y} d\log(\alpha/\phi)_n$$

Since

$$(\partial n/\partial \log\alpha_n)_{X,Y} - (\partial n/\partial \log X_n)_{Y,\alpha} =$$
$$[\partial n/\partial \log(\alpha/\phi)_n)_{Y,\phi} - (\partial n/\partial \log(\alpha/\phi)_n)y,_\alpha \quad \ldots\ldots(61)$$

symmetry suggests that this term be zero, so that as a function of Y and α/ϕ, the differential of n becomes

$$dn = [(\partial n/\partial \log X_n)_{Y,\alpha} + (\partial n/\partial \log Y_{n+1})_{X,\alpha}] d\log Y_{n+1}$$
$$+ (\partial n/\partial \log\alpha_n)_{X,Y} d\log(\alpha/\phi)_n \quad \ldots\ldots(62)$$

Justification for setting (61) equal to zero can be found by referring to a $\log X$ versus $\log Y$ diagram. On this type of plot, lines of constant α and constant ϕ are parallel and of unit slope. A little manipulation will show that if $\log Y_n - \log Y_{n+1}$ changes from one tray to the next, then it makes no difference if this change is accomplished by a change in α or ϕ, or both, the end result will be the same.

If n had been expanded by means of the Taylor formula about $\log\alpha_{n+1}$, and if Y_{n+1} had been eliminated from the resulting expansion, there would be the term

$$(\partial n/\partial \log\alpha_{n+1})_{X,Y} + (\partial n/\partial \log Y_{n+1})_{X,\alpha} =$$
$$[\partial n/\partial \log(\alpha_{n+1}/\phi_n)]_{X,\phi} - [\partial n/\partial \log(\alpha_{n+1}/\phi_n)]_{X,\alpha} \quad \ldots\ldots(63)$$

Following the same sort of reasoning that was employed in setting (61) equal to zero, this term can also be set equal to zero. There are then, the pair of equations

$$[(\partial n/\partial \log\alpha)_{X,Y} - (\partial n/\partial \log X_n)_{Y,\alpha}]_{\alpha=\alpha_n} = 0 \quad \ldots\ldots(64)$$

$$[(\partial n/\partial \log\alpha)_{X,Y} + (\partial n/\partial \log Y_{n+1})_{X,\alpha}]_{\alpha=\alpha_{n+1}} = 0 \quad \ldots\ldots(65)$$

The difference in sign that appears here is due to the fact that $\Delta\log\alpha$ plays a dual role. Near $X = X_{n+1}$, $\Delta\log\alpha$ behaves as $-\Delta\log X$, while near $Y = Y_n$, it behaves as $+\Delta\log Y$. Writing (64) and (65) for the same value of relative volatility

$$|(\partial n/\partial \log\alpha)_{X,Y}| = |(\partial n/\partial \log X_n)_{Y,\alpha}| = |(\partial n/\partial \log Y_{n+1})_{X,\alpha}| \quad \ldots(66)$$

and

$$(\partial n/\partial \log X_n)_{X,\alpha} = (\partial n/\partial \log Y_{n+1})_{X,\alpha} \quad \ldots\ldots(67)$$

Equation (67) simply states that total condensation of a part of the vapor stream and total vaporization of a part of the liquid stream yield the same results.

Substituting (64) in (62), the total differential for n becomes

$$dn = [(\partial n/\partial \log X_n)_{Y,\alpha} + (\partial n/\partial \log Y_{n+1})_{X,\alpha}] d\log Y_{n+1} +$$
$$(\partial n/\partial \log X_n)_{Y,\alpha} d\log(\alpha/\phi)_n \quad \ldots\ldots(68)$$

When α/ϕ is constant, Equation (4) becomes

$$\log(Y_{n+1}/Y_1) = -n\log(\alpha/\phi) \quad \ldots\ldots(69)$$

and differentiation yields

$$(\partial n/\partial \log Y_{n+1})_{\alpha/\phi} = -1/\log(\alpha/\phi)_n \quad \ldots\ldots(70)$$

Making the necessary substitutions in Equation (68)

$$-\log(\alpha/\phi)_n dn = d\log Y_{n+1} + \tfrac{1}{2}d\log(\alpha/\phi)_n \quad \ldots\ldots(71)$$

This is Equation (8) that was previously developed.

In terms of liquid compositions, the companion equation is

$$-\log(\alpha_{n+1}/\phi_n) dn = d\log X_n - \tfrac{1}{2}d\log(\alpha_{n+1}/\phi_n) \quad \ldots\ldots(72)$$

If the equilibrium relationship had been written in terms of the equilibrium constant

$$y_n = K_n x_n \quad \ldots\ldots(73)$$

there would be the pair of equations:

$$-\log(K_n x_n/y_{n+1}) dn = d\log y_{n+1} + \tfrac{1}{2}d\log(K_n x_n/y_{n+1}) \quad \ldots\ldots(74)$$

$$-\log(K_{n+1}x_n/y_{n+1}) dn = d\log x_n - \tfrac{1}{2}d\log(K_{n+1}x_n/y_{n+1}) \quad \ldots\ldots(75)$$

The derivation of these equations parallels that of (71) since the geometry of the $\log y$ vs. $\log x$ diagram is the same as the $\log Y$ vs. $\log X$ diagram.

The applicability of these equations is readily determined by evaluating the logarithmic composition terms, $\log(Y_n/Y_{n+1})$, $\log(y_n/y_{n+1})$, etc., for adjacent trays and then dividing the arithmetic average of the two by the logarithmic average. The result gives the fraction of the actual trays accounted for by these equations at that point. This can be shown from Equation (16) when $\log(\alpha_n/\phi_n) \equiv Q_n$ is linear in $\log Y_{n+1}$. Then, for one tray,[12]

$$\Delta n = \frac{\frac{1}{2}(Q_{n+1} + Q_n)}{(Q_{n+1} - Q_n)} \log(Q_{n+1}/Q_n) \quad \ldots\ldots(76)$$

gives the calculated number of trays. When Q_{n+1}/Q_n lies between 0.5 and 2, then Δn is less than 1.04.

APPENDIX C: MATHEMATICAL CONVENTIONS

A theoretical tray or plate is considered here as the difference operator E of the calculus of finite differences. E is such that $E\log Y_n = \log Y_{n+1}$. The subscript n records the number of times the operator E occurs. Since E is related to the differential

operator d of the differential calculus by the Taylor series expansion[13]: $E = \exp(d/dn)$; there is no difficulty with differential theoretical trays. Accordingly, the differential tray is taken as the differential operator such that $\log Y_{n+dn} = \log Y_n + d \log Y_n$. For a single theoretical tray it follows easily that

$$(E - 1) \log Y_n = \int_n^{n+1} d \log Y_n = \log(Y_{n+1}/Y_n).$$

With these conventions, differential trays and differential numbers of theoretical trays are permissible.

APPENDIX D: TRAY NUMBERING PROCEDURE

The theoretical plate number, n, can assume all values greater than zero and its integral values need not coincide with a physical boundary. However, n itself represents an arbitrary boundary or reference plane. Thus, the quantity and properties of the reflux leaving a plate and crossing a theoretical plate boundary bear the number of the plate as a subscript. Correspondingly, the counter-flowing vapor stream entering the plate carries the theoretical plate number increased by unity as a subscript. In effect, functional dependence upon n is indicated by a subscript even though n is not a true index of demarkation.

In this report, the counting of theoretical plates begins in the enriching section at $X_D = Y_1 = X_0$, and ends in the stripping section at X_B on the 45° diagonal of the McCabe-Thiele diagram in the equivalent binary system. The enriching section includes the condenser and the stripping section includes the reboiler.

Equation (31) determines the theoretical plate requirements for a separation from X_D to X_B. To determine the number of theoretical plates in the tower proper, it is necessary to deduct the equivalent number of plates for the reboiler and condenser. In the case of a total condenser and total reboiler the product compositions coincide with the terminal points of the tower operating lines and there is no correction. In the case of a partial condenser, equilibrium reboiler, and thermosyphon reboiler, the operating lines terminate before they reach the product compositions at X_D and X_B. It is necessary to extrapolate the operating lines to evaluate the auxiliary equipment. In Equation (31), this extrapolation was in effect accomplished by and evaluated by Equation (17). If correction is to be made to the total number of plates obtained from Equation (31), it should be done by means of Equation (17). Customarily, the extrapolations are performed at constant L/V ratio using the terminal flows at the top or bottom of the tower itself.

The number of theoretical plates at the bottom of the enriching section, e, and the number of plates at the top of the stripping section, $f-1$, are not necessarily equal unless the compositions of liquid and vapor at these points are equal. This is the case in Equations (29) and (30) where saturated liquid and vapor feeds are introduced at the intersection of the operating lines.

In the case of a partially vaporized feed in Equation (26), the operating lines terminate before they intersect. A separation effect results from the introduction of feed which is considered as a part of the distillation process and is included in the estimation of tray requirements. In Equation (31), this composition difference is evaluated along extrapolations of the operating lines near their intersections. A number of different mechanisms can be suggested for the coupling of the operating lines and the introduction of partially vaporized feed. The simplest situation occurs when the compositions of the liquid and vapor portions of the feed and the compositions at the intersection of the operating lines are the same and lie on the diagonal joining the equilibrium point (X_F, Y_F) and the point Z on the 45° diagonal on the McCabe-Thiele diagram in the equivalent binary system.

APPENDIX E: SAMPLE CALCULATIONS

Data: Edmister, W. C., "Hydrocarbon Absorption and Fractionation Process Design Methods", Tables 55, 58, 59. Reprinted from the Petrol. Eng.

Comp	F_s	Dx_D	Bx_B	$F_L x_F$	$F_V y_F$	α_F	α_D	α_B
C_1	26	26		1	25	20.6		
C_2	9	9		1	8	5.09		
C_3	25	24.6	0.4	7	18	2.06	3.12	1.86
C_4	17	0.3	16.7	8	9	1.00	1.00	1.00
C_5	11		11.0	7	4	0.429		
C_6	12		12.0	10	2	0.206		

Basis: Assume $(\partial n/\partial N)_s = 2.90$; $s = e$

Equation (13)

$$\frac{\log_{10} 2.06}{\log_{10} \phi_s} = 2.90/1.90; \phi_s = 1.61$$

Equation (27)

$$\frac{\dfrac{1.61X_s}{1 + 1.61X_s} - \dfrac{25/17}{1 + 25/17}}{\dfrac{X_s}{1 + X_s} - \dfrac{25/17}{1 + 25/17}} = \frac{-(8 + 7)}{18 + 9}$$

$$X_s = 1.09; \quad Y_{s+1} = 1.75$$

Equation (19)

$$\frac{\dfrac{24.6/0.3}{1 + 24.6/0.3} - (1.75/2.75)}{(1.75/2.75) - (1.09/2.09)} = \frac{L_s(x_{3s} + x_{4s})}{24.6 + 0.3}$$

$$L_s(x_{3s} + x_{4s}) = 76.2$$

Equation (40)

$$(Lx_1)_s = 26.0/(20.6 - 1) = 1.3$$
$$(Lx_2)_s = 9.0/(5.09 - 1) = 2.2$$

Equation (42) & Feed Balance

$$(Lx_5)_s = 11.0/(1 - 0.429/2.06) - 7 = 6.9$$
$$(Lx_6)_s = 12/(1 - 0.206/2.06) - 10 = 3.3$$

Reflux leaving the enriching section:

	C_1	C_2	C_3	C_4	C_5	C_6
$(Lx_i)_s$	1.3	2.2	39.7	36.5	6.9	3.3
Actual	1.34	2.41	37.0	37.7	8.13	3.42

Equation (18) (Enriching & Stripping Stepwise Application.)

$$-\Delta N = \left[\log_{10}\left(\frac{1.75}{24.6/0.3}\right) + \tfrac{1}{2}\log_{10}(2.06/3.12)\right] \frac{2.303 \log_{10}\left(\dfrac{\log_{10}2.06}{\log_{10}3.12}\right)}{\log_{10}(2.06/3.12)} +$$
$$\left[\log_{10}\left(\frac{0.4/16.7}{1.75}\right) + \tfrac{1}{2}\log_{10}(1.86/2.06)\right] \frac{2.303 \log_{10}\left(\dfrac{\log_{10}1.86}{\log_{10}2.06}\right)}{\log_{10}(1.86/2.06)}$$

$$N = 10.91 \text{ (Enriching + Stripping)}$$

Equation (31)

$$n/N = 2.303\,(2.90/1.90) \log_{10}2.90 = 1.62$$
n (including reb. & cond.) = 17.7; actual = 17

Assume maximum flows are given by Equation (45):

Equation (45)

$$L_n(x_l + x_h)_{n,\max} = 76.2 + 3.3 + 6.9 = 86.4; n < e$$
$$L_n(x_l + x_h)_{n,\max} = 76.2 + (7+8) + (1.3+1) + (2.2+1) = 96.7; \quad n > f - 1$$

Equation (19)

$$(Y/1 + Y)''_{n+1} = \frac{86.4(X/1 + X)'_n + 24.6}{86.4 + 24.6 + 0.3}; n < e$$

$$(Y/1 + Y)''_{n+1} = \frac{96.7(X/1 + X)'_n - 0.4}{96.7 - 16.7 - 0.4}; n > f - 1$$

Intersection of the operating lines for maximum flows yields:

$$Y''_{s+1} = 1.63; X''_s = 1.05; \phi''_s = 1.55$$

Equations (13) and (31) yield:

$$n''/N = 1.53;\ n'' = 16.7$$

Inclusion in Equation (31) of the term neglected in the differentiation of Equation (14) results in:

Equation (31a)

$$n = \frac{N(\partial n/\partial N)_s \log(\partial n/\partial N)_s}{(\partial n/\partial N)_s - 1} + \tfrac{1}{2}\int_0^n [(\partial n/\partial N) - 1]\, d \log \log \alpha_n$$

The correction term in Equation (31a) amounts to -0.32 in the first case and -0.24 in the second.

Data: Amundson, N. R., Pontinen, A. J., Ind. Eng. Chem., **50,** 730 (1958). Table IV, 15th iteration. Feed is vaporized on the feed tray: $X_F = X_f$; $Y_F = Y_f$. Cross plots of the data show that the intersection of the operating lines lies near the bottom of the feed tray. A check will be made of the number of trays

Item	s	x_B	x_D	x_1	y_2	x_f	y_{f+1}
C_3	0.200	0.009	0.853	0.910	0.903	0.233	0.367
C_4	0.370	0.473	0.0165	0.042	0.0387	0.495	0.509
α		2.00	3.00	2.38		2.00	
Moles	100	77.4	22.6				

(x_1 and y_2 are compositions of liquid leaving and vapor entering the condenser.)

$$Y_{s+1} \cong Y_{f+1} = 0.367/0.509 = 0.722$$
$$X_s \cong X_f = 0.233/0.495 = 0.470$$
$$\phi_s \cong 0.722/0.470 = 1.53$$
$$(\partial n/\partial N)_s = (\log_{10}2.00)/\log_{10}(2.00/1.53) = 2.60$$

$$-\Delta N = \left[\log_{10}\left(\frac{0.903/0.0387}{0.853/0.0165}\right) + \tfrac{1}{2}\log_{10}(2.38/3.00)\right] \frac{2.303 \log_{10}\left(\frac{\log_{10}2.38}{\log_{10}3.00}\right)}{\log_{10}(2.38/3.00)} +$$
$$\left[\log_{10}\left(\frac{0.722}{0.903/0.0387}\right) + \tfrac{1}{2}\log_{10}(2.00/2.38)\right] \frac{2.303 \log_{10}\left(\frac{\log_{10}2.00}{\log_{10}2.38}\right)}{\log_{10}(2.00/2.38)} +$$
$$\left[\log_{10}\left(\frac{0.009/0.473}{0.722}\right)\right]/\log_{10}2.00$$

$$N = 10.75 \text{ (Partial Condenser + Enriching + Stripping)}$$
$$n/N = 2.303(2.60/1.60)\log_{10}2.60 = 1.55$$
$$n \text{ (including reb. \& cond.)} = 16.7; \text{ actual} = 16$$

In the above example, heat of vaporization of the feed came from sensible heat in the feed. However, if the top tray and the feed tray act as heat transfer trays and heat effects are considerable, then stepwise application of Equation (17) may be necessary to avoid erratic results. Note that Equation (18) has been applied across the condenser itself because of the large change in relative volatility.

The sum of the combined keys has a maximum of 152.0 mol./hr. in the liquid leaving the top tray, and a maximum of 154 mol./hr. in the liquid leaving the third tray beneath the feed tray. The operating lines for these flows are:

$$(Y/1 + Y)''_{n+1} = \frac{152.0(X/1 + X)''_n + 22.6(0.853)}{152.0 + (0.853 + 0.0165)22.6};\ n < e$$

$$(Y/1 + Y)''_{n+1} = \frac{154.0(X/1 + X)''_n - 77.4(0.009)}{154.0 - (0.009 + 0.473)77.4};\ n > f - 1$$

Intersection of the operating lines yields, for the maximum flows:

$$\phi''_s = 1.46;\ n''/N = 1.44;\ n'' = 15.5$$

The calculated values of n properly straddle the actual value. The correction term in Equation (31a) amounted to -0.2 in both cases. Some of the slopes of the operating lines in the equivalent binary system in arithmetic and logarithmic coordinates are shown below:

n	$\frac{\Delta(Y/1 + Y)_{n+1}}{\Delta(X/1 + X)_n}$	$\frac{\Delta \log Y_{n+1}}{\Delta \log X_n}$
1 (cond.)	0.845	0.917
2 (top)	0.886	0.923
e	0.841	
s	0.848	0.909

Let $\log(\alpha/\phi)_n = Q_n - p_n$ where Q_n is linear in $\log Y_{n+1}$ and $p_n > 0$ when the operating line lies to the left of the linear approximation and zero otherwise. Let $\log(\alpha/\phi)_n = Q_n + q_n$ where $q_n > 0$ when the operating line lies to the right. Then the operating line and the linear approximation will yield the same value of n when

$$\int_0^n \left(\frac{1}{Q_n - p_n} - \frac{1}{Q_n}\right) d \log Y_{n+1} = \int_0^n \left(\frac{1}{Q_n} - \frac{1}{Q_n + q_n}\right) d \log Y_{n+1} \quad \ldots\ldots(83)$$

Hence,

$$\int_0^n \left|\frac{p_n dQ_n}{Q_n^2}\right| \leqq \int_0^n \left|\frac{q_n dQ_n}{Q_n^2}\right| \quad \ldots\ldots\ldots\ldots\ldots\ldots(84)$$

In general, when $p_n/Q_n^2 > q_n/Q_n^2$ then the linear approximation will yield less than the actual number of trays. This is the situation which exists when the intersection of the operating lines lies to the left of the linear approximation in logarithmic coordinates. (It is understood in the above that dQ_n changes sign at $\log Y_{s+1}$.) It is difficult to show that n'' will always be less than actual when ϕ_s'' is obtained from the maximum flows, although this appears to be the case. However, correction to n'' for the linear approximation can be made.

Data: Peiser, A. M., Chem. Eng., **67,** No. 14, 129 (1960). Sufficient information is not available for a tray check. Design conditions will be analyzed.

Comp.	x_F	y_F	x_B	x_D	x_e	y_f
7	0.0592	0.0137	0.0002	0.1871	0.0379	0.0844
8	0.1689	0.2243	0.0416	0.4351	0.3186	0.3877
9	0.2759	0.1712	0.3963	0.0380	0.4440	0.3191
10	0.2076	0.0706	0.2999	0.0003	0.1239	0.0797
Mols	831.20	168.80	614.70	385.30	660.62	885.13

Basis: Components 8 and 9 will be taken as the keys.

$Z = 0.750$

$Y_F = 1.312$ $\quad Y_{e+1} = 1.223$ $\quad Y_f = 1.215$

$X_F = 0.678$ $\quad X_e = 0.718$ $\quad X_{f-1} = 0.70$

$\alpha_F = 1.93$ $\quad \phi_e = 1.705$ $\quad \phi_{f-1} = 1.735$

The intersection of the operating lines is estimated with Equation (27):

$$Y_{s+1} = 1.185$$
$$X_s = 0.689$$
$$\phi_s = 1.72 = \tfrac{1}{2}(1.705 + 1.735)$$

Using Equations (12), (31) and (44):

$$(\partial n/\partial N)_s = \log_{10}(1.93)/\log_{10}(1.93/1.72) = 5.70$$
$$n/N = 2.303(5.70/4.70)\log_{10}(5.70) = 2.1$$
$$(L/L_M)_s = 5.70/4.70 = 1.22$$

Reverse fractionation in the stripping and enriching sections is avoided by preselection of the point of intersection of the operating lines in the equivalent binary system.

★ ★ ★

Factorial Design in the Study of Acid Leaching of Pegmatitic Uranium Ores[1]

D. G. FISHER[2], R. G. McINTOSH[3], R. L. EAGER[3] and A. B. VAN CLEAVE[3]

Factorial design of leaching tests done on pegmatitic uranium ores is an efficient method of studying the effects of changes in process variables, as the required information may be obtained with a minimum expenditure of effort.

The results of a complete five factor, two level, factorially designed experiment in which an "acid-cure" technique was used are discussed. The data obtained in two, half replicate, five factor, two level, tests in which a percolation leach technique was used, establish base levels of variables for further economic study of uranium recovery from Higginson Lake pegmatites.

A large fraction of the known potential uranium reserves of the Canadian shield region of Northern Saskatchewan occurs in the form of pegmatitic deposits containing 0.10% or less of U_3O_8. Mawdsley[(1)] has described the geology of some of these deposits. The predominant minerals are feldspar and quartz but considerable amounts of biotite and smaller amounts of other minerals are also present. The uranium occurs mainly as small crystals of uraninite disseminated in the rock. The uranium values in these pegmatites show a tendency to concentrate in the fines during comminution[(2)], which supports the suggestion that the uraninite is associated with the biotite or that it occurs along grain boundaries which are readily cleaved. Chemical and spectrographic analyses of Saskatchewan pegmatites indicate that usually only trace amounts of carbonate, sulphide, phosphate, arsenate, molybdenum, cobalt, copper, zinc, nickel and chromium are present. Thorium in amounts comparable to the uranium content is sometimes present. The low acid consuming character of the rock, as indicated by chemical analyses, has been confirmed by leaching tests which indicated that high uranium recoveries could be obtained by leaching the ore at 50 to 60% pulp density for periods of from 48 to 72 hours with a solution containing 36 lb. of concentrated H_2SO_4 per ton of crushed ore (<0.185 in. 23% minus 35 mesh) at ambient temperature and without the addition of an oxidizing agent[(3)].

The results of leaching tests to be described in this paper were obtained using samples of a 15 ton lot of pegmatitic ore from the Anglo Barrington Mines property near Higginson Lake in Northern Saskatchewan. The average grade of the ore was 0.07% of U_3O_8. Preliminary leaching tests, in which several techniques were used with this ore have been reported[(4)].

The purpose of this paper is to discuss the application of factorial design of experiments to the study of the variables affecting the recovery of uranium by acid leaching, using both "acid-cure" and percolation leach techniques. The problem is to evaluate the effects of a number of process variables; such as, time, temperature, amount of acid, acid concentration, oxidizing agent and particle size, on the recovery of uranium from a pegmatitic ore. The most economical investigation is made by arranging the experiment according to an ordered plan in which all factors are varied in a regular way. Provided that the plan has been correctly chosen, it is possible to determine not only the effect of each individual factor, but also the way in which each effect depends on the other factors, that is the interactions. Thus a more complete picture is possible than would be obtained by varying each of the factors one at a time while keeping others constant. Statistical analysis can be applied to the results of such designs and it is possible, if necessary, to have the design provide its own estimate of experimental error[(5)].

A factorial design enables one to obtain the required information with the required degree of precision and with a minimum expenditure of effort. If some previous knowledge is available regarding the effects of the factors and the interactions, it may be possible to reduce the effort still further by using a fractional factorial design[(6)]. The advantages of using factorial designs may be summed up as follows:

1. When there are no interactions the factorial design gives the maximum effeciency in the estimation of the effects.
2. When interactions exist, their nature being unknown, a factorial design is necessary to avoid misleading conclusions.
3. In the factorial design the effect of a factor is estimated at several levels of the other factors, and conclusions hold over a wide range of conditions.

The application of factorial design to "acid-cure" and percolation leach technique of recovering uranium illustrates the usefulness of the method in assessing the effects of process variables and in estimating the conditions that would result in maximum profit in a commercial operation.

Experimental

A. Acid-Cure Leaching

In "acid-cure" leaching the crushed ore is mixed with sufficient strong sulphuric acid solution to wet the pulp, which is then acid-cured for a period of time prior to washing to remove the pregnant solution. The procedure followed was:

[1]*Manuscript received October 18, 1960; accepted March 18, 1961.*
[2]*Carbide Chemicals Company, Montreal, Que.*
[3]*Department of Chemistry and Chemical Engineering, University of Saskatchewan, Saskatoon, Sask.*
Based on a paper presented at the C.I.C. Western Regional Conference, Regina, Sask. September 9, 1960. Contribution from the Department of Chemistry and Chemical Engineering, University of Saskatchewan, Saskatoon, Sask.

TABLE 1
FACTOR LEVELS FOR ACID CURE LEACHING EQUIPMENT

400 g samples of crushed ore				
Factor	Base Level	Unit Interval	(−) Factor Level	(+)Factor Level
Temperature, °C.	30	10	20	40
Amount of H_2SO_4, lb/ton	27	9	18	36
Volume of acid solution, ml.	60	20	40	80
Time, hr.	24	8	16	32
Particle size			<1.41 mm (−14 mesh)[a]	<4.76 mm (−4 mesh)[b]

[a]Sample II Table 2 [b]Sample I Table 2

(1) 400 gm. samples of crushed ore and the desired volume of sulphuric acid solution were added to sealers which were rolled at room temperature (23±3°C.) for 45 min. at 50 r.p.m. to ensure adequate mixing.
(2) The samples were let stand in a constant temperature oven (t±0.5°C.) for specified times.
(3) 200 ml. of wash solution (distilled water adjusted to pH 2 with H_2SO_4) was added and the sealer rolled for 10 min.
(4) The pregnant liguor was removed by suction filtration.
(5) The residue was repulped in the orignal sealer with 200 ml. of wash solution by rolling for 10 min.
(6) The residue was again filtered and repulped with another 200 ml. of solution as before.
(7) The residue was dried at 105°C. for 12 hours and sampled for uranium analysis.
(8) The volumes of pregnant solution and the two washings were measured and samples taken for uranium and R_2O_3 analysis. The fluorophotometric method of analysis [7] was used for duplicate or triplicate analyses for uranium.

A complete five factor, two level, factorial design was set up and the leaching tests performed in a random order. The factors and the levels chosen are summarized in Table 1. (Screen analyses for the samples used are shown in Table 2.) The levels were chosen to cover a range of convenient operating conditions and to include conditions which gave satisfactory uranium recoveries in previous experiments[3,4]. The range between the upper and lower level of each factor was chosen so that the expected change in uranium recovery, produced by changing the level of one factor, would be approximately the same for each factor, thus minimizing the chance that the effect of changing one factor would over shadow the effects of other variables. The range between the two levels of any factor was made large enough to ensure that expected differences in uranium recoveries would be large enough, when compared to the experimental error, to be tested effectively in the 32 tests. The factors and factor levels were chosen so that all treatments would be subject to the same experimental error.

The per cent recoveries of U_3O_8 in the leach liquor (including washings) for each of the 32 tests in the complete five factor design are shown in Table 3. The amounts of ignited R_2O_3 that would be obtained from the neutralization of all of the leach liquor from 400 gm. samples of ore are also shown. These latter figures give an indication of the amount of iron, aluminum, silicon, etc. dissolved during the leaching process. It is evident that the greatest change in the weight of the ignited R_2O_3 precipitates is produced by varying the amount of acid used and, that the amount of contaminants in the pregnant solution can be minimized by using the minimum amount of acid necessary for satisfactory uranium recoveries in a given time interval. Separate experiments indicated that between 8 and 20% of the acid soluble R_2O_3 fraction of the ore was dissolved in these leaching tests.

An analysis of variance, by the method of individual comparisons[5] was done on the U_3O_8 recovery values coded according to the formula, $\phi = \mathrm{Sin}^{-1}\sqrt{\%\ U_3O_8\ \text{recovered}}$. The statistical analysis showed that the main effects of the five factors were all significant at the 1% level. That is, it can be concluded, with only a 1% chance of being wrong, that within the range studied, increasing the temperature, or increasing the amount of sulphuric acid or the volume of solution, or increasing the leaching time, or decreasing the average particle size, all result in a significant increase in the per cent of U_3O_8 extracted from the ore.

The interactions between: (a) temperature and time of leaching; (b) amount of acid and particle size; (c) volume of solution and particle size; (d) amount of acid and volume of solution; were also significant at the 1% level. The interaction between temperature and volume of solution was found to be significant at the 5% level. The magnitudes of the various interactions are summarized in Tables 4 to 8 where the average per cent U_3O_8 extracted in the 8 tests* at the indicated levels of each pair of factors is shown. None of the other possible interactions were found to be significant.

The results shown in Table 4 indicate that the time factor has a larger effect at 20°C. than at 40°C. The most probable reason for this interaction would be that the rate of leaching at 40°C. is so much greater than the rate at 20°C., that the extraction has proceeded practically to its full extent in 16 hours at the higher temperature level. If shorter leaching times has been selected this interaction might not have been significant.

The amount of acid-particle size interaction shown by the data in Table 5 may be explained by assuming that 18 lb. of acid per ton of −14 mesh ore does not provide enough acid to fully extract the uranium, since a larger fraction of the acid would be consumed by reaction with the more finely divided rock. When 36 lb. of acid per ton of ore is used, the amount of uranium extracted is significantly greater with −14 mesh ore because more of the uranium mineral is in positions more accessable to acid attack in the time allowed.

*Except in Table 7 where average U_3O_8 recoveries for 4 tests are given.

TABLE 2
PARTICLE SIZE DISTRIBUTION OF CRUSHED ORE SAMPLES USED IN "ACID-CURE" AND IN PERCOLATION LEACH TESTS

Particle Size Interval		Percent				
mm.	Standard Tyler Mesh.	Sample I	Sample II	Sample III	Sample IV	Sample V
<4.76, >1.41	−4+14	56.80	0.94	57.6	18.4	23.6
<1.41, >0.23	−14+65	31.92	75.31	34.4	64.7	58.1
<0.23, >0.074	−65+200	7.58	16.43	6.8	11.3	9.4
<0.074	−200	3.70	7.32	1.2	5.6	8.9

TABLE 3

PERCENT RECOVERY OF U_3O_8 AND AMOUNT OF IGNITED R_2O_3 IN LEACH LIQUORS FROM FACTORIALLY DESIGNED "ACID-CURE" LEACHING EXPERIMENTS

400 gm. sample I (−4 mesh)

H_2SO_4 lb./ton	Vol. ml.	20°C.				40°C.			
		16 hr.		32 hr.		16 hr.		32 hr.	
		U_3O_8	R_2O_3	U_3O_8	R_2O_3	U_3O_8	R_2O_3	U_3O_8	R_2O_3
		%	g	%	g	%	g	%	g
36	40	84.3	1.96	87.2	2.50	87.0	2.86	87.3	2.92
36	80	86.0	1.60	89.3	2.08	88.7	2.64	88.3	2.91
18	40	84.0	1.89	86.0	1.54	83.5	1.65	86.8	1.58
18	80	80.3	1.14	82.2	1.25	84.6	1.51	83.7	1.57

400 gm. sample II (−14 mesh)

H_2SO_4 lb./ton	Vol. ml.	20°C.				40°C.			
		16 hr.		32 hr.		16 hr.		32 hr.	
		U_3O_8	R_2O_3	U_3O_8	R_2O_3	U_3O_8	R_2O_3	U_3O_8	R_2O_3
		%	g	%	g	%	g	%	g
36	40	87.9	2.30	91.0	2.86	92.0	3.17	91.2	2.96
36	80	89.9	2.15	94.7	2.64	96.0	3.00	95.5	3.08
18	40	83.6	1.51	86.2	1.66	85.2	1.71	85.1	1.60
18	80	83.7	1.43	88.2	1.65	89.3	1.57	89.2	1.63

The volume of solution-particle size interaction shown by the data in Table 6 may be explained as follows. With −4 mesh ore, changing the volume of solution from 40 to 80 ml. resulted in a slight decrease in the amount of uranium extracted probably because the actual concentration of acid would be smaller with the larger volume of solution with resultant decrease in the rate of acid attack. With −14 mesh ore, however, the uranium extraction is considerably more efficient when the larger volume of solution is used. This could be due to incomplete wetting of the solid particles when 40 ml. of solution is used on

TABLE 4

TEMPERATURE-TIME INTERACTION, "ACID-CURE" LEACHING

		Temperature		
		20°C.	40°C.	
Time	16 hr.	84.9	88.3	% of U_3O_8 recovered
	32 hr.	88.2	88.8	

TABLE 5

AMOUNT OF ACID-PARTICLE SIZE INTERACTION "ACID-CURE" LEACHING

		Amount of Acid		
		18 lb./ton	36 lb./ton	
Particle size	−4 mesh	87.8	87.2	% of U_3O_8 recovered
	−14 mesh	86.3	92.3	

TABLE 6

VOLUME OF SOLUTION-PARTICLE SIZE INTERACTION "ACID-CURE" LEACHING

		Volume of Solution		
		40 ml.	80 ml.	
Particle size	−4 mesh	85.8	85.4	% U_3O_8 of recovered
	−14 mesh	87.8	90.8	

TABLE 7

TEMPERATURE-VOLUME OF SOLUTION INTERACTION "ACID-CURE" LEACHING

		−14 mesh ore		−4 mesh ore		
		Temperature				
		20°C.	40°C.	20°C.	40°C.	
Volume of solution	40 ml.	87.2	88.4	85.4	86.1	% U_3O_8
	80 ml.	89.1	92.5	84.4	86.4	recovered

TABLE 8

AMOUNT OF ACID-VOLUME OF SOLUTION INTERACTION "ACID-CURE" LEACHING

		Amount of Acid		
		18 lb./ton	36 lb./ton	
Volume of solution	40 ml.	85.1	88.5	% of U_3O_8 recovered
	80 ml.	85.2	91.1	

−14 mesh ore where the surface area would be considerably greater than in the case of −4 mesh ore, where 40 ml. of solution were judged sufficient to effectively wet 400 gm. of ore.

The data shown in Table 7 indicate that the major interaction between temperature and volume of solution is due to the results obtained with the −14 mesh samples. The effect of temperature is probably more evident when the −14 mesh ore is treated with 80 ml. of solution than with 40 ml. of solution, because of more effective wetting of the particles by the larger volume of solution as was suggested in explaining the volume of solution-particle size interaction above.

The apparent interaction between amount of acid and volume of solution, shown by the data of Table 8, can also be explained as being due to the effect of volume of solution and the surface area of the ore particles as discussed above.

In addition to providing data for testing the main effects of the five factors, this factorial design showed that satisfactory uranium recoveries are possible with "acid-cure" leaching techniques on this type of ore. However, this technique may not be practical as a commercial process because of the large amount of energy required to mix the ore and the solvent. In contrast, percolation leaching can be adapted to the treatment of large tonnages of ore. Further experiments were designed to test the effects of possible process variables on the extraction of uranium by a percolation leach technique.

B. Percolation Leaching

The work involved in carrying out a complete factorial design comprising 2^n tests when n factors are tested at two levels can frequently be lessened by the use of fractional factorial dseigns[5,6]. That is, it is possible to investigate the main effects and the more important interactions by using only a fraction of the number of tests required for the complete factorial experiment. This procedure is justified when it is known from previous tests that the effects of higher order interactions are negligible or when a sufficiently reliable estimate of experimental error has been established. However, if it is assumed that interactions of all orders are real, it follows that in a half replicate factorial design each effect is confused with another effect. Confused effects are termed "aliases" and it is imperative to determine the aliases for any proposed fractional factorial design in order to avoid confusion of important effects. Since it appeared that higher order interactions between leaching variables could safely be neglected, a half replicate factorial design was set up to test the effects of time, temperature, concentration of acid, concentration of oxidizing agent and particle size on recovery of uranium when a percolation leach technique is used.

All percolation leach tests were conducted in a cabinet which permitted both temperature and humidity control. The air in the cabinet was continuously circulated by means of a fan. The leaching apparatus is shown diagramatically in Figure 1. Four such units were located in the cabinet. Crushed ore samples weighing 200 gm. were placed in the 4-in. Buchner funnels and the acid solution was forced up through the ore bed by means of a finger pump, at a rate which was slow enough to prevent ore particles from being carried off in the overflow as it returned to the mixing reservoir. Evaporation losses were further minimized by tape sealing an inverted beaker over the funnel collecting the overflow and by taping a flat cover over the mixing reservoir. Tests begun by placing the desired amount of leach solution in the mixing reservoir, bringing the entire system to the desired temperature and then starting the circulation of the leach liquor. At the conclusion of a test, the circulating pump was stopped and as much as possible of the leach liquor was drained into the mixing reservoir before being removed for measurement of volume and uranium analysis. The residue was washed by circulating 100 ml. of wash liquor (water adjusted to pH 2 with H_2SO_4) through the system for ½ hr. The first wash liquid was drained from the system and the process repeated with a second 100 ml. portion of wash liquid. The volumes of both washings were measured and retained for uranium analysis. The leached ore sample was washed a third time by removing it from the Buchner funnel and pulping it with 100 ml. of distilled water. The residue was collected by suction filtration, dried, and analysed for uranium. The third wash liquid was also collected and analysed for uranium.

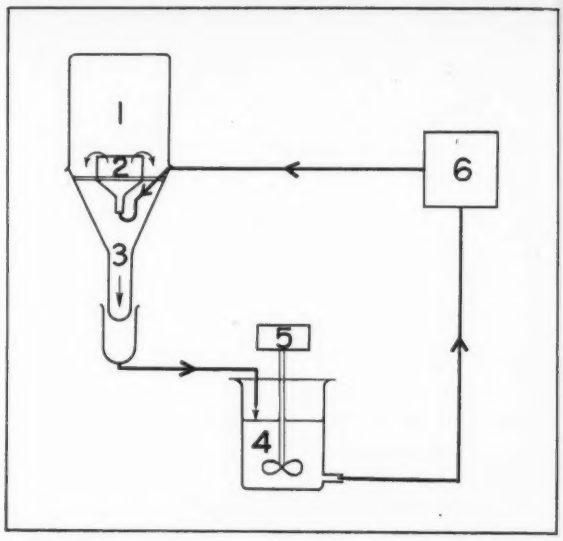

Figure 1—Schematic flow diagram of Percolation Leach apparatus.

Legend: 1. 21. beaker; 2. Buchner funnel containing 200 g. of ore; 3. glass funnel; 4. Leach liquor in 600 ml. beaker; 5. stirrer; 6. circulating pump.

The factor levels chosen for one half replicate factorial design I are shown in Table 9. Although earlier tests had not indicated the necessity of adding an oxidizing agent to obtain high uranium recoveries from this type of ore, it was of interest to see whether the presence of $NaClO_3$ would significantly affect uranium recoveries, hence, the factor levels 0 and 4 lb./ton of $NaClO_3$ were chosen. The levels of other factors are similar to those used in previous experiments. After the experimental design had been chosen the 16 individual tests were randomized by drawing numbers from a hat.

Screen analyses for ore samples III and IV used are given in Table 2. It will be noted that Sample III corresponds closely in size range fractions to Sample I, but that Sample IV shows a larger fraction of coarse particles than did Sample II, hence, it is designated as −8 mesh rather than −14 mesh.

The per cent uranium recoveries obtained in the tests of this half replicate factorial design are summarized in Table 10. In general, the uranium recoveries obtained by this leaching technique are very satisfactory, as high as 96% and the pregnant solution contains practically no suspended solids. Uranium could be recovered directly from such solutions by ion exchange or solvent extraction without employing a preliminary clarification step.

TABLE 9

FACTOR LEVELS FOR PERCOLATION LEACH DESIGN I

200 gm. samples of Crushed Ore
Volume of Leach Solution 400 ml.

Factor	Base Level	Unit Interval	(−) Factor Level	(+) Factor Level
Temperature °C.	35	10	25	45
Amount of H_2SO_4 lb./ton	27	9	18	36
Amount of $NaClO_3$ lb./ton	2	2	0	4
Time hr.	24	6	18	30
Particle size			<2.38 mm (−8 mesh)[a]	<4.76 mm (−4 mesh)[b]

[a]Sample IV Table 2 [b]Sample III Table 2

The responses were coded and subjected to statistical analysis by the method of Yates[6]. The analysis of variance indicated that three of the main effects, temperature, amount of acid and amount of oxidizing agent were significant at the 1% level. The effect of time was significant only at the 5% level and the particle size factor was not significant under the conditions of this experiment. Only one interaction, that between temperature and particle size was found to be significant and that at the 5% level. Increasing the temperature from 25°C. to 45°C., the amount of H_2SO_4 from 18 to 36 lb./ton of ore, and the addition of 4 lb./ton of $NaClO_3$ all significantly increase the extraction of uranium. Despite the observation that time appeared as significant only at the 5% level, it is certain that time is a controlling factor in the leaching mechanism as could be substantiated by choosing lower levels for this variable. The analysis does indicate that uranium recoveries would likely not be significantly increased by employing leaching times beyond 30 hours. The lack of significance in the particle size factor indicates that virtually all of the uranium oxide in the crushed rock is accessible to acid attack even in the −4 mesh material.

TABLE 10

PERCENT RECOVERY OF U_3O_8 IN LEACH LIQUORS FROM ONE-HALF REPLICATE FACTORIALLY DESIGNED PERCOLATION-LEACH, DESIGN I

200 gm. sample III (−4 mesh)
400 ml. acid solution

		25°C.		45°C.	
H_2SO_4 lb./ton	$NaClO_3$ lb./ton	18 hr.	30 hr.	18 hr.	30 hr.
36	0	—	89.5	87.7	—
36	4	90.5	—	—	94.4
18	0	85.5	—	—	83.9
18	4	—	89.2	90.2	—

200 gm. sample IV (−8 mesh)
400 ml. acid solution

		25°C.		45°C.	
H_2SO_4 lb./ton	$NaClO_3$ lb./ton	18 hr.	30 hr.	18 hr.	30 hr.
36	0	86.4	—	—	93.7
36	4	—	95.3	96.1	—
18	0	—	83.9	88.0	—
18	4	83.0	—	—	94.6

TABLE 11

TEMPERATURE-PARTICLE SIZE INTERACTION PERCOLATION LEACH DESIGN I

		Particle Size		
		−8 mesh	−4 mesh	
Temperature	25°C.	87.2	88.7	% U_3O_8 recovery
	45°C.	93.1	89.1	

Although the temperature—particle size interaction is confused with the three factor interaction, amount of acid—amount of oxidizing agent—time, the latter has been assumed to be negligible. A two-way table of mean per cent U_3O_8 recoveries calculated from the data in Table 10 is shown as Table 11. Increasing the temperature from 25°C. to 45°C. has a larger effect on the −8 mesh material than on the −4 mesh material. Thus, in spite of the absence of particle size as a main effect, it appears that higher uranium recoveries would be obtained with more finely crushed ore at 45°C. An economic balance would, of course, have to be made to justify the high temperature—fine particle size leaching method in practice. The revenue from increased recoveries would have to more than offset the increased grinding and heating costs to justify using these conditions.

In preforming the tests for percolation leach design I, it was observed that the volume of solution used (400 ml. per 200 gm. sample) was considerably larger than necessary and as pointed out above, particle size variation in the range investigated did not show a significant effect. Consequently a second half replicate factorially designed percolation leach experiment with factor levels as indicated in Table 12 was carried out. The particle size distribution of the ore sample V used in this design is given in Table 2. Note that the particle size distribution for Sample V is very similar to that for Sample IV. The experimental procedure employed was the same as outlined above for fractional factorial design I. The per cent uranium recoveries obtained in the tests of design II are shown in Table 13. Analysis of variance for the uncoded per cent U_3O_8 recoveries for this design showed the effects of temperature, amount of oxidizing agent, and time to be significant at the 1% level, and the effect of amount of acid to be significant at the 5% level. Neither the volume of acid solution or any of the first order interactions were significant at these levels.

As expected, the significance of the time factor is more evident in design II than in design I, because of the choice of a lower base level. The principal effect of increasing the temperature or of adding an oxidizing agent appears to be to increase the rate of solution of the uranium mineral, so that a given uranium recovery can be attained in a shorter time if elevated temperature and an oxidizing agent are used. The same uranium

TABLE 12

FACTOR LEVELS FOR PERCOLATION LEACH DESIGN II

200 gm. samples of crushed ore

Factor	Base Level	Unit Interval	(−) Factor Level	(+) Factor Level
Temperature °C.	35	10	25	45
Amount of acid lb./ton	27	9	18	36
Amount of $NaClO_3$ lb./ton	2	2	0	4
Time hr.	9	3	6	12
Volume of acid solution, ml.	162.5	37.5	125	200

TABLE 13

PERCENT RECOVERY OF U_3O_8 IN LEACH LIQUORS FROM ONE-HALF REPLICATE FACTORIALLY DESIGNED PERCOLATION-LEACH DESIGN II

200 gm. sample V (−8 mesh)
125 ml. acid solution

		25°C.		45°C.	
H_2SO_4 lb./ton	$NaClO_3$ lb./ton	6 hr.	12 hr.	6 hr.	12 hr.
18	0	71.6	—	—	92.5
18	4	—	88.0	88.0	—
36	0	—	82.5	87.3	—
36	4	84.0	—	—	93.3

200 gm. sample V (−8 mesh)
200 ml. acid solution

		25°C.		45°C.	
H_2SO_4 lb./ton	$NaClO_3$ lb./ton	6 hr.	12 hr.	6 hr.	12 hr.
18	0	—	80.2	82.9	—
18	4	80.0	—	—	89.0
36	0	79.0	—	—	91.5
36	4	—	88.6	87.5	—

recovery can be achieved at lower temperatures, and without the presence of an oxidizing agent, if a longer contact time can be used. Since the base level for volume of acid solution was set lower for design II than for design I, the actual concentration of acid was sufficiently high for effective leaching at both levels of volume of solution, so variation in this factor did not prove to be significant. In practice, therefore, the least volume of solution that would allow effective circulation of the acid solution through the ore bed should be used. Considering the results of fractional designs I and II, it is evident that uranium recoveries of the order of 95% can be obtained by percolation leaching of −8 mesh ore at 45°C. with as little as 18 lb. of H_2SO_4 per ton of ore for 24 hours, with oxidizing agent present. Similar recoveries can be obtained, if up to 36 lb. of H_2SO_4 per ton of ore is used without the addition of an oxidizing agent, although a somewhat longer contact period might be required. The high uranium recoveries and the "crystal clear" pregnant solutions obtained in the percolation leaching of Higginson Lake pegmatitic ore makes this method attractive as a possible commercial method for use with this type of ore.

Conditions which would result in maximum U_3O_8 recovery could be arrived at by using the results of designs I and II to select points along the path of steepest ascent at which further tests should be done. It is evident that by using higher temperatures, longer time, and larger amounts of acid in the presence of an oxidizing agent, that higher recoveries of U_3O_8 would be obtained. However, that point at which the increasing costs exceed the profit achieved by increasing the recovery would soon be reached. Therefore, the profit associated with the recovery of uranium by any leaching method should be chosen as the response to be maximized now that approximate base levels for the significant factors have been established. Cost estimates to be associated with each of the significant factors, temperature, time, amount of acid, amount of oxidizing agent and particle size would have to be estimated to establish the profit obtainable at a given recovery level. The above reported factorially designed experiments, using estimated profit as the response could then be used as a starting point to determine the levels of the process variables that would be used in plant practice. The value of factorial design in minimizing the number of tests necessary to establish the desired operating conditions is evident.

Acknowledgement

The authors are indebted to the Saskatchewan Research Council for a grant in aid of this work. One author (D. G. F.) expresses his appreciation of the National Research Council for the bursary awarded to him. The assistance of Anglo-Barrington Mines, Ltd. in supplying the ore sample is gratefully acknowledged.

References

(1) Mawdsley, J. B., The Radioactive Pegmatites of Saskatchewan, A/CONF. 15/P/225 (1958).

(2) VanCleave, A. B., Beneficiation of Low Grade Pegmatitic Uranium Ores, Trans. Can. Inst. Mining Met., LIX, 433 (1956).

(3) Gunn, Brad., Cavers, S. D., and VanCleave, A. B., The Extraction of Uranium from a Saskatchewan Pegmatite Granite, Can. J. Tech., **34**, 379 (1956).

(4) VanCleave, A. B. and Eager, R. L., Beneficiation of Low Grade Pegmatites, A/CONF. 15/P/230 (1958).

(5) Davies, O. L., Design and Analysis of Industrial Experiments, Oliver and Boyd, London (1956).

(6) Fractional Factorial Experiment Designs for Factors at Two Levels, Nat. Bur. Standards Applied Math. Series, 48, (1957).

(7) Centanni, F., Ross, A. M., and De Sesa, M. A., Fluorometric Determination of Uranium, WIN 34 (1956), Anal. Chem. 27, 1651 (1956).

★ ★ ★

Reactions in a Fluidized Coke Bed with Self-Resistive Heating[1]

H. S. JOHNSON[2]

When electrodes are inserted in a fluidized bed of conductive coke particles, an electric current can be passed with sufficient power to raise the bed to a high temperature. This device becomes a chemical reactor when the fluidizing gas is appropriately chosen. The reaction conditions which obtain in such a reactor are sometimes of especial value in producing favorable yields in chemical reactions.

The design and operating characteristics of laboratory scale units are described. These are usually Vycor tubes fitted with rubber stoppers through which electrical and gas connections are made. Even with such simple apparatus, it is possible to operate at 1500°C.

Several chemical reactions have been studied in detail using reactors of this type. Among these are some which show commercial promise, such as the high temperature reaction of ammonia and hydrocarbons to form hydrogen cyanide.

A fluidized bed of conductive particles can be heated by the passage of electric current between electrodes which dip into the fluidized bed, and in fact, such a system is a useful heat source, or chemical reactor. The physical arrangement is shown in Figure 1.

When used as a chemical reactor, the coke bed is fluidized by the reactant gas or mixture, which is thereby heated very rapidly to the bed temperature. The main application of such a reactor is to the following types of chemical reaction:

(1) reactions with substantial energy requirements. This applies equally to sensible and latent heat, but most especially to the higher temperature levels — say above 1800°F.

(2) reactions which are favored by rapid heating.

(3) reactions which are favored by high temperature, either through thermodynamic or kinetic effects.

The types of chemical reactions which can be carried out in such reactors are sometimes limited by the nature of the bed material. So far, only carbon has given satisfactory results, and carbon becomes reactive with various gases, oxygen, water, CO_2 and others, at moderately elevated temperatures. Thus, when it is proposed to include such gases as reactants, the existence of the reactions with carbon has to be considered.

Previous references to reactors of this type are quite rare, and appear to be confined to the patent literature. A German patent to F. Winkler of I. G. Farbenindustrie in 1928[1] is of particular interest, but, for whatever reason, the proposal did not lead to commercial utilization.

Design Considerations Applied to Laboratory Reactor

(1) **Electrode Entry:** It became apparent quite early that side-entering electrodes would not be operable. The reason for this is that, at elevated temperatures, the segment of reactor wall separating the electrode entry points becomes conductive, and is soon seriously damaged. It seems to be a general rule that the electrode should not enter at a hot zone, especially at points where it contacts the wall and the fluidized bed simultaneously. It can also be concluded that, in a 2-electrode system, one electrode could enter at side or bottom, but the other must not.

(2) **Radiation Shield:** It is advisable to shield the electrode entry points from direct radiation from the fluidized bed. A radiation shield in the form of a false roof can be used, but when operating at high temperatures, it must be assumed that any electrical insulator will become conductive. The only completely safe insulator in this region is a gap left between solid elements. For this reason, on the laboratory scale, radiation shields are made in segments supported by the electrodes and thermocouple well. (Figure 2)

(3) **Fluidization:** For safe electrical operation, the coke particles must be in motion in the vicinity of the electrodes. If a continuous path of stationary particles exists between electrodes, local overheating, resulting in very large currents, frequently occurs. Good dispersion of the fluidizing gas is therefore an important aid to steady operation. On the laboratory scale, a porous-disk diffuser is very useful. When this is not practicable however, multi-jet dispersers or bubble cap types can be used. Materials of construction are porous carbon, graphite, and Vycor.

Thermal insulation of laboratory reactors is kept to a minimum so that the Vycor tube will be cooler than the bed, which may operate at temperatures far above the quoted service temperature of Vycor. In most of our laboratory work, therefore, the greater part of the input energy is lost to the air. With the combination of air-cooling and the low thermal conductivity of Vycor, it is quite possible to operate a laboratory reactor at 1500°C. using rubber stoppers for end closures.

In commercial reactors, heat losses must be minimized and refractories must therefore be capable of withstanding temperatures equal to those in the fluid bed. Very important practical developments have been made in a pilot plant installation under the supervision of another research group at Shawinigan. These developments include features of design and material selection that make sustained high temperature operation feasible, and also certain process developments connected with hydrogen cyanide manufacture.

[1]*Manuscript received November 11, 1960; accepted February 17,1961.*
[2]*Research Group Leader, Shawinigan Chemicals Limited, Shawinigan, Que.*
Based on a paper presented at the C.I.C. Chemical Engineering Conference, Quebec City, November 7-9, 1960.

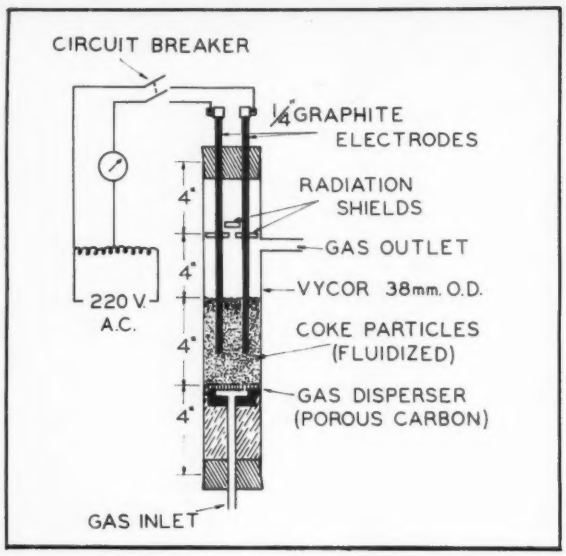

Figure 1—Fluidized coke reactor with self-resistive heating.

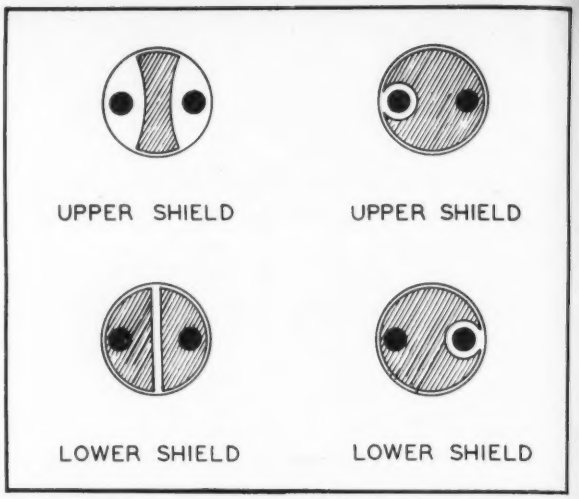

Figure 2—Forms of radiation shield used in laboratory reactor.

Electrical Properties

Because of the motion of the conductive particles, the electric current in the electrofluid reactor is not entirely steady. Moreover, the current depends upon the degree of fluidization. When the particles are not in motion, heat is generated in the path between the electrodes and is not readily dissipated, so that the path becomes very hot. Under these circumstances, local temperatures can become high enough to vaporize carbon, leading to agglomeration of coke particles.

Under most conditions, Ohm's law is approximately obeyed. This is best shown by connecting an oscilloscope to show the current-voltage relationships. The strict Ohm's law relationship is represented by a straight line when current is plotted against voltage. Any curvature, or loop formation is a measure of the deviation from Ohm's law. Sketches of some of the observed patterns are shown in Figure 3. It must be emphasized that in the normal operation of the electrofluid reactor, Ohm's law is obeyed, and that the cases shown in Figure 3 include undesirable deviations from normal practice. Some understanding of these deviations clarifies the preferred operation.

As the A.C. voltage is increased from zero, it is quite common to see the patterns shown in Figure 3 appear in succession. In particular at the higher range of voltage (about 200 volts per inch) alternation between type (2) and type (3) is quite common. Type (3) is considered to be characteristic of arcing as can be shown by withdrawing one of the electrodes from the fluid bed so that an arc is visible above the surface. In this situation the pattern is of type (3). It may be noted that the average current under arcing conditions can be lower than under non-arcing conditions, even though the voltage is higher. If the average current, as measured on an ammeter, is plotted against average voltage, the above sequence is represented as shown in Figure 4.

At point A, there can be a sudden decrease in current. This is thought to represent the onset of arcing. Because of the lower current, the temperature will drop, the arc is extinguished and operation returns to the high-current level, whereupon the cycle repeats.

Thermal Efficiencies

Most fluid bed reactors are heated by combustion of fuel, often in a separate chamber from the reaction zone. Heat transfer from burning fuel has two characteristics which make it less efficient at high temperatures (above 1800°F.).

(1) The rate of heat transfer depends on the temperature difference between the flue gas and the fluid bed. At temperatures above 2200°F. this constitutes a serious limitation on production rate.

(2) When heat is being transferred at a high temperature level, only a relatively small fraction of the total sensible heat in the flue gas can be transferred to the fluid bed. Recovery of the remainder, by low-temperature heat transfer, e.g., raising of steam, is required if reasonably efficient fuel utilization is to be realized.

These limitations of rate and efficiency of heat transfer at high temperatures do not apply to the electro-fluid reactor since the energy is fed directly to the reactant system, and the efficiency of electrical heating is not affected by the tempera-

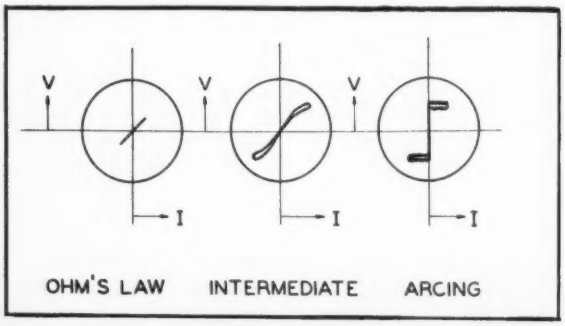

Figure 3—Types of oscilloscope patterns observed in electrofluid reactor operation.

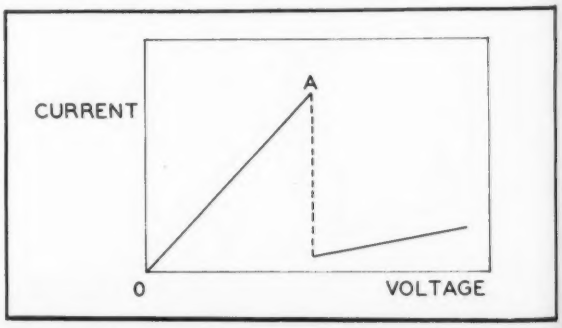

Figure 4—Ammeter-voltmeter measurements in electrofluid reactor (schematic).

ture level at which it is transferred, except in the minor effect, common to all types of heaters, of increased shell losses.

Applications

(1) **CS_2 from petroleum coke and hydrogen sulphide.** Available thermodynamic data show that the reaction between H_2S and carbon is favored at high temperatures[2]. By extrapolation it can be estimated that at 1327°C., 59.2% of the H_2S fed reacts to form CS_2, 26.6% reacts to form the elements, and the remainder is unchanged. Since carbon is a reactant, and the electrodes are of graphite, successful operation obviously depends on a very large difference in reactivity between graphite and the carbon in the fluid bed. Using the coke derived in the petroleum industry by fluid coking of residues, and briefly referred to as fluid coke, this condition is satisfactorily fulfilled.

In a 38 mm. O.D. laboratory reactor, operating at temperatures in the vicinity of 1500°C., about 70% of the H_2S was converted (i.e., not recovered) with apparent efficiencies to CS_2 in the range 90-100%. These were thought to be higher than the true values because of conversion of sulphur contained in the petroleum coke, forming additional CS_2.

Experiments of longer duration were made in a 5-inch I.D. reactor at 1400°C. These indicated that graphite would be a satisfactory construction material. Conversion of H_2S was estimated at about 55%, with efficiencies to CS_2 again in the range 92-94%. The low yield of elemental sulphur, compared with the thermodynamic prediction, may be noted.

Feed rate of H_2S was approximately 5-6 s.c.f.m./cu. ft. of petroleum coke, in both the 34 mm. and the 5-inch reactors, but this can be varied within limits which depend chiefly on coke particle size. Production rates corresponding to the above feed rate are 15-20 lb. CS_2/cu. ft. coke/hr.

The coke used in this work was commercial petroleum coke from a refinery fluid coker. It was usually screened to remove particles coarser than 20 mesh, and calcined in an open dish at temperatures above 900°C. in order to impart electrical conductivity. Actual power requirement for a 38 mm. laboratory reactor operating at 1500°C. is approximately 1 kw., or approximately 10 amp. at 100 v. For a 51 mm. O.D. reactor at 1500°C., the power requirement is approximately 2.6 kw., or 13 amp. at 200 volts.

(2) **CS_2 from petroleum coke and sulphur.** Commercial synthesis of CS_2 is usually carried out using wood charcoal, which is sufficiently reactive to permit operation at 700-800°C. Even at such temperatures, heat transfer imposes limitations on the production rate of an externally-fired reactor. In the electrofluid reactor, heat input is not a problem, and it was therefore of interest to determine at what temperature fluid petroleum coke would react at a reasonable rate.

It is known that the yield in this reaction is not greatly affected by temperature[3], and that an equilibrium yield of 85% could be expected at 1200°C. Although the heat of reaction is close to zero at 1000°C., the sensible heat required to dissociate sulphur vapor and heat it to reaction temperature is still sufficient to make the reaction suitable for this type of reactor.

Sulphur can be fed to the bottom of the reactor as vapor at, or above, the boiling point; or the liquid can be fed through a wide graphite pipe which, at a point near the bottom of the reactor, becomes hot enough to vaporize the sulphur. In the latter method, nearly all of the thermal energy involved is supplied by the fluid coke reactor.

It was found that at 1100°C. the reaction proceeded rapidly, with a conversion of 70% being obtained in the laboratory. On a larger scale of operation, where longer contact times would be possible, higher conversions can be expected. Laboratory production rates were approximately 20 lb. CS_2/cu. ft. of coke/hr.

In this temperature range, silicon carbide components are rapidly attacked. Again, graphite was found to be the most useful material of construction for the reaction zone.

(3) **HCN from ammonia and hydrocarbons.** A nearly ideal reaction for the electrofluid reactor is the synthesis of the highly endothermic HCN from ammonia and hydrocarbons, or ammonia and coke. The heat of formation of HCN (gas) at 77°F. is approximately 60,300 B.t.u./lb. mole. Moreover, the reaction is favored by rapid heating. Further, since HCN itself is not thermodynamically stable with respect to its elements, the HCN must be removed from the reaction zone as quickly as possible. When all of these factors are considered, the electrofluid reactor is seen to be particularly well-suited for this synthesis.

By way of orientation, it may be pointed out that the dominant route to HCN from petroleum is the Andrussow process[4] for partial combustion of a mixture of CH_4 and NH_3 over a Pt catalyst at about 1000°C. Exit gases contain about 8% HCN, and a typical yield on CH_4 is 70%, on NH_3 60%. Other high temperature processes using noble metal catalysts are known.

The object of the laboratory work was to evaluate the non-catalytic reaction between ammonia and hydrocarbons in which the fluid coke merely supplies the heat required.

A Canadian patent[5] contains examples of operation at 1400-1600°C., using propane and methane as hydrocarbons. In these experiments, the atomic ratio of nitrogen to carbon was varied, but was generally not far from unity. Gas feed rates are related to the size of coke particles used, and in these experiments were in the range 5-10 volumes of feed gas (at room temperature) per volume of coke per minute. When the hydrocarbon is propane, the concentration of HCN in the off-gas from the reactor is about 25% by volume, unreacted ammonia about 0.6% by volume. The yield of HCN on ammonia fed is 85-90%.

(4) **HCN from ammonia and coke.** This reaction is equally well-suited to the electrofluid reactor. Laboratory trials have shown that, in the absence of specific catalysts, the yield of HCN is lower than when hydrocarbons are used as the source of carbon.

Other Reactions

The foregoing gives an idea of the methods used in studying certain reactions which have been of particular interest. In the five-year period since the development of the electrofluid reactor, numerous reactions have been studied. Some of these are merely listed:

(1) CO_2-C
(2) H_2O-C
(3) Chlorinations: TiO_2-Cl_2-C
SiO_2-Cl_2-C
Al_2O_3-Cl_2-C
(4) Hydrocarbon cracking.
(5) Metal oxides and sulphur, H_2S, CS_2 to give metal sulphides.
(6) Heating applications: The electrofluid bed may be used as a preheater for chemical reactants, e.g., to preheat the recycle gas stream in iron reduction processes.
(7) Pyrolysis of acetic acid and acetone to give ketene.

Acknowledgements

The contributions of A. H. Andersen and D. C. Downing to this work are acknowledged. D. C. Bean and J. Reid did much of the experimental work. The author wishes to thank the management of Shawinigan Chemicals for permission to publish this work.

References

(1) German patent 457,179 (1928). F. Winkler, assignor to I.G. Farbenindustrie.
(2) Owen, A. J., Sykes, K. W., Thomas, D. J. D., and White, P., Trans. Faraday Soc., **49**, 1198 (1953).
(3) Owen, A. J., Sykes, K. W., and Thomas, D. J. D., Trans. Faraday Soc., **47**, 419 (1951).
(4) Andrussow, L., Z. Angew. Chem., **48**, 593 (1935).
(5) Canadian Patent 573,348 (1959). Johnson, H. S., and Andersen, A. H., assignors to Shawinigan Chemicals Limited.

★ ★ ★